2014

Design and Development of Heterogenous Combustion Systems for Lean Burn Applications

Anthony Terracciano
University of Central Florida

DESIGN AND DEVELOPMENT OF HETEROGENOUS COMBUSTION SYSTEMS FOR LEAN BURN APPLICATIONS

by

ANTHONY CARMINE TERRACCIANO
A.A Broward College, 2010
B.S.M.E University of Central Florida, 2013

A thesis submitted in partial fulfillment of the requirements
for the degree of Master of Science in Mechanical Engineering
in the Department of Mechanical and Aerospace Engineering
in the College of Engineering and Computer Science
at the University of Central Florida
Orlando, Florida

Spring Term
2014

Major Professors: Nina Orlovskaya and Subith Vasu Sumathi

ABSTRACT

Combustion with a high surface area continuous solid immersed within the flame, referred to as combustion in porous media, is an innovative approach to combustion as the solid within the flame acts as an internal regenerator distributing heat from the combustion byproducts to the upstream reactants. By including the solid structure, radiative energy extraction becomes viable, while the solid enables a vast extension of flammability limits compared to conventional flames, while offering dramatically reduced emissions of NO_x and CO, and dramatically increased burning velocities. Efforts documented within are used for the development of a streamlined set of design principles, and characterization of the flame's behavior when operating under such conditions, to aid in the development of future combustors for lean burn applications in open flow systems. Principles described herein were developed from a combination of experimental work and reactor network modeling using CHEMKIN-PRO. Experimental work consisted of a parametric analysis of operating conditions pertaining to reactant flow, combustion chamber geometric considerations and the viability of liquid fuel applications. Experimental behavior observed, when utilizing gaseous fuels, was then used to validate model outputs through comparing thermal outputs of both systems. Specific details pertaining to a streamlined chemical mechanism to be used in simulations, included within the appendix, and characterization of surface area of the porous solid are also discussed. Beyond modeling the experimental system, considerations are also undertaken to examine the applicability of exhaust gas recirculation and staged combustion as a means of controlling the thermal and environmental output of porous combustion systems.

This work was supported by ACS PRF #51768-ND10 and NSF IIP 1343454.

I wish to dedicate this work to my dad, Anthony Salvatore Terracciano. Without you, I would not have developed an appreciation of cars or engines which inspired me to study Engineering. Thanks for being my best friend and widening my field of view beyond what lies directly before of me.

Rest in Peace

August 5th, 1958 – January 12th, 2008

ACKNOWLEDGMENTS

I would like to thank all of the individuals whom have helped me during the development of the work provided herein. A special appreciation is given to my Fiancé, *Diana Bateman,* and my family for putting up with me through the long, and obscure, hours which I used to complete my Master's work.

I would like to pay special thanks to *Dr. Subith Vasu* and *Dr. Nina Orlovskaya* for their guidance through the process of my research and academic development. An equal thanks to both *Dr. Louis Chow*, and *Dr. Alain Kassab* as both committee members and outstanding professors; subject matter presented in their formal classes greatly developed the critical thinking needed to complete the research herein.

In addition, special thanks are given to my colleagues in Dr. Nina's research group: *Manuel Robayo*, *Richard Stadelmann*, *Zhilin Xie*, *Amjad Aman*, *Billy Hughes*, and *Ben Beaman*. Comradery offered by their experiences helped me to maintain motivation when things were going less than spectacular. Combined, the groups varied technical expertise often provided me with additional insight to troubles encountered during the research process.

I would like to thank my friends *Kelsey Dyal* and *Pretam Choudhury* for their support and encouragement offered through the long nights which I used to complete this work.

The members of the experimental design team which produced an invaluable research tool: *James Wilson*, *Jennifer Jackson*, and *John Lundy*; which I had the pleasure of working with.

Thanks to *Dr. Peter Glarborg* from the Technical University of Denmark for providing assistance with the development of a chemical mechanism.

This work was supported by ACS PRF #51768-ND10 and NSF IIP 1343454.

TABLE OF CONTENTS

LIST OF FIGURES viii

LIST OF TABLES xiv

CHAPTER ONE: INTRODUCTION 1

1.1 Why Combustion in Porous Media 1

1.2 Visualization of a Porous Combustor 4

1.3 Basics of Combustion 5

1.3.1 Reaction Pathways and the Transition State 7

1.3.2 Gas Phase Combustion 8

1.3.3 Catalytic Combustion 9

1.3.4 Series of Reactions 10

CHAPTER TWO: LITERATURE REVIEW 17

2.1 Theory of Porous Burners 17

2.1.1 Combustion Chamber Geometric Dependence 17

2.1.2 Material Considerations 21

2.1.3 Reactant Flow Considerations 24

2.2 Modeling of Porous Combustion 26

2.2.1 Analytical Analysis of Porous Combustion 27

2.2.2 Numerical Analysis of Porous Combustion 32

2.2.3 Numerical Solutions and the Mechanism Dependency 36

2.3 Porous Burner Designs 38

2.3.1 Fuel Selection for Porous Combustors 38

2.3.2 Novel Uni-Directional Flow Combustors 40

2.3.3 Reciprocating Flow Porous Combustors 43

CHAPTER THREE: LEAN APPLICATIONS OF HETEROGENOUS COMBUSTION 46

3.1 Enhancement of Pilot Flames 46

3.2 Ignition Devices in Internal Combustion Engines 48

3.3 Energy Extraction via Reclaimed Fuel Sources 48

3.4 Radiative Emitters 49

CHAPTER FOUR: EXPRIMENTAL SETUP 51

4.1 Double Feedback Loop Burner 51

4.1.1 Flow Loop Design 52

4.1.2 Combustion Chamber Design 55

4.2 Combustion Event Modeling 58

CHAPTER FIVE: RESULTS AND DISCUSSION 67

5.1 Double Feedback Burner 67

5.1.1 Double Feedback Burner Experimental Results 67

5.1.2 Double Feedback Burner Modeling Considerations 71

5.2 Exploratory Modeling Work 72
5.2.1 Determination of Solid Length 72
5.2.2 Exhaust Gas Recirculation Analysis 75
5.2.3 Staged Injection 77
CHAPTER SIX: CONCLUSIONS 82
APPENDIX A: REDUCED CHEMICAL MECHANISM RATES 84
APPENDIX B: THERMODYNAMICS DATA 92
REFRENCES 98

LIST OF FIGURES

Figure 1) Model of a axial flow heterogeneous combustor, showing the preheating δ_p and flame regions δ_L. 4

Figure 2) Temperature distribution within an adiabatic porous combustor. 5

Figure 3) Energy Pathway of Reactants, showing the activation energy barrier and the maximum extractable energy of the system. 7

Figure 4) A visual representation of a reaction system of N_2, H_2, and O_2. 8

Figure 5) Simple model of a catalytic surface reaction where diatomic oxygen directly interacts with surface vacancies. 10

Figure 6) Adiabatic flame temperature of an air methane mixture over a wide range of equivalence ratios, generated using the GRI 3.0 Mechanism[40]. 15

Figure 7) Reaction diagram of methane combustion in the lean oxidation regime. 16

Figure 8) Cylindrical axial and spherical porous combustor flowing charge gasses axially with radial dependence of flame within the porous solid. 18

Figure 9) Image of Silicon Carbide Porous Media, ~8.5 pores per linear inch (ppin). 18

Figure 10) Microstructure view of porous silicon carbide using optical microscope. 19

Figure 11) Energy release within a control element as compeared to the advection losses. 20

Figure 12) Expressed relation between flame speed ratio and heat recirculation efficiency across various equivalence ratios. 25

Figure 13) Physical domain representation of an isothermal solids interaction with a as described by Takeno et al. Upstream Boundary on the left, fluids moving in the positive x direction. With a solid of finite length occurring from 0 to L. 28

Figure 14) Plot of stable flow rates produced as a solution to an Eigen Function for a porous burner as produced by Takeno [67]. 30
Figure 15) Calculation of the excess enthalpy flame of the Upper branch of Eigen solutions [67]. 31
Figure 16) Calculation of the excess enthalpy flame of the Lower branch of Eigen solutions [67]. 31
Figure 17) Transient combustion wave displayed with temperature peaks corresponding to 300 second intervals within a porous combustor [68]. 32
Figure 18) Temperature and heat production output plot of the region immediately surrounding the flame peak intensity within a porous combustor [69], note the arrow indicates the direction of flow. 33
Figure 19) Chemical Conversion plot of carbon containing species as a function of distance within a modeled porous flow reactor [69]. 34
Figure 20) Droplet life time as a function of wall surface temperature adopted from [88]. 39
Figure 21) Two types of liquid fuel nozzles for use with porous combustors [89]. Top: pressurized air injector. Bottom: Pressurized swirling air injector. 40
Figure 22) Non premixed flame burner [91]. 41
Figure 23) Two stage porous combustor [93]. A steel screen is used to inhibit flame movement, radiative emissions are allowed to pass through Quartz tubing, and the energy is collected from a radiation to fluid heat exchanger. 42
Figure 24) The five step process associated with the closed chamber combustion device developed by Hanamura. 44

Figure 25) Reciprocating flow burner design showing combustion section, insulation, and ignition point [10]. 44
Figure 26) Reciprocating flow porous combustor, combustion chamber shown with oscillating valve series to control flow directions. [95]..... 45
Figure 27) Enthalpy transfer, from products initially at the burned temperature, to reactants at the unburned temperature [96]..... 46
Figure 28) Venturi design inlet for a surface stabilized heterogeneous combustor. An inlet at the center, for gaseous fuel, contracts producing a pressure drop; using pressure as the driving force ambient air will then be drawn in to the Venturi. 47
Figure 29) Closed combustion chamber with Porous Media used in lieu of a spark igniter as described by [97]..... 48
Figure 30) Combustion chamber design for combustion in porous media which allows for the emission of radiative energy from the combustion chamber length through a small opening. 50
Figure 31) Flow loop of the double feedback burner with each component outlined and the location of the 6 steady states as they correspond to the location of the burner. 52
Figure 32) CAD Depiction of concentric heat exchanger. 53
Figure 33) Vaporization Chamber showing liquid fuel needles and method of reactant delivery. 54
Figure 34) Steel foam as attached to the access hatch of the vaporization chamber. 54
Figure 35) Outlined thermodynamic Cycle outlining the relative locations of the thermodynamic states between the sections within the combustor..... 55
Figure 36) 2D representation of the combustion chamber showing dimensions, green alumina inserts, red silicon carbide porous media, thermocouple ports, as well as the silicon carbide

structure. From right to left, each of the instrumentation ports are referred to as *0~7*. Dimension a) 25.4mm, b) 152.4, c) 63.5mm, d)50.8mm. 56

Figure 37) Arrangement and packing of the combustion media, radiation scattering media and wall screen protectors. 57

Figure 38) Assembled porous combustor with instrumentation hookups shown on the combustion chamber. 58

Figure 39) Control volume analysis of porous media. 59

Figure 40) Comparison between real surface area (red) of micro and mesio pores as compared to effective convective surface area (blue) [107]. 60

Figure 41) In depth geometric analysis of porous media showing void openings, voids, and unformed openings. These are shown in conjunction with characteristic webbing lengths and widths used in calculations. 60

Figure 42) Regular dodecahedron. Used to illustrate idealized structure of the porous media. ... 61

Figure 43) FCC Crystal Structure. Used to orchestrate the arrangement of voids within a porous structure. 62

Figure 44) Discretization of porous section overlaid on the combustion media for comparison purposes. 65

Figure 45) Convection coefficient for an isothermal horizontal cylinder as a function of exterior surface temperature. 66

Figure 46) Temporal dependency of an experimental run of the double feedback burner, temperature profile is taken from *4*. 67

Figure 47) Temperature plot of the vaporization chamber for the double feedback burner. 68

Figure 48) Partial combustion chamber thermocouple plot missing thermocouples 0 and 3 as these were damaged at an earlier point in the experiment. 69
Figure 49) Step wise flow rate drops maintaining constant equivalence of 0.50, plotted along with the output temperature at *4*. 70
Figure 50) Combustion chamber outlet temperature *4* time evolution starting from initial point at which mass flux was changed. 71
Figure 51) Comparative data between the model, and experimental system using gaseous fuel at an equivalence of 0.50 over a range of flow rates. 72
Figure 52) CHEMKIN-PRO temperature profiles of Double-Feedback Burner at 49.75 SLPM. 73
Figure 53) Augmented temperature profile corresponding to the Double-Feedback burner at 55.00 SLPM and equivalence ratio of 0.60. 74
Figure 54) Carbon deposition along the combustion chamber inlet, white arrow pointing to carbon deposition along the wall, with the apparent reaction zone outlined in orange. Spacing between each thermocouple tap center is 2.166 cm. 75
Figure 55) Representation of an EGR system which features pathways for the exhaust to reroute. 76
Figure 56) Temperature reduction as a result of EGR implementation at a recirculation flux of 2.5%. 76
Figure 57) Reductions in the NO_x and CO concentrations, respectively, for a heterogeneous combustor featuring EGR with a recirculation flux of 2.5%. 77
Figure 58) Porous combustor with staged inlet. 78
Figure 59) Temperature profile of the gas phase for 80 SLPM at an equivleance ratio of 0.55 through a heterogenous reactor. 79

Figure 60) Comparison of a single inelt and double inlet reactor by examination of the thermal output. 80

Figure 61) Comparison of CO and NOx output for single inlet and double inlet deisgn over varying overall equivleance ratios. 81

LIST OF TABLES

Table 1) Selected Compounds arranged in order of heats of formation at reference conditions. Compounds exist in the gas phase unless otherwise listed. 6

Table 2) Excerpt of H_2/O_2 chemistry. 13

Table 3) Compositions of important gaseous species from Biogas and Landfills. 49

Table 4) Selected materials properties of SiC and Al_2O_3. 57

LIST OF VARIABILES AND CONSTANTS

Latin Alphabet

A Arrhenius Equation Pre-Factor [cm^3/s]

A Area [cm^2]

A_c Area of Conduction [cm^2]

A_{surf} Area of a Surface [cm^2]

A_v Area of Gas Flow [cm^2]

C_p Constant Pressure specific Heat [$J/(kg \cdot K)$]

D Diameter [cm]

D_{12} Diffusion Coefficient [cm^2/s]

D_e Equivalent Diameter [cm]

D_w Webbing Diameter [cm]

E_a Activation Energy [cal/mol]

F_d Drag Force [N]

K Reaction Rate [$cm^3/(mol \cdot s)$]

K_c Equilibrium Constant [atm^n]

K_F Formation Reaction Constant [atm^n]

K_f Forward Reaction Rate Constant[$cm^3/(mol \cdot s)$]

K_P Pressure Specific Equilibrium Constant [atm^n]

K_r Reverse Reaction Rate Constant[$cm^3/(mol \cdot s)$]

L_R Reactor Length [cm]

Le Lewis Number [Unitless]

N_L Number of Voids Length [Unitless]

N_p Number of Voids Planar [Unitless]

Nu_D Nusselt Number [Unitless]

P_t Total Pressure [atm]

Pe Peclet Number [Unitless]

Pr Prandtl Number [Unitless]

Q Thermal Power [W]

Q_e External Heat Flow [W]

R_u Universal Gas Constant [8.314 J/(mol*K)]

R Non-Dimensionalized mass flux [Unitless]

R_T Thermal Shock Resistance [kW/m]

Ra_d Rayleigh Number [Unitless]

Re Reynolds's Number [Unitless]

S_L Laminar Flame Velocity [cm/s]

T Temperature [K]

T_{ba} Adiabatic Flame Temperature [K]

T_{out} Outlet Gas Temperature [K]

T_s Solid Phase Temperature [K]

T_x Temperature as a Function of Axial Position [K]

V Gas Velocity [cm/s]

X Arbitrary Chemical Species [Unitless]

Y Mole Fraction [Unitless]

d_m Section Diameter [cm]

f Non-Dimensionalized Heat Transfer [Unitless]

h Convection Coefficient [$W/(cm^2 \cdot K)$]

h Specific Enthalpy [kJ/kg]

$\dot{m}$ Mass Flow [kg/s]

$\dot{m}''$ Mass Flux Per Unit Area [$kg/(s \cdot cm^2)$]

q'_{loss} Heat Loss Per Unit Length[W/cm]

q_r" Radiative Heat flux

q''_{surf} *Heat Flux Through A Surface [W/cm^2]*

$\dot{q}_{chem}$ *Heat Release Via Chemical Reactions [W/cm^3]*

$\dot{q}'_{surf}$ *Heat Release Via Surface Reactions [W/cm^2]*

r Dimensionless Mass Flux [Unitless]

r_e *Equivalent Radius [cm]*

x Position Variable [cm]

i Counting Indicy [Unitless]

j Counting Indicy[Unitless]

n Exponential Index [Unitless]

t Time [s]

k_f *Thermal Conductivity of a Fluid [W/m]*

$\Delta H_f°$ *Heat of Formation [kJ/mol]*

Δx_i *Discretization of Arbitrary Position[cm]*

Greek Alphabet

Λ_s *Mass Burning Velocity Eigen Value [Unitless]*

α Dimensionless Enthalpy Relation [Unitless]

β Reactant Preheating Energy Ratio [Unitless]

Velocity Rate [Unitless]

δ Length of Reaction Zone [cm]

δ_L *Length of Flame Thickness [cm]*

δ_p *Length of Gas Preheat [cm]*

ε Hemispherical Total Emissivity [Unitless]

η Mass Flux of Product Fraction [Unitless]

θ Non-Dimensionalized Solid Gas Temperature Difference [Unitless]

ι Firing Rate [W]

κ Dimensionless Heat Flux Coefficient [Unitless]

ν Kinematic Viscosity [cm^2/s]

ξ Non-Dimensionalized spatial variable [Unitless]

ρ_f *Fluid Density [kg/cm^3]*

τ Non-Dimensionalized Temperature[Unitless]

τ_s *Dimensionless Solid Phase Temperature [Unitless]*

φ Equivalence Ratio [Unitless]

$\bar{\varphi}$ *Overall Equivalence Ratio [Unitless]*

ψ Ratio of Actual to Laminar Flame Speed [Unitless]

ω Rate of Production [matrix]

CHAPTER ONE: INTRODUCTION

1.1 Why Combustion in Porous Media

As the world continues to grow, with "developing countries" entering into the post industrial age, the need to derive means of producing efficient thermal energy will have an increasing importance. Recent advances in the gasification process of coal [1, 2] and declines on the return rates from oil drilling [3] both bring change to the nature of combustion; future combustors will need to better utilize resources than current technology while burning fuels with increased variability in their composition. Combustion in porous media can offer increased stability, reduced emissions, and higher firing rates than existing combustion technology; supplementing these enhanced lean burn characteristics, combustion in porous media can also act as a valuable tool in the reformation of fuel stocks for the production of syngas.

Combustion processes are series of chemical reactions, recombining unreacted molecules at a high energy potential, to various combinations of molecules at a lower energy potential. Combustion, being an irreversible process, generates large concentrations of entropy [4]. ; though, what can be done to a combustion reaction to reduce the inefficiencies which occur when formulating low formation enthalpy products, allowing near theoretical heat to be obtained?

Supposing combustion was initiated at a higher temperature, through imposing a regenerator into the system, the total fuel needed to produce a mixture at a high temperature is greatly lessened as combustion is starting from a point of higher enthalpy. Weinberg [5] proposed the inclusion of an in combustion event regenerator, which has ignited the study into combustion in porous media. Emplacing a solid structure with high surface area into the space in which combustion is designed to occur, the combustion reaction dynamics change due to the

heterogeneous nature of the solid-gas interactions. A solid structure within the combustion region provides a structure through which thermal energy readily propagates.

Weinberg never directly expressed the utilization of porous media within a combustion reaction, merely the idea of internal heat recirculation leading to more efficient combustion; the high temperature offered by heat recirculation could produce high reaction rates of combustion processes accompanied with high thermodynamic efficiency, and high heat transfer rates. As a result of the reactant preheating, one of the sought after abilities of porous combustion is the possibility of exhibiting a localized flame temperature in excess of the fuel mixture's adiabatic flame temperature. However, the localized superadiabatic temperature will be within the region of the flame region only as exhaust gas temperatures will always exhibit a thermodynamic upper bound of the adiabatic flame temperature.

Weinberg proposed several advantages of such a combustion technique, high temperatures afforded by the porous structure enable a heightened thermal potential, coning the phrase "excess enthalpy combustion" which is more commonly referred to as superadiabatic combustion. Superadiabatic combustion is a combustion regime in which the flame exists at a temperature above that of the adiabatic flame temperature. Extreme temperatures offered by superadiabatic combustion enable for increased heat extraction potentials and significantly faster combustion processes [5]; he even proposed the excess enthalpy combustion would be able to produce reaction products of higher organization by sudden gas quenching [5].

Matrix stabilized porous combustion also yields higher burning velocities and leaner flammability limits than open flames [6]. Furthermore, combustion completely submerged within porous media occurs without a flame [7] similar to catalytic combustion [8]. Simultaneously, porous media burners also feature low CO and NO_x emissions [6, 9, 10]. As the insertion of a

solid structure also allows for the direct control of particulate emissions [7]. The porous structure's ability to regulate heat flux also enables combustion capable of burning low calorific value fuels [9] and ultra-low equivalence ratios.

A porous solid structure can be implemented in several ways into a combustion reaction. Open flow systems can constitute surface combustors, more commonly known as radiant burners, [11-13] or immersed flame porous combustors [6, 14, 15] which have the flame stabilized within the voids of the porous matrix. Closed combustion systems can use a porous structure in multiple alternate ways. What is common between all these techniques is the solid structure is generally made of a thermally stable ceramic and the solid transmits heat to the gas.

As with any fluid flow device, it is necessary to consider the mechanics of the fluids which progress through the devices. Entire fields of study are dedicated to the effects which the nature of fluid flow affects the combustion characteristics of a system [16]; combustion systems under high pressure as would be experienced in Brayton Cycle turbines are particularly susceptible to thermoacoustic instabilities [17, 18].

1.2 Visualization of a Porous Combustor

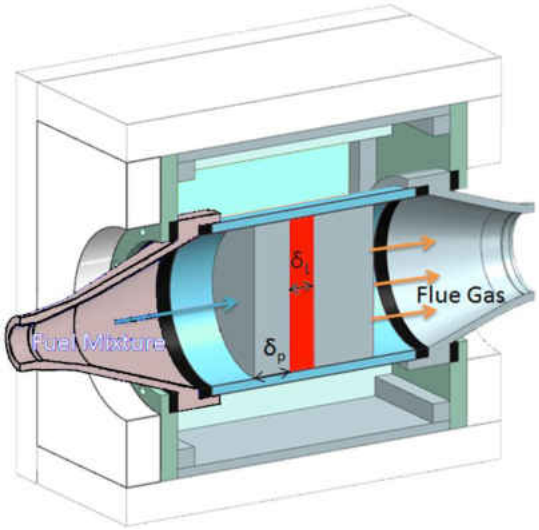

Figure 1) Model of a axial flow heterogeneous combustor, showing the preheating δ_p and flame regions δ_L.

Within the combustion chamber, a formal definition of the flame thickness is given as δ_L, corresponding to the region of peak chemical heat release. Prior to the flame thickness there is a preheating zone denoted by δ_p, the bounds of the preheat zone are defined by the length of flow from the combustion chamber inlet, until the gas and solid phase temperature reach thermal equilibrium marking the beginning of the chemical reaction. In reference to the flame's position within the porous media, these definitions are visible in Figure 1

Within heterogeneous combustion, when the flame exists within the solid, the various modes of heat transfer are working to modify the structure of the flame. Within Figure 2, the region beyond the flame, heat is convectively transferred from the post combustion gasses into the solid. Heat then conducts and radiates through the solid structure upstream through the flame.

Within the preheating region, heat is again convectively transferred from the solid structure to the gas.

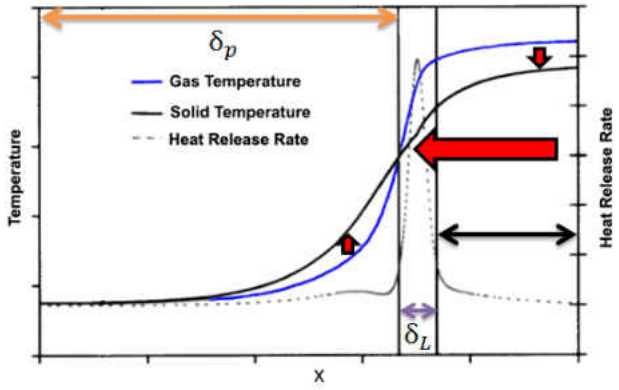

Figure 2) Temperature distribution within an adiabatic porous combustor.

1.3 Basics of Combustion

Products of combustion reactions exist in a configuration which requires less energy to maintain a stable form than the reactants. Akin to conventional combustion, combustion within a porous media mandates three components, assuming a monopropellant is not being used, to maintain a stable combustion reaction: an oxidizing agent, a reducing agent, and an energy source for ignition of the reactants are required. However, the key element which makes combustion in porous media so unique is the ability to run the mixture at equivalence ratios well beyond normal combustion limits due to internal heat transfer; extension of these limits can be further increased by including a catalytically active solid material.

One of the two primary chemical reagents needed for a combustion reaction is referred to as an oxidizer. Oxidizers are a classification of molecules which strip electrons from other compounds in the reaction. By nature oxidizers are typically electronegative; elemental oxidizers are organized on the periodic table around fluorine with the next two most electronegative elements occurring as oxygen and chlorine respectively [19]. Outside of

aerospace applications, the oxidizing agent which is most widely utilized across combustion devices is the diatomic oxygen occurring in air [4]; however, the enhancement of the oxidizer stream by pure oxygen injection [20] is common. The selection of air is governed by its' availability and low cost of retrofitting.

Reductants, commonly referred to as fuels, are the second necessary chemical group consumed by combustion reactions. Fuels utilized within a combustion reaction may take a variety of forms; though most fuels will exhibit a high amount of bond energy within the molecular structure and a high formation enthalpy relative to its mas compared to reaction byproducts like CO_2 and H_2O [21]. Located in Table 1.1 several common combustion compounds of a C-H-N-O-S system are displayed, arranged in order of the highest formation enthalpy to the lowest. Formation enthalpy is derived from the energy within the chemical bonds of a structure, compared to some defined base, it is common practice in combustion analysis to apply the ground state as N_2, O_2, H_2, C (solid), and S (solid) at conditions of 1 atm and 298.15K.

Table 1) Selected Compounds arranged in order of heats of formation at reference conditions. Compounds exist in the gas phase unless otherwise listed.

Molecule Name	**ΔH_f° (kJ/mol)**		**Molecule Name**	**ΔH_f° (kJ/mol)**
C (Carbon)	716.67		S (Sulfur)- Solid	0.000
N (Monatomic Nitrogen)	472.68		H_2S (Hydrogen Sulfide)	-20.50
O (Monatomic Oxygen)	249.17		NH_3 (Ammonia)	-45.90
S (Monatomic Sulfur)	276.98		CH_4 (Methane)	-74.87
H (Monatomic Hydrogen)	218.00		C_2H_6 (Ethane)	-84.81
O_3 (Ozone)	142.67		CO (Carbon Monoxide)	-110.53
SH (Mercapto)	139.33		COS (Carbonyl Sulfide)	-138.41
NO (Nitric Oxide)	90.29		H_2O (Water)	-241.83
SO (Sulfur Oxide)	5.007		C_8H_{18} (Octane)	-250.31
O_2 (Diatomic Oxygen)	0.000		H_2O (Water)	-285.10
N_2 (Diatomic Nitrogen)	0.000		SO_2 (Sulfur Dioxide)	-296.84
H_2 (Diatomic Hydrogen)	0.000		CO_2 (Carbon Dioxide)	-393.52
C (Carbon)- Solid	0.000		SO_3 (Sulfur Trioxide)	-395.77

Within a combustion event, interaction of the electron clouds between the fuel and oxidizer cause the fuel to chemically decay, and the recombination of the chemical elements which constitute the reactants results in the formation of the reaction byproducts. Products of the

reaction are composed of the same elements which the reactants are comprised of, though in a form with reduced energy contained with the chemical bonds. As continuity is maintained across the chemical species, the reaction byproducts will occur in a much higher molar quantity as compared to the reactants.

1.3.1 Reaction Pathways and the Transition State

Clarification of a reaction process can be assisted through a visual representation, of the transition state theory [22]. Figure 3 is a graphical overview of transition state theory which is comprised a curve of the energy potential of the reactants as they progress through the chemical reaction, black, and three additional denotations. In plots of this nature, the x axis is referred to as the reaction coordinate, which is an abstract representation of the reactions completion progress. Separating the local minima is the saddle point of the reaction which characterizes the "transition state." Noting the initial and finial minima, the products of the reaction, energy denoted by the blue line, exist at a lower energy state than the reactant potential, denoted by the green dotted line.

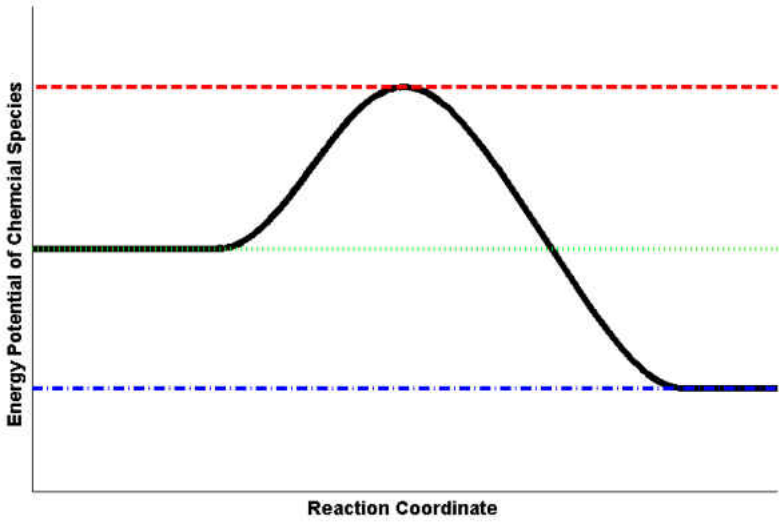

Figure 3) Energy Pathway of Reactants, showing the activation energy barrier and the maximum extractable energy of the system.

Prior to the reaction, at the x axis zero, the chemical species of the reactants contain a given chemical energy potential. As the reaction progresses, additional energy is introduced to the reactants resulting in a positive first derivative until a maxima occurs; the differential of energy between the maxima and the initial is known as the activation energy. Once the activation energy has been supplied, the reaction molecules enter a transition state which exists for only a short instance until a viable pathway for the reactants to continue to the post reaction minima. In a theoretical combustion system, the difference in energy between the green and blue lines represents the maximum energy which can be extracted from the combustion reaction.

1.3.2 Gas Phase Combustion

The aforementioned transition state is what allows a single chemical reaction to occur. However, within combustion systems there are often hydrocarbons containing several C-C bonds, and as a result the direct formation of products from reactants is an unlikely event. For a reaction to proceed there are several steps undertaken by the reactants, on the progression to the byproducts. A simple overview is explained in Figure 4, which shows a simple interaction process between N_2, H_2, and O_2.

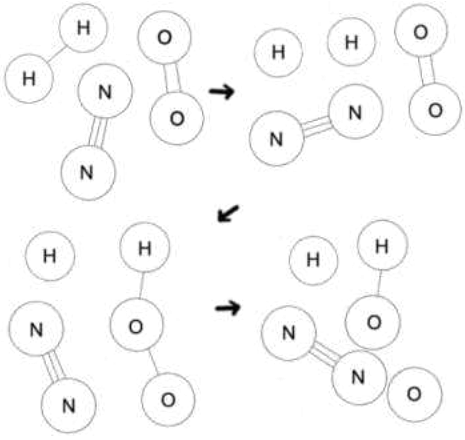

Figure 4) A visual representation of a reaction system of N_2, H_2, and O_2.

In Figure 4, the first state identifies diatomic N H and O; a collision occurs between the H_2 and the N_2. N_2, having the stronger bond, acts as a solid body and assists to split the H_2 into two-H radicals. With the H radicals free, these split and one of the H's are attracted to the O_2 to form HO_2, a pseudo stable combustion radical. Upon the interaction of HO_2 with N_2 the dissociation of HO_2 occurs forming two additional radicals O and OH. Rates at which compounds are produced and consumed are functions of: equilibrium constants, availability of the chemical species, the number of bodies considered for the reaction, activation energy for the reaction, collision frequency and the temperature dependent forward reaction rate [23].

1.3.3 Catalytic Combustion

Catalysts exists in many forms, ranging from enzymes [24] to injected gas phase compounds to reduce NO_x concentrations [25]; however, for the purposes of the text following catalysts refers to solid structures which interact with a reacting flow. Catalytically enhanced combustion allows, for the targeting of reducing concentrations of pollutants such as NO_x [26], VOC's [27], and SO_x [28]. Inclusion of catalysts within a combustion reaction leads to a regime of combustion referred to as "catalytically enhanced combustion."

A catalyst operates undergoing a mass hysteresis [8, 29]. On the surface of the catalyst exposed to a reacting flow, a localized disruption in the structure of the catalyst surface, which are known as surface vacancies, where a bond can be made from mass in the free reactant flow stream [30]. Examining Figure 5, it can be seen the free floating O_2 approaches the surface vacancies. Assuming there is sufficient energy the collision which occurs between the O_2 atom and the surface will disrupt the double bond. At the point of bonding on the catalyst surface, the electron configuration of the O molecule is complementary to the exhibited open electron configuration and geometric spacing exhibited by the vacancy. Once bonded, the oxygen atom

now denoted by O(s) representing a surface species closes the surface vacancy and forms a structure which allows for secondary bonding existing in parallel to the formation of a gas phase O radical.

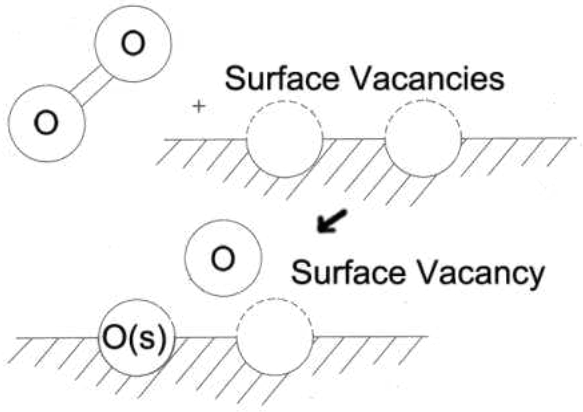

Figure 5) Simple model of a catalytic surface reaction where diatomic oxygen directly interacts with surface vacancies.

1.3.4 Series of Reactions

Combustion processes are typically "fast" compared to other types of flow problems, requiring only milliseconds for ignition of stationary reactants [31] once sufficient energy is provided to allow chemical shifts. In a combustion process with a homogeneously mixed reacting flow, the limiting factor is the reaction rate of the fuel and oxidizer. Reaction rates are a function of temperature and are specific to the chemical composition of the fuel and oxidizer. Temperature dependence governs the rate at which a reaction occurs, expressed as k, or the reaction rate coefficient through a modified form of the Arrhenius

(1).

Temperature dependence of a reaction rate is dependent upon the rate at which molecules collide, and have sufficient energy to chemically interact A. A temperature dependence of activation energy, E_a, the energy needed to reach the transition state by compounds expressed as

exponential function and an exponential temperature dependence which ranges accordingly to the n power. Essentially, the equation yields the corresponding rate at which a collision of fuel and oxidizer molecules will result in reaction propagation.

$$k(T) = A \cdot T^{n} \cdot e^{\frac{-E_a}{R_u \cdot T}} \tag{1}$$

While it is possible for a combustion system to form reaction byproducts directly from its initial reactants, this rarely happens; in most instances, there are several intermediary compounds which occur sequentially and simultaneously to form products from reactants. Chemical reactions regardless of their rates and final equilibrium concentrations exhibit a degree of complexity beyond the direct formation of products from reactants.

Examining the single step reaction of methane and air as equation (2), it can be seen that fuel and oxidizer is directly converted to products with nitrogen acting as an inert third body. However, the energy needed for this reaction to occur is rather high, and the global reaction takes the form of a first law efficiency; biased on this reaction the amounts of extractable energy biased on complete combustion can be produced. However, equation (2) is actually a state function where the process itself is more appropriately described over several partial reactions which vary according to the temperature range across the reaction regime [32]. A simplified chemical model for methane in porous media is expressed as equations (3) through (6) [33] which allows for the creation of intermediates and incomplete products.

$$CH_4 + 2\cdot(3.76\cdot N_2 + O2) \rightarrow CO_2 + 2\cdot H_2O + 7.52\cdot N_2 \tag{2}$$

$$CH_4 + 2\cdot H + H_2O \rightarrow CO + 4\cdot H_2 \tag{3}$$

$$CO + H_2O \rightarrow CO_2 + H_2 \tag{4}$$

$$2\cdot H + M \rightarrow H_2 + M \tag{5}$$

$$3\cdot H_2 + O_2 \rightarrow 2\cdot H_2O + 2\cdot H \quad (6)$$

When utilizing mechanisms with a plethora of reactions, it is typical to break down a large mechanism into several groups arranged with similar molecular complexity; this hierarchal structure follows the tendency of reactions to occur. Following the vernacular proposed by Green, [34], a mechanism seed is a base subset of reactions which are the lowest common denominator of the combustion system. Mechanism seeds are at the base of a hierarchical structure of reaction complexity and are crucial to accurate numerical representation of physical systems.

The H_2 and O_2 base chemistry seed mechanism is greatly responsible for the accurate prediction of ignition delay times [35]; while both the CO and H_2 base chemistry are the most important reactions in the accurate prediction of laminar flame speed analysis in methyl and methylene species combustion [36]. When considering combustion of larger hydrocarbons: i-octane, n-dodecane, and n-hexadecane the complexity of the necessary intermediates to represent the system increases considerably. In these, long chain hydrocarbon combustion analyses, a "full" mechanism which accurately depicts the oxidation of lighter hydrocarbons: methane, ethane, and propane become seed mechanisms [37].

Chemical mechanisms contain many reactions which form a series of species specific differential rate equations. A subset of hydrogen and oxygen reactions [38, 39] are presented in Table 2. Presented are specific reactions with Arrhenius Constants. For this system, examinations of seven molecular species are considered across five reactions. To make use of such data the formation of differential equations are used to generate the net rate of production across each species.

Table 2) Excerpt of H_2/O_2 chemistry.

	Chemical Reaction	**A (cm^3/(mol·s))**	**n**	**E_a (cal/mol)**
1)	$OH+H_2 \leftrightarrow H+H_2O$	2.14E+08	1.5	3449.0
2)	$O+H_2O \leftrightarrow OH+OH$	4.50E+04	2.7	14550.0
3)	$HO_2+H \leftrightarrow OH+OH$	8.40E+13	0.0	400.0
4)	$HO_2+O \leftrightarrow OH+O_2$	1.63E+13	0.0	-455.0
5)	$HO_2+OH \leftrightarrow H_2O+O_2$	3.60E+21	-2.1	9000.0

Using O_2 as an example species, differential equation rates of production from specific reactions can be produced based on the mole fractions of the reactants within the mixture and the temperature dependent Arrhenius rate constants which are presented as equations (7) and (8). These can be summed together across any of the, *i* reactions contained within the mechanism of *j* species, forming the net rate of production for the specific compound expressed in the general sense of equation (9). When a considered mechanism is "large" rather than using the form proposed in equation (9), it is convent to represent a combustion system in a matrix form (9).

$$\frac{\boldsymbol{d_4[O_2]}}{\boldsymbol{dt}} = \boldsymbol{K_4(T)} \cdot \boldsymbol{[HO_2]} \cdot \boldsymbol{[O]} \tag{7}$$

$$\frac{\boldsymbol{d_4[O_2]}}{\boldsymbol{dt}} = \boldsymbol{K_4(T)} \cdot \boldsymbol{[HO_2]} \cdot \boldsymbol{[O]} \tag{8}$$

$$\frac{\boldsymbol{d[X_j]}}{\boldsymbol{dt}} = \sum_{\boldsymbol{i}} \frac{\boldsymbol{d_i[X_j]}}{\boldsymbol{dt}} \tag{9}$$

$$\boldsymbol{\omega} = \begin{bmatrix} \boldsymbol{K(T)_{1,1}} & \cdots & \boldsymbol{K(T)_{1,j}} \\ \vdots & \ddots & \vdots \\ \boldsymbol{K(T)_{i,1}} & \cdots & \boldsymbol{K(T)_{i,j}} \end{bmatrix} \tag{10}$$

It is also of importance to note, for every chemical reaction which features a "↔" symbol also features a reverse reaction tabulated from the given reaction rate and the equilibrium constant for that chemical system. Formally, these quantities are related as expressed below in equation (11). Where K_c, the equilibrium constant, is derived from the thermodynamic

equilibrium of all species involved in the reaction, and subscripts F and R denote forward and reverse, respectively.

$$\boldsymbol{K_c = \frac{K_F}{K_R}} \tag{11}$$

For cases of reactions invariant of timescale, the achievement of thermodynamic equilibrium constitutes the termination of a combustion reaction. At thermodynamic equilibrium, for the case of an adiabatic reaction process, the maximum conventional temperature of the flame is achieved, known as the adiabatic flame temperature. Equation (12) denotes the likely products of methane combustion across equivalence ratios ranging from .25 to 5, when using air as an oxidizer.

$$\begin{aligned} &CH_4 + 2 \cdot \ (O_2 + 3.76 \cdot N_2) \ \rightarrow \\ &\quad a \cdot CO_2 + b \cdot H_2O + c \cdot H_2 + d \cdot CO + e \cdot O_2 + f \cdot NO + g \cdot N_2O + h \cdot N_2 \\ &\qquad + \sum i_j \cdot (C_nH_m)_j \end{aligned} \tag{12}$$

In order to solve the coefficients for the products at thermodynamic equilibrium, an equal number of equations must be generated for the constants. For any chemical systems a number of equations equal to the number of chemical species can immediately be generated. Once an atomic species balance has been considered is then necessary to take into account the net equilibrium of products and reactants, equation (13); using this equation a series of additional equations can be generated. Equation (14) for example, allows for the expression of enthalpy conservation between the products and reactants which at equilibrium sums to zero.

$$0 \leftrightarrow \ \sum n_j \cdot X_j \tag{13}$$

$$0 = \sum n_i \cdot \left(\Delta H_{f0_j} + \Delta H_j\right) \tag{14}$$

Additional equations necessary to determine the remaining coefficients are derived from the partial pressure of each constituent gas species, equation (15); from which specific equilibrium constants as a function of partial pressures and of formation constants $K_f(T)$ which are equilibrium constants for formation reactions when the references are usually taken as species with zero energy potential as shown in Table 1 are able to be generated. In Figure 6, the adiabatic flame temperatures for an air methane mixture in an open flow system are conveyed as a function of equivalence ratio with a peak temperature at equivalence of 1.038 producing a temperature of 2327K.

$$P_i = P_{abs} \cdot \frac{n_i}{\sum n_j} \tag{15}$$

$$K_p = \prod_j {P_j}^{n_j} \tag{16}$$

$$K_p = \prod_j {K_f(T)_j}^{n_j} \tag{17}$$

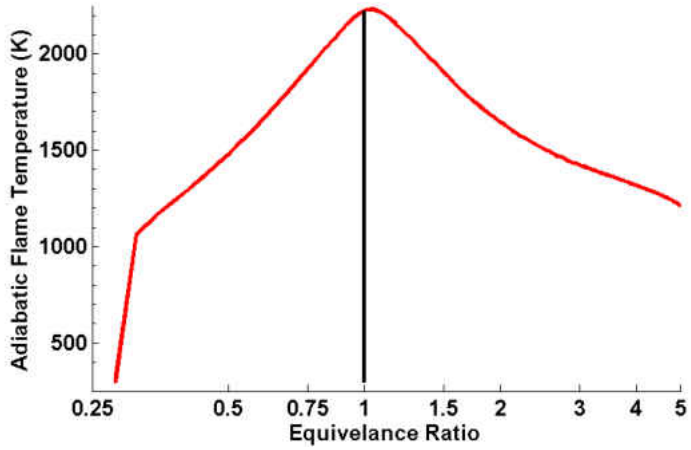

Figure 6) Adiabatic flame temperature of an air methane mixture over a wide range of equivalence ratios, generated using the GRI 3.0 Mechanism[40].

For lean combustion operating on methane and air, a streamlined pathway of chemical species has been included Using the GRI 3.0 mechanism [40], along with the Glarborg [39] sulfur model and key reactions [41-44] a mechanism was generated for reduced complexity of reacting systems across the equivalence ranges 0.4-1.1, pressure ranges of 0.1 atm to 20 atm, and initial temperatures as low as 1200K in ignition delay tests.

From this streamlined process the following outlined pathways of methane oxidation were found to be prominent and are graphically represented in Figure 7. Four primary pathways are employed to CO_2 formation, after all methane is converted to methyl: a higher order hydrocarbon pathway, a methyl subspecies path, and a methylene path. Methylene prominently interacts with nitrogen forming several nitrogen containing subspecies prior to oxidizing completely.

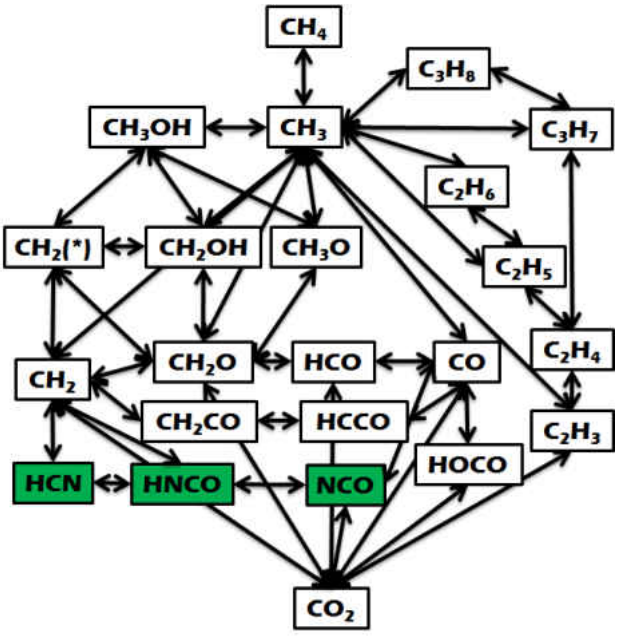

Figure 7) Reaction diagram of methane combustion in the lean oxidation regime.

CHAPTER TWO: LITERATURE REVIEW

2.1 Theory of Porous Burners

Design principles of porous combustors are widely varied, various designs offer their own specific key features. While it is impossible to examine the field within its entirety, some of the notable points of heterogeneous combustion in porous media are outlined in the following text. A detailed theory of the operation of a porous burner is presented. Examples of interesting porous burner designs are presented which have developed to suit various experimental and practical needs. With a finalized review which is pertinent to the explicit modeling of porous combustion systems.

2.1.1 Combustion Chamber Geometric Dependence

Within an open flow porous combustion system, the selection of the geometric configurations of the combustion chamber is of great importance. Open flow porous burners are afforded flexibility of the geometric configuration of the flow within the porous structure; reactant flow can undertake a Cartesian configuration, cylindrical axial flow, cylindrical radial flow or spheroidal flow [45-47].

The solid medium which the flame is to be immersed in must provide a balance depending on the intended operational temperature spectrum of the burner. The macroscopic properties of the porous solid play a role in determining optimal effects, while the pore size determines heat and fluid flow dependencies.

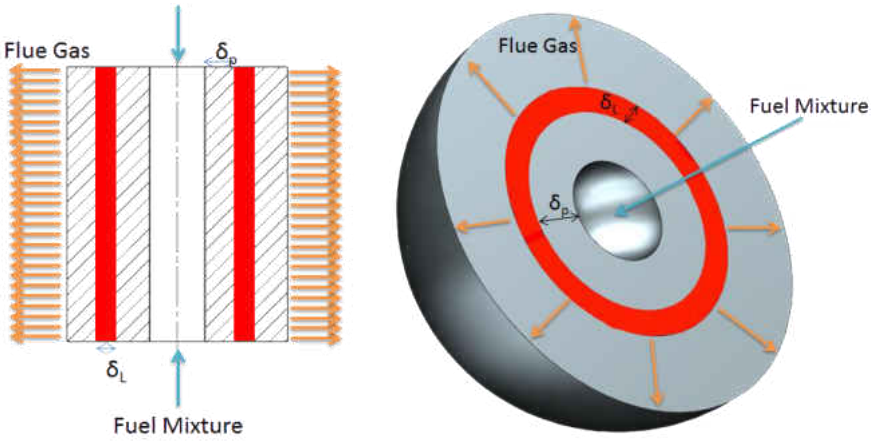

Figure 8) Cylindrical axial and spherical porous combustor flowing charge gasses axially with radial dependence of flame within the porous solid.

For the corresponding modeling and experimental aspects of the work provided herein, Figure 9 and Figure 10 depict the porous solid used prior to being fired through the burner. Figure 9 displays bulk surface characteristics, used for heat transfer calculations, of the silicon carbide porous structure used. As can be seen in the figure, there is no preferred orientation of the material and the structure of the solid is assumed to be random. Analysis of such an object is characterized by voids, the space occupied by gases, and webs, the solid structure which encloses the voids.

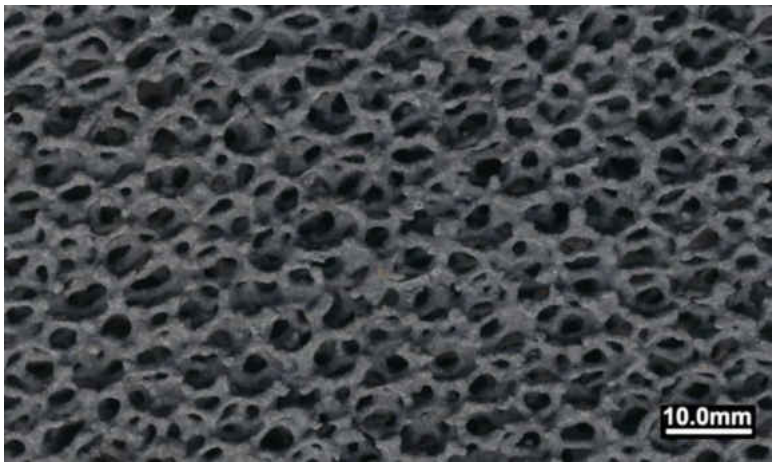

Figure 9) Image of Silicon Carbide Porous Media, ~8.5 pores per linear inch (ppin).

When examining the silicon carbide in greater magnification as can be seen in Figure 10, the complexity of the seemingly homogeneous surface disintegrates. Observing the differences in the light reflection patters, it is observable that several phases are simultaneously present within the material. Furthermore from the figure it can be seen the solid structures surface exhibits a high degree of roughness on the nano-scale, to supplement the fissures viewable on the ceramic surface.

These small scale discontinuities present a large contribution to the modeling of the porous structure. Roughness on the surface ensures a turbulent airflow over single solids. However, the characteristics of the surface create a localized site distribution of the various solids when considering catalytic reactions.

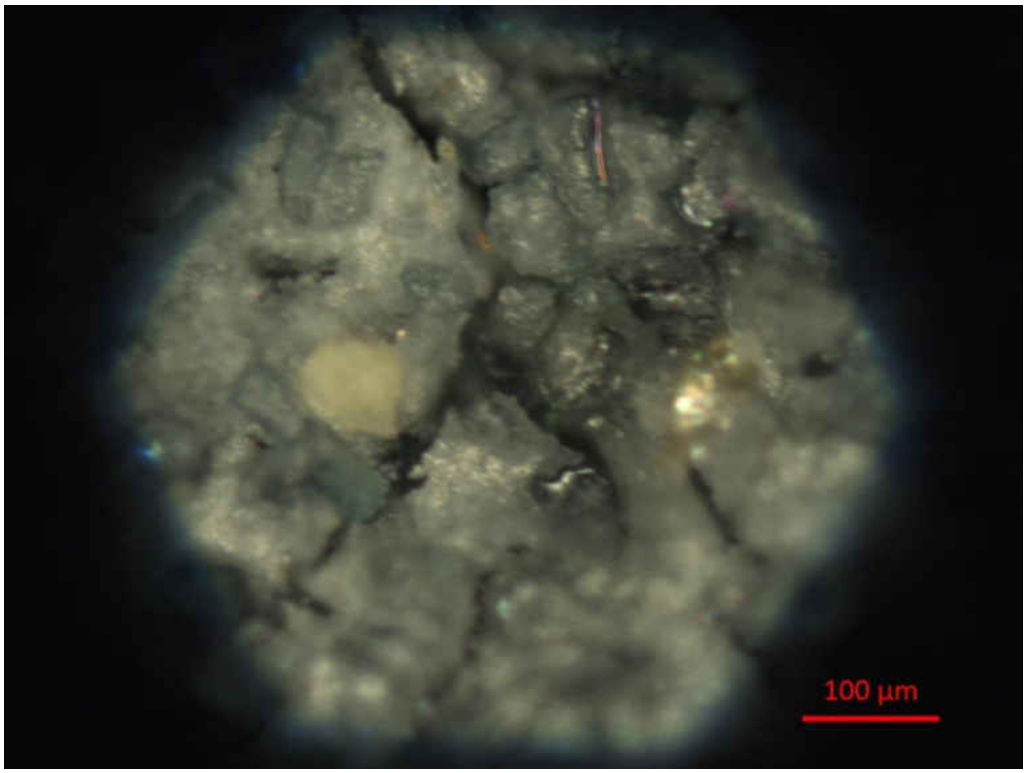

Figure 10) Microstructure view of porous silicon carbide using optical microscope.

The macroscopic dimensions of a combustion chamber play a significant role in the stability of a burner as the solid length required to produce an excess enthalpy flame increased with increasing flow rate [48]. However the dimensions on the pore scale greatly dictate the heat transfer characteristics. A modified form of the Peclet number was derived shown below in (18. The number is a rough indicator as for the allotment of flame propagation within an inert porous media, with the critical Pe*=65±45 [49]. The number is a ratio of the heat released from combustion within a given pore, as compared to the heat absorbed convectively into the pore therefore, for effective flame ignition Pe/Pe* >> 1. where S_L is the laminar flame speed, d_m is the equivalent diameter of the combustion section, and α_f is the thermal conductivity of the reactants.

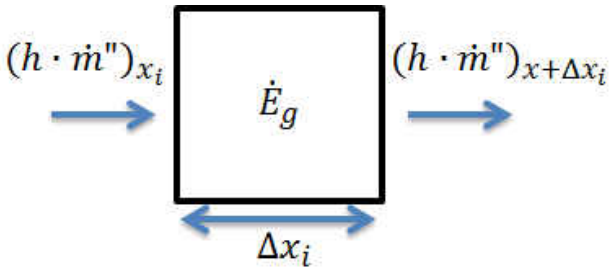

Figure 11) Energy release within a control element as compeared to the advection losses.

$$Pe = \frac{S_L \cdot d_m}{\alpha_f} \tag{18}$$

It is of importance to note this process only manages to take into account convective heating of the solid, and does not include any radiative terminology. Gasses have a emissive structure which is related to the rotational and vibrational spectra of molecules which comprise the gas [50]. As a result, discrete peaks of radiative interaction occur; as a result radiative emission and absorption of gasses is strongly dependent upon its mixture temperatures. Depending on the constituent mixture of the unreacted flow, the radiative influence may falter. For example, CO_2 has discrete peaks of radiative emission around across a wide but discontinuous spectrum: 1.06 μm, [51], 2.0 μm 2.7 μm, 4.3 μm, [52] 9.4 μm 10.4 μm [53].

2.1.2 Material Considerations

Porous media is an arbitrary term which can apply to a wide facet of materials [9]; depending on the type of porous structure the associated defining characteristics will vary. Even with such variations, the function of the porous structure remains unchanged: conduct heat and act as a surface which preferentially interacts with the ongoing combustion reactions. A literature search reveals the porous structure is commonly made of some type of ceramic or in burners which are made to run extremely lean a metallic insert is used such as FeCrAlY [54]. Regardless of the composition of the structure, it must withstand the intensity of the harsh environment associated with the formation of radicals during combustion.

Porous burners are inherently dependent non only of the geometric configurations of the immersed solid structure but also on the material properties of the structure. Where often CO emissions are strongly dependent upon the type of porous media being utilized [10]. As a baseline, whatever porous solid immersed within the combustion reaction must be able to withstand the high temperature oxidizing environments of a reaction environment. Though, characteristics of a suitable material must take into account chemical and thermal reactivity prior to implementation; as Zhdanok et al [55] demonstrated the solid phase's ability to regulate heat within the combustion reaction directly controls properties of the flame.

Prior to examining heat transfer properties of a possible material, it is necessary to ensure the structure remains stable within the operating environment. The spectrum of temperatures which the materials will be exposed to in some cases can reach 1600 K, and as a result the material must ensure such structures will not degrade. Simultaneously, the structure exists within a chemically harsh environment due to the formation of free radicals within the combustion reactions. From one experiment within the combustion chamber utilizing silicon carbide signs of

melting upon temperatures in excess of 1600 K was observed [56]. For long lasting structures this limits the viable materials selection choices to steels with high chromium and molybdenum content, SAE designator 3xx which remain viable up to 1500 K , or ceramics. A short list of ceramics compiled from burners described within literature include: alumina (Al_2O_3), cordierite ($(MgFe)_2Al_3(Si_5AlO_{18})$), Mullite ($2Al_2O_3SiO_2$ or $3Al_2O_3SiO_2$), and partially stabilized zirconia (PSZ).

Further considerations of thermal transfer characteristics play a dominant role in the selection of a material to be included as material properties of the solid matrix play a predominant role in determining the operating range of the burner [57]. The purpose of the solid structure is to mitigate and control heat flux through the system. For example, the thermal capacity of the immersed solid is a distinguishing feature of the burners operation; in situations where the burner must reach steady state quickly it is desirable to have a limited thermal mass conversely, for a burner which is to remain stable for long periods of time it is favorable to utilize a structure with a heightened thermal mass as additional stability will be offered.

Both intraphase and interphase heat transfer characteristics of the desired material play a dominant role in the burners operation. A burner designed to operate in a specific temperature regime should have favorable thermal conductivity and radiadiative emissivity on that operating range. For example, burners which are designed to be radiative emitters from their downstream components could utilize alumina as a downstream flame holder as Al_2O_3 is characterized with high transparency for near infrared emission light and a sharp decrease of transmittance at the 3.0 μm wavelength [58].

Chemical considerations regarding the surface chemistry of the immersed solid plays a determine role. A particular solid structure may have desirable effects such as catalytic activity,

or negative effects which inhibit the effectiveness of the reaction. In a particular series of circumstances it was found when using a particular Yttrium biased ceramic, the combustion flame would exist as if there was no interaction with the porous media [56]. In this particular series of experiments it was also found when utilizing pre-vaporized heptane showed the droplets would collect on the surface of the yttrium resulting in the additional phase of a combustion reaction [56].

Of particular interest are the characteristics of the degradation of the solid phase. Using silicon carbide, or SiC as an example, at high temperatures the solid phase will interact with the flow stream. Oxygen will adhere to the SiC surface and reform bonds to create quartz, SiO_2, and CO, $SiC \rightarrow SiO$ & $SiO_2 \rightarrow SiO_x(g)$ [59]. CO will evolve off the surface and a nano layer of SiO_2 forms with smaller active sub layers.

Growth of the layer is then controlled by the rate at which diffusion of gasses through the surface layer occurs [60]. While the doping of SiC with borides such as ZrB_2 have been shown to decrease the rates of solid phase oxidation [61]; the long term viability of a SiC structure requires further investigation. Susceptibility of surface scale formation decrease dramatically at a lower temperature, the rates of oxidations can be reduced significantly [59, 61, 62].

Selection of an emplaced solid phase also requires considerations of the fuel's chemical composition as hydrocarbons of various complexity feature different burn characteristics; however it is also important to consider the fuels purity as quantities of impurities are not significant on a thermodynamic scale, but greatly affect the environmental impact of a combustion system and its long term stability. When sulfur is present in fuel, the combustion flue gasses high tendency to form sulfuric acid [63]. In large furnace installations, trace concentrations of sulfur dramatically affect the composition along the walls which route

combustion gasses dramatically affecting the corrosion process [64]; such exposure of sulfur compounds can dramatically affect the long term viability of a flame immersed solid if care is not taken to appropriately select a viable material.

2.1.3 Reactant Flow Considerations

Selection of a fuel is a crucial endeavor, even within ordinary flame theory the burning characteristics of fuels vary, in both the radicals which are formed but also in the velocity in which reactants cross the boundary of the flame. From a design perspective, when formulating a burner to run on multiple fuel sources, considerations of the chemical composition of the fuel must be accounted for as the volumetric flow rate must be in agreement with burning characteristics of the flame. This of course is not to say a burner can't be formulated to run on both natural gas and kerosene, but rather that considerations must be taken for the oxidation characteristics of both fuel flow types.

The selection of a fuel and the operational range of an equivalence ratio for a porous combustor is pertinent to its design, as it has been shown with increasing equivalence ratio, the heat recirculation efficiency decreases [57]. A dimensionless parameter was crafted titled the flame speed ratio, given here the symbol ψ, is seen in (19), examination of the flame velocity in this manner allows for comparisons of reactant flux, taking into account for the effective equivalence ratio of the reacting mixture. Furthermore it was found there are definite trends between the percent of heat recirculated, (20) where ι is the firing rate and the energy transferred to the gas from the solid, and the flame speed ratio.

$$\boldsymbol{\psi} = \frac{\boldsymbol{S_{L_{actual}}}}{\boldsymbol{S_L}} \tag{19}$$

$$\boldsymbol{\beta} = \frac{\dot{m}_f \cdot (h_{\delta_p} - h_0)_f}{\iota} \tag{20}$$

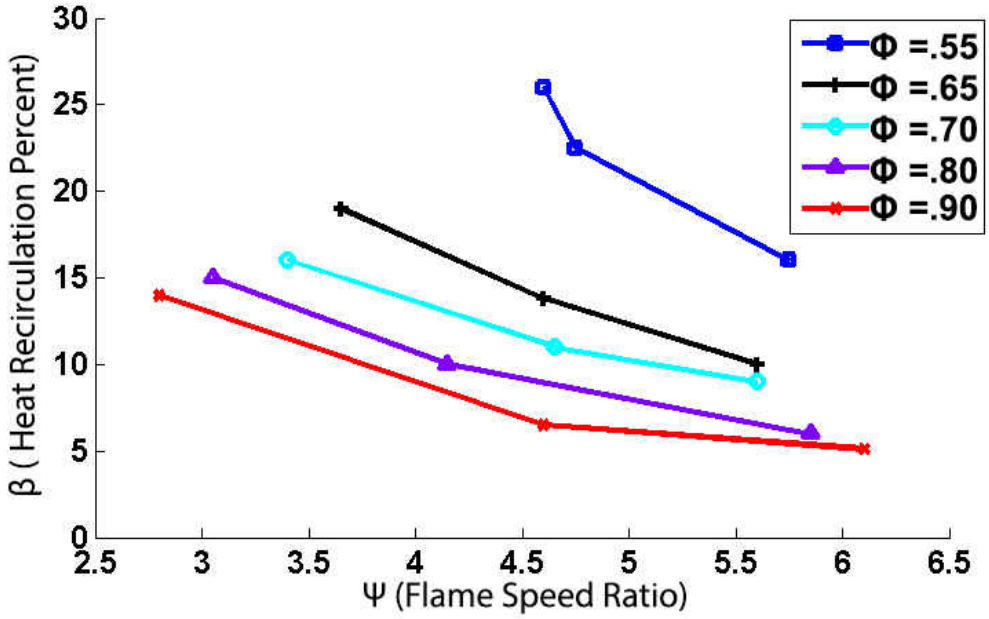

Figure 12) Expressed relation between flame speed ratio and heat recirculation efficiency across various equivalence ratios.

Examining Figure 12, and taking into the relations expressed by equations (19) and (20), important characteristics of porous burners can be made. While porous burners are able to operate at extremely low equivalence ratios, there is a necessity to circulate more heat to the reactants prior to ignition. Considering at a lower equivalence ratio, the firing rate of the burner is chemically hindered there is a considerable drop-off in the net heat which can be extracted from the burners output. However, it is important to note at increased flame speed ratios, across all equivalence ratios, the energy necessary to recirculate energy from the reactants dramatically decreases; thus conveying porous burners are exceptionally efficient when producing high velocity reactant flows.

2.2 Modeling of Porous Combustion

In order to produce a valid model of any system, the model must "*accurately enough*" represent the processes of the system being modeled. When modeling such a system, the key variables of interest are temperatures of the gas and solid phases. More detailed models are able to consider additional parameters such as locational concentrations and final equilibrium concentrations. Coupling of the dependencies within porous media combustion creates quite the task when analyzing such processes in either a numerical or analytical manner. When analyzing combustion in porous media several common assumptions are made as adopted from J.R. Howell et al [6]:

- The fuel air mixture is completely premixed as it enters the burner at a known temperature and equivalence ratio.
- Flow within the burner is incompressible and one dimensional.
- The pressure drop across the porous media is negligible as compared to channel flow.
- Gas within the porous media can be treated as transparent.
- To maintain a 1 D spatial model, the walls of the combustion device are assumed adiabatic. *As a note, this is an accepted invalid assumption* .

Comments regarding the aforementioned assumptions are pertinent to understanding of the behavior of heterogeneous combustion. Foremost, the assumed adiabatic nature of combustion in porous media is a common assumption but should only be considered for initial iterations as external heat loss greatly increases the preheating length and the likelihood of flame quenching [65]. Secondly, although it is not outlined by J.R. Howell et all it is assumed all gases considered are ideal. Thirdly, for reactors which have combustion dimensions in which the ratio

of the length of the combustion chamber in the flow direction and orthogonal to this direction approach zero, the effects of multidimensional effects become increasingly important [66].

Assuming a homogenous fuel and air mixture allows for the production of a system where the rate limiting step can be attributed to reaction rates opposed to the diffusive fluxes of chemical species within a reacting stream. Combining assumptions regarding pressure drop and incompressible flow allows for the determination of the flow velocity directly as a function of temperature. Treatment of the gas as non-participating in the radiative Heat Transfer process allows the equation which links the energy balance between the gas and solid phase to be linear. Given the high spectral dependence of gasses and their participation in radiation, this is assumed valid. Combined, these assumptions allow the temperature defined reaction rate to determine the thickness of the reaction zone and the temperature gradient [32].

2.2.1 Analytical Analysis of Porous Combustion

A theoretical study was considered on the insertion of a finite length porous solid to act as an internal heat recirculation device was performed by Takeno et al [67] as an extension of laminar flame theory. Their early model provides a large degree of quantitative insight as to how combustion in porous media operates and sought to predict the existence of limits of the system. From Figure 13 which is the physical representation of the system modeled by Takeno, with the green structure being the length of the solid which the flame interacts with.

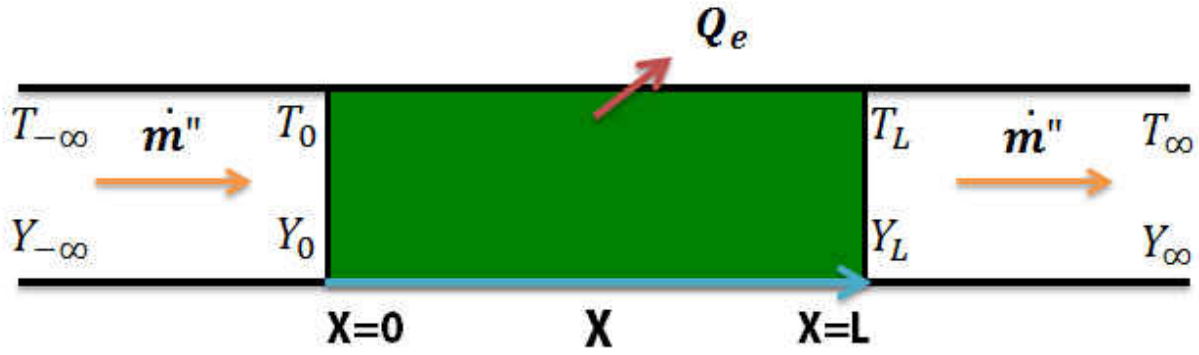

Figure 13) Physical domain representation of an isothermal solids interaction with a as described by Takeno et al. Upstream Boundary on the left, fluids moving in the positive x direction. With a solid of finite length occurring from 0 to L.

In addition to momentum conservation, continuity of mass flux and atomic species, solution of the flame theory as it interacts with a solid requires the solution to equation (21), the energy flux equation as an extension of diffusion flame theory; is consistent of a conduction term, advection term, enthalpy release term and an interphase heat transfer term. Additionally, equation (22) quantifies the net thermal losses through the solid. Solutions of the equation are then produced according to a series of mass flux dependent Eigen values, expressed as equation (23).

$$\frac{d}{dx}\left(k_f \frac{dT}{dx}\right) - \dot{m}'' \cdot C_p \cdot \frac{dT}{dx} + \dot{\omega} \cdot (\Delta Hf^\circ{}_1 - \Delta Hf^\circ{}_2) + h \cdot (T_s - T_x) = 0 \qquad (21)$$

$$Q_e + \int_0^L h \cdot (T_x - T_s)\, dx = 0 \qquad (22)$$

$$\Lambda_s = \frac{k_f \cdot \rho \cdot K(T_x)}{\dot{m}''_s{}^2 \cdot C_p} \qquad (23)$$

Solutions of equation (21) are then non-dimensionalized. Of importance to this discussion, replacement of the spatial domain variable x with ξ, and temperature variable T with τ allows for a simplification in solution presentation. Mass flux is also reduced to the

nondimensionalized parameter r which is a ratio of the actual mass flux as compared to the laminar.

$$\xi = \frac{\dot{m}'' \cdot C_p}{k_f} \cdot x \tag{24}$$

$$\tau = \frac{T_x - T_u}{T_{ba} - T_u} \tag{25}$$

$$\tau_s = \frac{T_s - T_u}{T_{ba} - T_u} \tag{26}$$

$$r = \frac{\dot{m}''}{\dot{m}''_s} \tag{27}$$

The findings of Takeno produce a series of stable states of the combustion system. The dependencies according to their model take into account heat transfer parameters between the solid structure and the working fluid, temperature dependent combustion rates and the necessary activation energy for combustion. For a given flow rate there exists a plurality of steady states for the system which is dependent on the amount of unreacted fuel initially within the system. Above a critical mass flow rate for any system, no stable condition of the system exists and the introduction of heat loss reduces this maximum mass flux. For the test case presented in [67] Figure 14, a locus of Eigen Values indicating the solutions of the solid phase temperature as a function of mass flux.

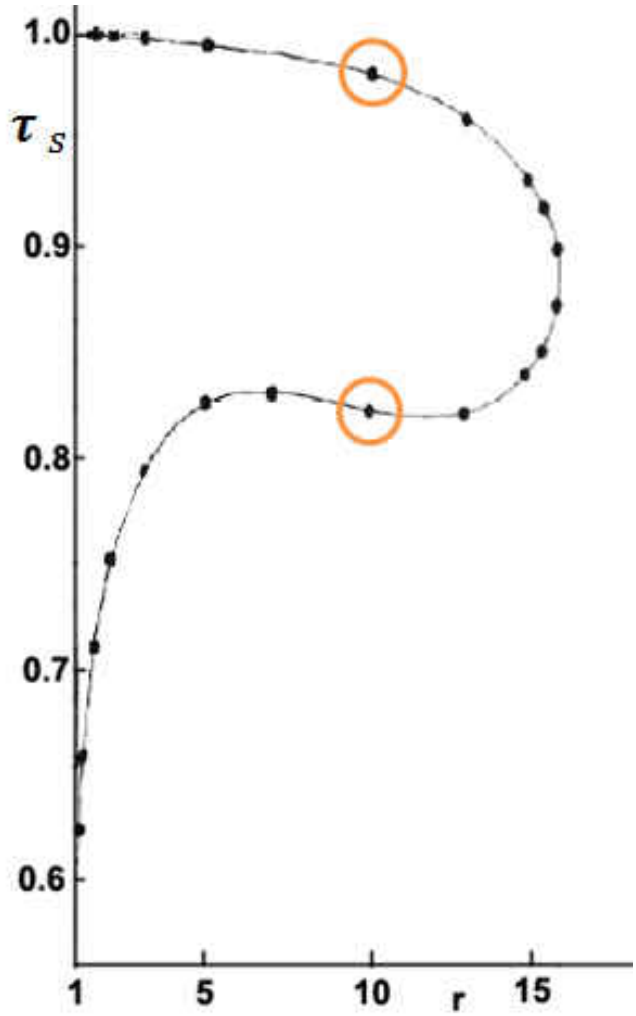

Figure 14) Plot of stable flow rates produced as a solution to an Eigen Function for a porous burner as produced by Takeno [67].

Examining the two solutions produced at the flow rate r=10 from Figure 14, an upper branch solution, one in which the fuel is completely oxidized prior to the termination of the porous media is presented as Figure 15. A supplementary lower branch solution is also presented in Figure 16; solutions of the lower branch have a lower solid temperature than the upper branch and produce a flame which reaches completion beyond the length of porous media.

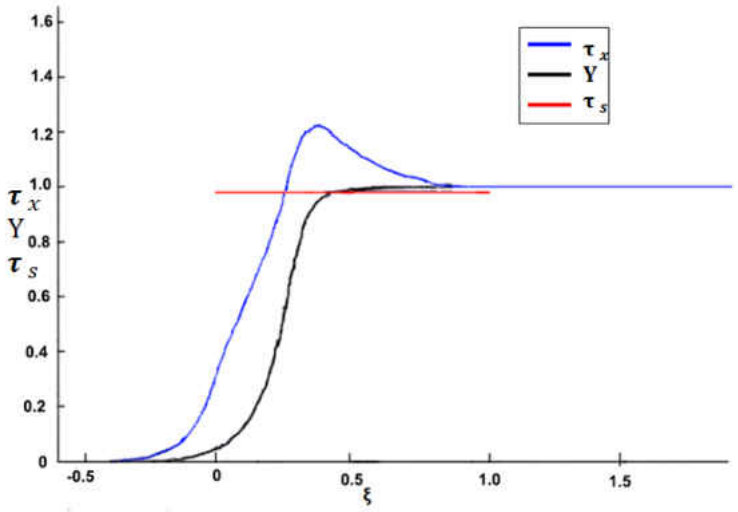

Figure 15) Calculation of the excess enthalpy flame of the Upper branch of Eigen solutions [67].

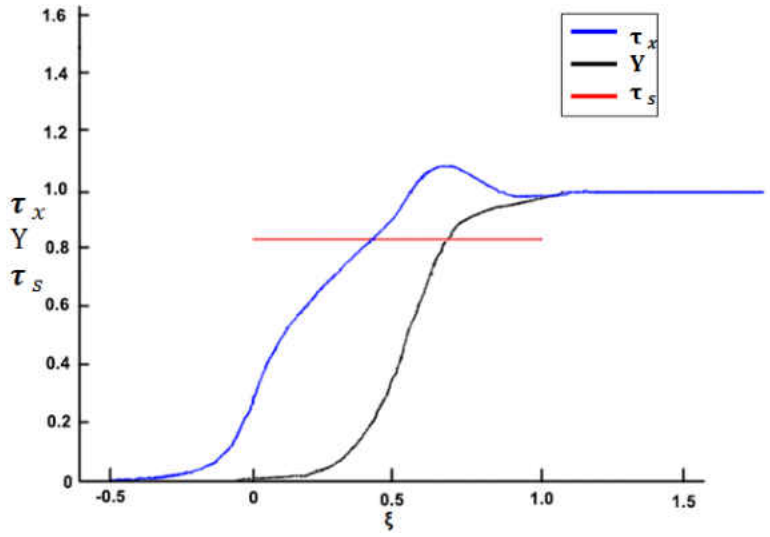

Figure 16) Calculation of the excess enthalpy flame of the Lower branch of Eigen solutions [67].

Foutko et al, [68], discusses the analytical analysis of transient combustion waves within porous combustors; this work builds off of the postulated idea proposed by Hanamura. Within this transient flame model, it is assumed a single step, temperature dependent, reaction. Further assumptions of the model assume a specific heat which is invariant of temperature, though a thermal conductivity term which takes radiative effects into account for conduction within the

solid with dependencies upon the defined external radiative and convective heat loss, and approximated ignition temperature.

Foutko et al conveyed sustained superadiabatic combustion occurring when the velocity of the combustion wave does not match the velocity of the reactant flow, causing the flame front to shift. For their model, if the provided heat exchange coefficient of the solid structure exceeds a critical value, the combustion heat release rate can exceed the supply rate from the porous solid to the gas; from this point the gas phase reaction can then be treated as an explosion [68].

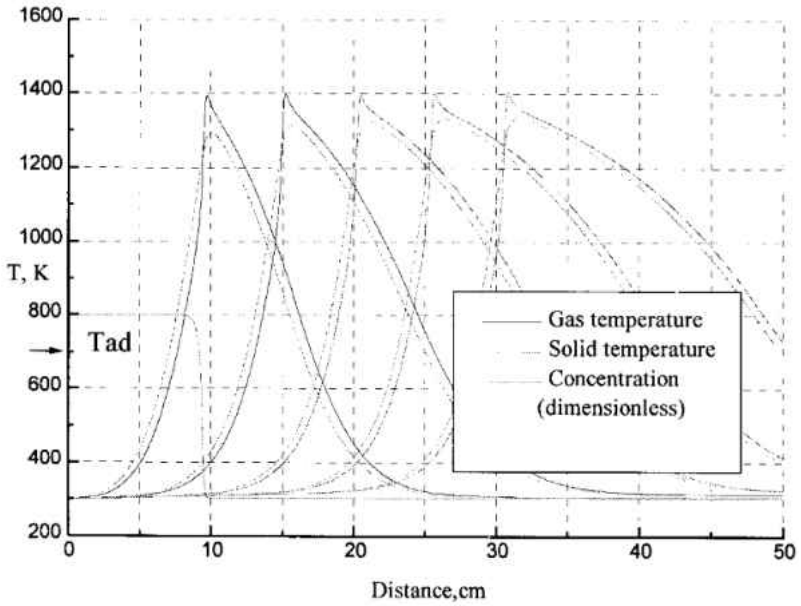

Figure 17) Transient combustion wave displayed with temperature peaks corresponding to 300 second intervals within a porous combustor [68].

2.2.2 Numerical Analysis of Porous Combustion

Adopted from an output of a model, produced by Henneke and Ellzey [69], the basis for analyzing a single simulation output is explained. When analyzing a specific event corresponding to the burner it is convenient to utilize a graph as shown in Figure 18, which features an abscissa of length with the dependent variables plotted on the Y axis. To analyze any simulation the three most encompassing traces which are to be considered are: temperatures of

the gas and solid phase along with the net heat release rate. Heat release rates are useful as they exist as a single global expression representing the chemical model.

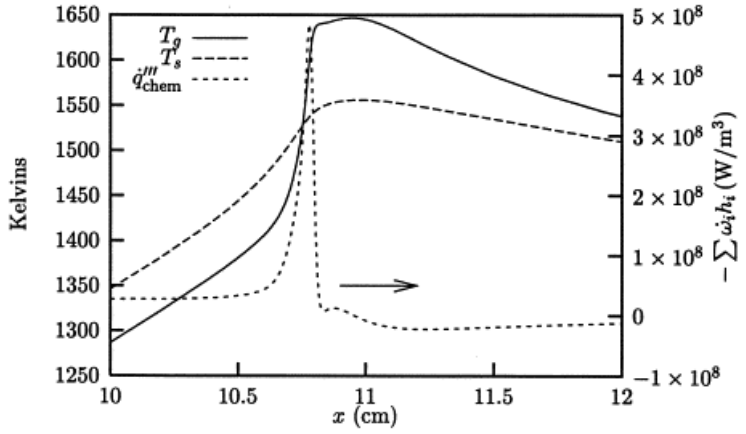

Figure 18) Temperature and heat production output plot of the region immediately surrounding the flame peak intensity within a porous combustor [69], note the arrow indicates the direction of flow.

Analysis of the population of various species contained within the chemical model will reveal further details which are glossed over by the heat release rate plot. Figure 19 displays the corresponding mass fractions of the CH_4 within the reacting flow as well CO and CO_2. Following the plot of CH_4, it can be approximated the reaction begins at the location where the mass fraction of CH_4 begins to sharply decay; to better represent the location of reaction initiation the analysis of radical onset can also be examined. Displaying the CO-CO_2 plots are a common indicator of reaction completion as CO_2 is the final product of the combustion reaction and is also responsible for a significant portion of the overall heat release as disruption of the triple bond contained within CO to CO_2, on the order of 293 kJ/kmol.

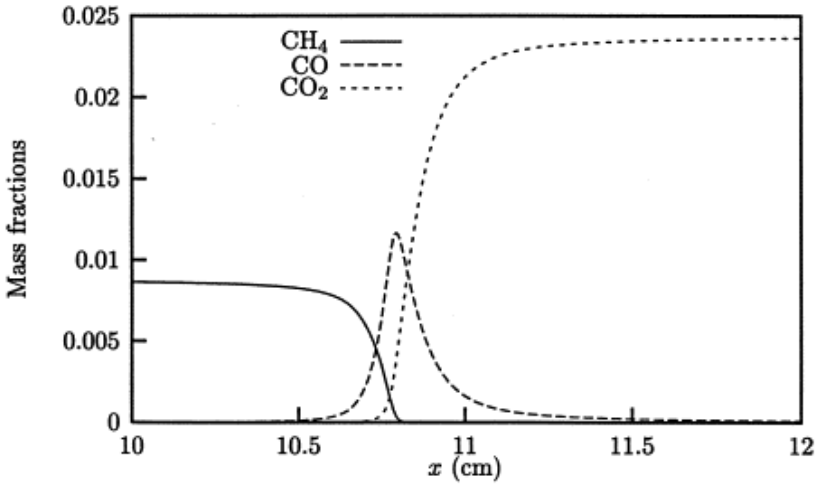

Figure 19) Chemical Conversion plot of carbon containing species as a function of distance within a modeled porous flow reactor [69].

A model proposed, by Henneke [69], for a packed bed porous burner operates on the principles of a one-dimensional model, including gas-phase transport, radiation, interphase heat exchange, and solid conduction. It is important to note, the model produced assumes not an isothermal solid, but rather thermal equilibrium between the gas and solid phases. When defining scales of combustion, it was considered formulated such that the thickness of the reaction zone to be the smallest possible scale; meaning considerations of the scales at which individual species occur will shift out of existence quickly. They also assume the solid is only used as a heat recirculation tool and does not influence the chemical reactivity. Their research sought to explicitly examine the validity of modeling ultra-lean conditions.

The treatment of the solid phase radiative loss model was fixed using Marshak's boundary conditions, a solution geared towards surfaces with azimuthal symmetry which produces a recurrence relation [70]. The solid phase neglected the secondary convective effects on the solid. Further assumptions for the radiative exchange dictate the time constant required for

radiative properties versus those of chemical properties can allow for a quasi-equilibrium radiative exchange.

When running their model, initially the mixture and flux of the inlet flow was held constant at an equivalence ratio of 0.15, and inlet flow velocity of 43 cm/s. Based on comparative data of experimental work produced by Zhdanok et al [55] Henneke was also able to determine diffusive effects within porous combustion are negligible at lean equivalence ratios.

A model proposed by Barra et al [57], builds off the model proposed by Henneke [69], seeks to examine the effects of heat recirculation from the combustion byproducts into the incoming reactants of a packed bed burner. Their proposed model incorporates a 1D volume average approach assuming thermal disequilibrium between solid and gas phase of the burner. Their proposed model for porous burner heat recirculation accounts for: solid to gas conduction, solid to solid radiation, convective heat transfer between the solid and gas species diffusions, dispersions and detail chemistry of several species through a discrete summation. In addition to the simplistic burning evaluations characterizing the combustion reaction, several other variations of system behavior were observed across various equivalence ratios.

The burner used in this study features a combustion section comprised of two varying pore size of partially stabilized zirconia as produced by Khanna et al [71]. The upstream section with a length of 3.5cm and 25.6 ppcm is followed by a downstream section of 3.9 ppcm which is 2.55 cm in length. The design was selected to produce a stable operating range of components. The proposed reaction model in assumption to the generally aforementioned components, assumes: Catalytic, buoyancy, Dufour and Soret effects are negligible. It also assumes the time constant associated with radiation equilibrium is significantly shorter than those associated with chemistry and fluid mechanics; thus enabling radiation to be treated as a quasi-equilibrium

problem. To complement the various constraint equations, it is assumed the only heat lost from the solid occurs as a function of radiation to a black body at a temperature of 298K, upon exit of the combustion reaction the change in chemical species terminates, and there is no diffusive flux of energy from the gas phase at the upstream and downstream ends.

2.2.3 Numerical Solutions and the Mechanism Dependency

When considering a chemical mechanism, its intended temperature [72], pressure range [73], and equivalence ratio [74] dictate the reactions which are needed to model a combustion evbent. In short, what works to accurately predict the flame speed, equilibrium concentrations, and ignition delay in one scenario, will not necessarily reflect others. Determining the appropriate purpose of a mechanism also dictates its importance; suppose in addition to flow analysis, temperature profiles and pollutant formation are also needed to accompany a CFD simulation.

As the complexity of the problem increases, the feasibility of implementation a large mechanism quickly dwindles and a reduced target mechanism, for say NO_x formulation [75], may be needed. Alternatively, some simulation events which investigate strictly the chemical behavior of a of a fuel reforming system may favor larger mechanisms having logarithmically more reactions such as the Lawrence Livermore National Laboratory Mechanism [76] to accurately predict trace compound species.

Often times, a prepackaged mechanism selected for a numerical combustion investigation will have a surplus of reactions and species needed to represent a combustion system suited for engineering applications and the given conditions which are being considered. Often times, numerical stiffness of the rates of production matrices and the variability in the expected time scales of the radicals involved [77]; as a direct result of the aforementioned numerical difficulties

of complex reaction mechanisms, excessive computational times require the pruning of irrelevant data from the mechanism. When preforming a mechanism reduction, it is first necessary to define a reasonable scheme to which the reduction process may be evaluated.

Schemes for mechanism reduction range from the extremely simple concept of examining the rate controlling reactions for subsequent species [78] or assuming homogeneous concentrations of radicals, Quasi-Steady-State-Approximations, [79]. Intricate methods for mechanism reduction include analysis of manifold space, created by the perturbation a chemical system with each molecular species representing a degree of freedom in multi-dimensional space [80] using theoretical analysis on the nonlinear dynamics of chemical systems. Often times, several techniques will be used in conjunction with one another [81] to provide a limiting mechanism.

Given any technique or combination thereof of mechanism reduction the endeavor is only worthwhile if, the reduced mechanism must accurately compare to both the initial mechanism and the combustion system which it is representing. Accurate depiction of changes in results according to variation reaction pressure, finalized concentrations of chemical species on appropriate timescales, and close approximation of ignition delay are all important characteristics which must be considered [82].

While simplification of a mechanism provides invaluable solutions for the modeling of complex systems, it is often difficult to discern as to which reactions and species are negligible in the grander scheme. Reactions which are important at a given temperature range may not be within the exception of a specific series of initial conditions. None the less, removal of such reactions can impair the validity of the overall model. Implementation of basic concepts of graph theory is useful when considering the reduction of a chemical system [77].

2.3 Porous Burner Designs

2.3.1 Fuel Selection for Porous Combustors

Gaseous fuels are typically consistent of the lighter alkanes (CH_4, C_2H_6, and C_3H_8) hydrogen and carbon monoxide[83, 84]. When designing a system to operate with these fuels, it is typical to have fuel and air premixed upstream of the combustor as differences in the kinematic viscosity, Prandtl Number, and thermal conductivity, of the fuel compared to air are negligible.

Combustors operating on liquid fuel require considerations of a three phase reaction environment, as opposed to a two phase environments which is seen in gaseous combustion. External environmental considerations, such as cool temperatures, may impair the ability of the fuel system as is similar with diesel trucks. Implementation of bio fuels and other large hydrocarbons have characteristically high gelling temperatures. Fuel gelation can be addressed through implementation of fuel blending [85], introduction of additional heat to the fuel [86] or through forced agitation of the fuel within its reservoir.

Beyond ensuring liquid fuel will be suitable in the intended operating conditions, delivery of the fuel to the sustained chemical reaction must prove to be stable. Liquid fuel introduction in porous combustion is widely grouped into two groups: fuel-vaporization and fuel-spray [87]. When considering a fuel vaporization system it is important to ensure optimal temperatures for the vaporization of the fuel [88]. In a vaporization liquid fuel delivery scheme, a solid surface introduces heat to the liquid fuel causing evaporation. As a function of the surface temperature, Figure 20, conveys a qualitative expression of droplet life time as a function of wall surface temperature.

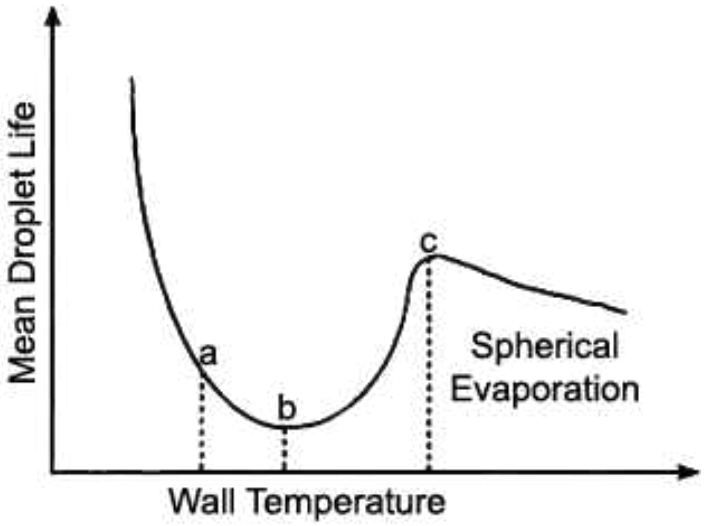

Figure 20) Droplet life time as a function of wall surface temperature adopted from [88].

If the wall temperature is less than that at *a,* the fluid boiling point then, evaporation is lengthy as it is controlled by the partial pressure of the fuel in the gas phase. Beyond the boiling point, the wall temperature can increase while maintaining a layer of fluid on the surface up to some specific temperature *b*. At this temperature the maximum evaporation rate of the fuel occurs this temperature related rate is known as the Nukiyama Point. Further increasing the surface temperature decreases the heat flux until the next maxima known as the Leidenfrost Point; a transition occurs at this temperature where there is always a layer of gas between the surface and the liquid inhibiting heat transfer.

In addition to the liquid vaporization method, a pressurized stream of fuel can also be used to create an evenly dispersed fuel-air mixture. Displayed below, in Figure 21, are two fuel nozzles used in a study on porous combustion [89]. While the interaction of fuel and air as they are emitted from the nozzle, it is typical for pressurized fuel streams to be used in conjunction with a dispersant, typically air to create a homogenous mixture of fine fuel droplets. When considering a fuel nozzle, it is important to select a nozzle for the given flow considerations

which will produce adequately small droplets as droplet size has been shown to strongly influence the combustion characteristics [90].

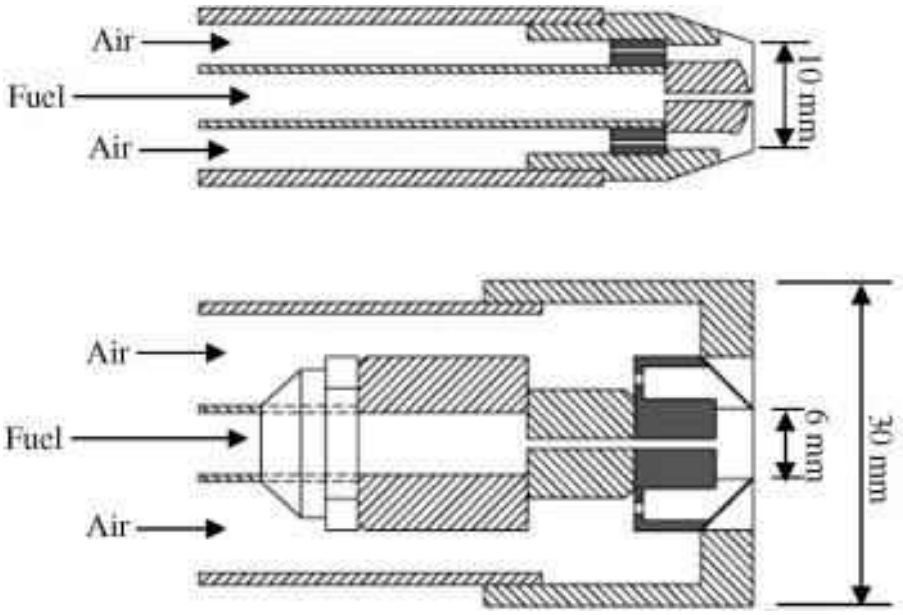

Figure 21) Two types of liquid fuel nozzles for use with porous combustors [89]. Top: pressurized air injector. Bottom: Pressurized swirling air injector.

2.3.2 Novel Uni-Directional Flow Combustors

A combustor with a non premixed fuel stream was constructed to examine the influence of fuel mixing on performance within porous media combustion [91]. Portrayed in Figure 22, the burner had a split fuel stream where a swirling device in the center introduced angular momentum into the fuel stream; the air stream was introduced radially to the fuel stream and the span of the channel which allowed the air to mix was designed which allowed controlling of the mixing length.

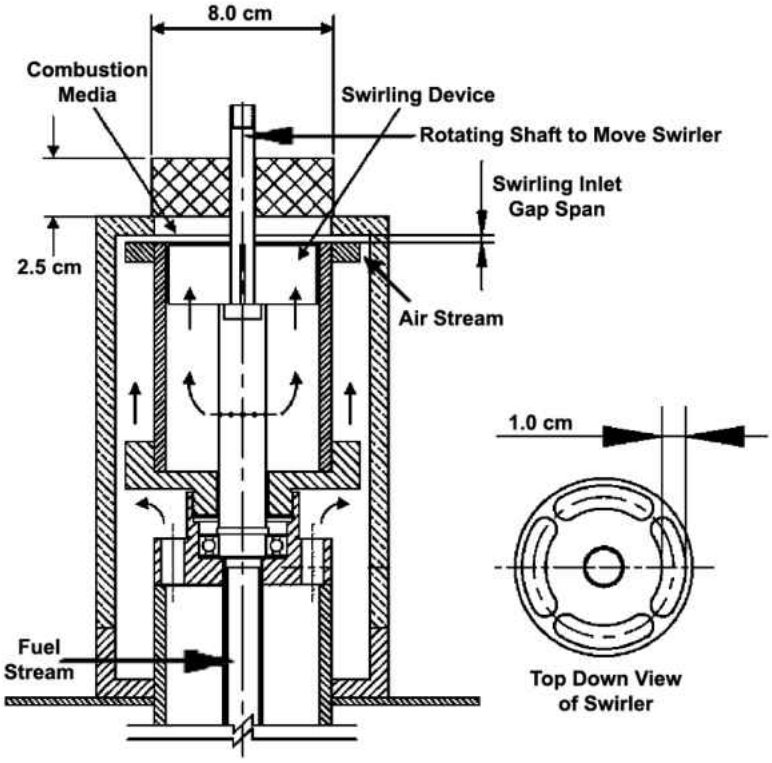

Figure 22) Non premixed flame burner [91].

From analysis of their experimentation, the appropriate gap distance was bounded by two concepts, which are believed to control the fuel and oxidizer mixing process. Producing a smaller gap forces more radial mixing of the two flow streams, though if there is not enough distance from the exit plane of the swirler to the inlet plane of the porous medium, mixing does not have sufficient time to occur. From the worst combination of swirling rate, no swirl, and gap distance the gas temperatures were limited to 1098K 8ppm of NO_x and 2200 ppm of CO_2; conversely the highest attempted swirling rate and optimal mixing length produced an exit plane temperature of 1453K, 1ppm of NO_x and 800 ppm of CO_2 at an equivalence ratio of 0.833.

The previous example considered a single stage combustion process. By allowing several independent stages to exist in series, the efficiency of combustion can be better controlled as the reactant profiles can be considered at each stage uniquely [6]; thereby allowing for a reduction of

CO and NO_x while maintaining radiant output [92]. A multi stage series combustor design also enables better use of the downstream radiative losses as encountered by a single stage combustor by specific targeting of the temperature of the porous solid at the exit plane.

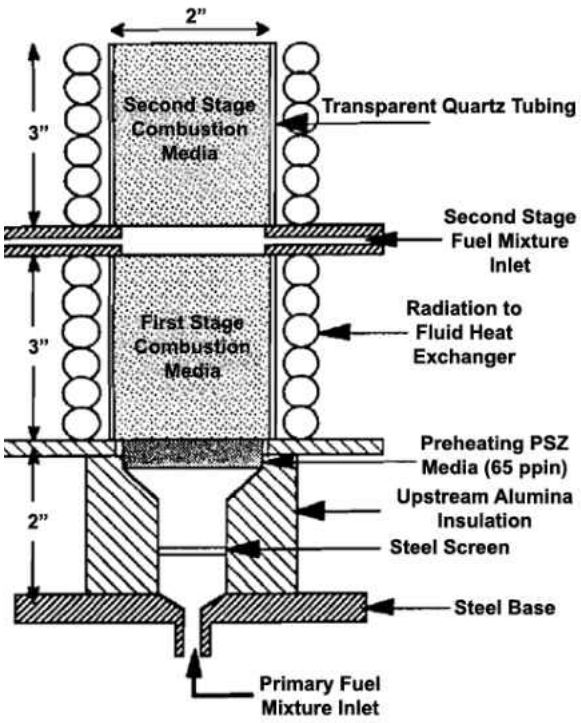

Figure 23) Two stage porous combustor [93]. A steel screen is used to inhibit flame movement, radiative emissions are allowed to pass through Quartz tubing, and the energy is collected from a radiation to fluid heat exchanger.

Each of the combustion chambers featured a porous structure comprised of partially stabilized zirconia (PSZ) ceramic, with a transparent quartz sleeve surrounding the porous medium, allowing the porous structure to emit radiative energy to a coil containing flowing water allowing regulation of the solid phase temperature. At the primary fuel air mixture system, methane and air are delivered as a single flow to the first of the two combustors. A steel mesh is emplaced shortly after the entrance. A small region is allowed to exist following the steel mesh to ensure proper flow distribution. Between the steel mesh and the first stage combustion chamber, a 65 ppin PSZ porous ceramic was implemented to cause rapid preheating.

Following the first stage of combustion, the primary component combustion byproducts, were introduced to the second stage, supplemented with additional gas delivery comprised of unreacted methane and air. The unreacted gasses were mixed into the first stage flow stream utilizing four jets directed radially inward. As a result of the additional flow added to the system, the second stage burner will have a higher mass flux than the primary burner due to the increased reactant flux.

Burner ignition mandated the use of a flame, introduced to the downstream section of the second combustion chamber and allowed to migrate upstream. Upon the flame boundary reaching the beginning of the second porous media, the flame would delay at this point. The flame was not allowed to propagate further until enough heat had saturated first porous section, at this time the flame would jump across the vacancy.

2.3.3 Reciprocating Flow Porous Combustors

Hanamura et al [94] postulated a reciprocating combustion system. A constant volume process over five steps similar to an Otto cycle is employed within this burner. The device utilizes two crank shafts each with their own corresponding piston for a single combustion chamber. Outlined in, Figure 24, the five step process begins with ejecting exhaust gasses through a displacement piston while simultaneously drawing in a fuel mixture, similar to a two cycle engine. As the displacement piston compresses the mixture (1). The fluids are then compressed within the combustion chamber (2). Prior to completing the displacement piston compression stroke, the gasses are passed through the porous medium and ignited from the previous gasses (3). The expansion of the gasses causes the power piston to displace downstream while the displacement piston maintains constant position near the porous medium (4). The

return of the power piston then causes the gasses to diffuse through the porous medium and cause the return of the displacement piston to complete the cycle (5).

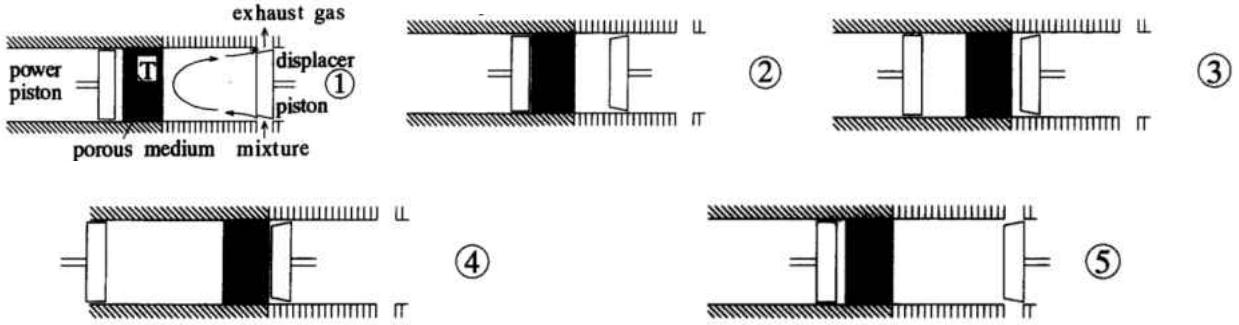

Figure 24) The five step process associated with the closed chamber combustion device developed by Hanamura.

Building from the theoretical analysis of a reciprocating flow combustor, Hoffman [10] operates utilizing a common inlet and exit of reactant gasses. The routing of the gasses through the insulated combustion chamber cycles at a common time interval. The gas pathing is controlled through the symmetric operation of a series of solenoid valves. A figure of the reciprocating flow burner can be seen in Figure 25. An external view of characteristic auxiliary systems for a reciprocating flow combustor can be seen in Figure 26.

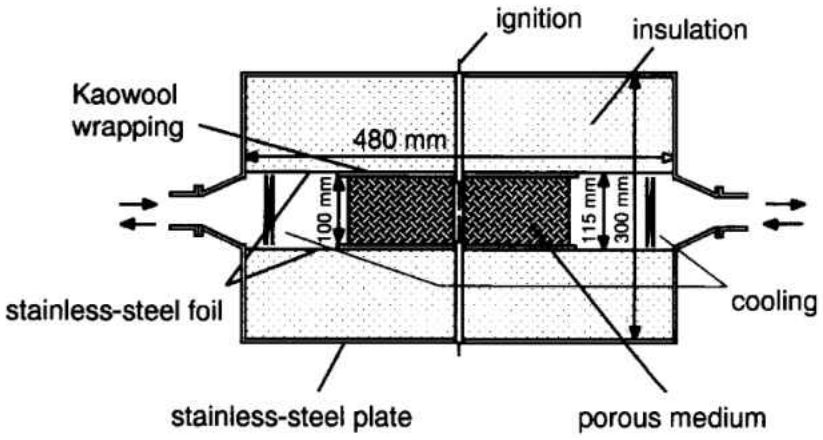

Figure 25) Reciprocating flow burner design showing combustion section, insulation, and ignition point [10].

At steady state, a reciprocating flow combustor will produce a flame front which moves through the porous structure in accordance with a half cycle time constant. At some point the flow direction is reversed and a symmetric temperature profile is produced. Characteristically a plateau will form when examining the solid phase temperature at an optimal time constant. A temperature profile of this nature will allow minimal emissions from the ends of the porous burner as the thermal potential at these regions is reduced compared to the peak temperatures

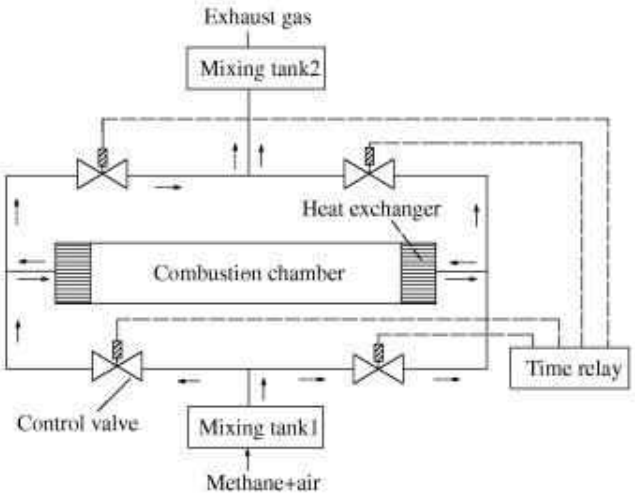

Figure 26) Reciprocating flow porous combustor, combustion chamber shown with oscillating valve series to control flow directions. [95]

CHAPTER THREE: LEAN APPLICATIONS OF HETEROGENOUS COMBUSTION

3.1 Enhancement of Pilot Flames

Many household devices: water heaters, furnaces, ranges, ect, which operate on natural gas require a small flame which is always on to provide ignition energy for larger flame which is needed when the appliance is under load. Emplacement of a porous combustor can dramatically reduce the fuel demands of the devices when they are in their standby state while reducing the heating demands the standby flame emplaces on HVAC systems.

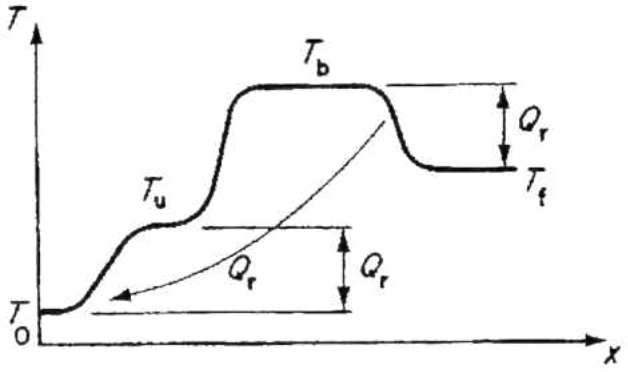

Figure 27) Enthalpy transfer, from products initially at the burned temperature, to reactants at the unburned temperature [96].

Heterogeneous combustion enables reactant preheating through enthalpy transfer from the reaction byproducts Figure 27. Preheating of the reactants enables the initiation of combustion at lean limits which are far less than that of a conventional flame; operating a flame which is only needed at short times on less fuel will reduce the net fuel consumption by the device. However reducing the enthalpy which is generated emplaces a lessened load on HVAC systems further reducing the net energy needs of the device.

Often the amount of energy which is extracted from the combustion process in this standby state is un needed and the exhaust gasses merely heat the inside of the structure which the devices are emplaced.

Using a venturi design, Figure 28, a pressurized head of gaseous fuel can be employed to also draw in air towards a porous medium. The flame would then exist within the medium under standby mode and when a load is needed to ignite the primary flame, from the Takeno analytical model it is known a rich flame will be longer. A series of valves at the fuel source are then used to enrich the fuel flow to the heterogeneous pilot flame while simultaneously allowing fuel flow to the primary burner will cause the flame to exit and simultaneously ignite the larger burner. Once lit, the excess fuel to the pilot flame can be terminated and it can resume its standby mode until ignition energy is again needed.

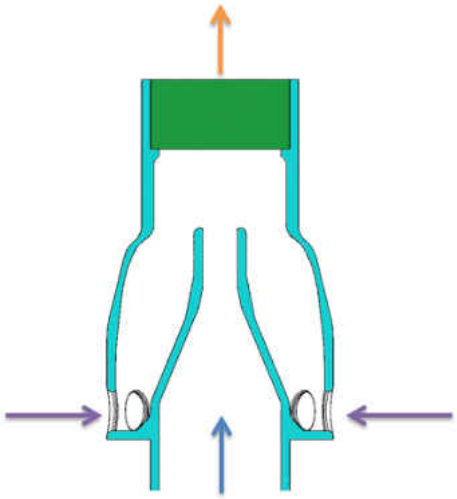

Figure 28) Venturi design inlet for a surface stabilized heterogeneous combustor. An inlet at the center, for gaseous fuel, contracts producing a pressure drop; using pressure as the driving force ambient air will then be drawn in to the Venturi.

3.2 Ignition Devices in Internal Combustion Engines

A control mass combustor with a porous medium is exemplified in Figure 29. The design features direct injection to the combustion chamber; with a porous media structure immediately interacting with the injected fuel flow. In this design for an internal combustion engine, porous media replaces a spark plug as an ignition source; the fuel is supplied the necessary thermal energy to cause the fuel to vaporize and subsequently decay into its radical composition.

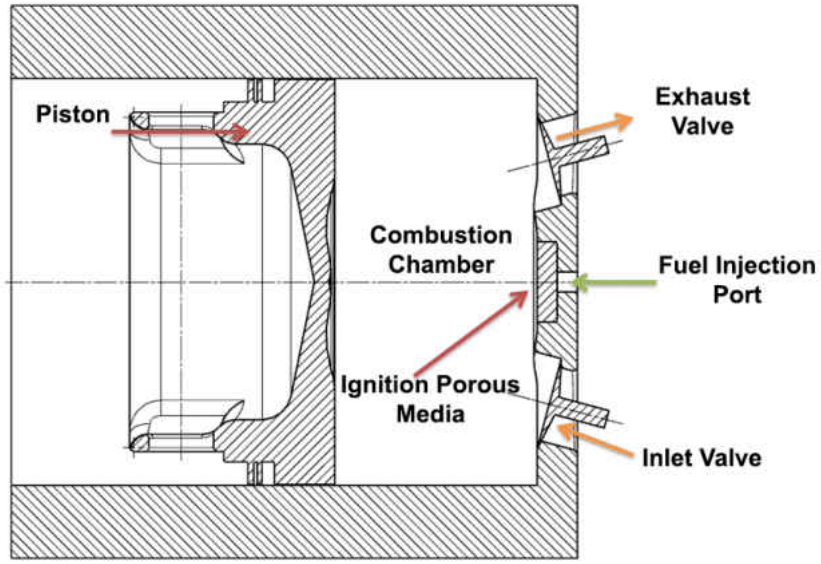

Figure 29) Closed combustion chamber with Porous Media used in lieu of a spark igniter as described by [97].

3.3 Energy Extraction via Reclaimed Fuel Sources

Preheating gasses within a porous solid enable a vast reduction in the necessary fuel concentration. Porous media burners have been shown to be effective for the oxidation of VOC's when the mass fraction of combustible compounds in the fuel stream is on the order of 2% [98].

Porous combustors which are able to sustain a flame on low quality fuels, combined with the ability to dramatically reduce emissions make porous combustors perfect for the combustion of reclaimed fuel sources which have a considerable fraction of other pollutants.

Shown in Table 3 are the respective major species which constitute biogas, gas from sewage treatment facilities with anaerobic digesters; and landfill gas, gas which is produced naturally at landfills by the decomposition of organic solid matter. As displayed within the table there is a considerable amount of methane produced by such sources, however there is also a large amount of inert CO_2 and a small but significant fraction of H_2S.

Table 3) Compositions of important gaseous species from Biogas and Landfills.

[99, 100]	**Biogas**	**Landfill Gas**
CH_4	40~75 (% Vol)	45~60 (% Vol)
CO_2	25~40 (% Vol)	40~60 (% Vol)
H_2S .	0.1~1 (% Vol)	0~1 (% Vol)
Misc.	1.6~6.7 (% Vol)	0.2~ 2.6 (% Vol)

3.4 Radiative Emitters

Solids at elevated temperatures, as encountered in porous media burners is a perfect source of thermal radiation. A simple method of quantifying the efficiency of the radiative emission from the downstream section of a porous burner was proposed by Khanna et al [71]. Equations formulated within the model were used to quantify the theoretical radiative heat output at the exit plane of the combustion chamber as emitted by the solid porous media. Their model proposed this heat content could be expressed as both a form of the enthalpy difference of the working fluid from the inlet conditions as compared to the combustion section and the radiative power. Expressions correlating these variables are observable as equations (28) and (29).

$$[h(T_{in}) - h(T_{out})] \cdot \dot{m} = Q_{theoretical} \tag{28}$$

$$Q_{theoretical} = \varepsilon \cdot \sigma \cdot A \cdot T_{out}^4 \tag{29}$$

A heterogeneous combustor designed for the emissions of radiative energy can be designed to operate in a manner which allows the emissions of energy from either along the body length or at the exit plane. In either of these cases, enclosures can be crafted which promote the focused emissions of radiative energy.

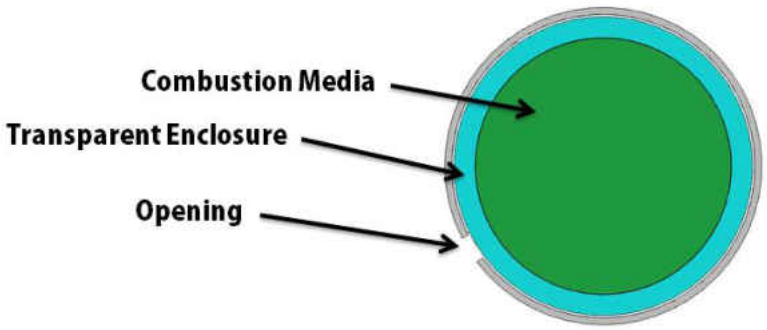

Figure 30) Combustion chamber design for combustion in porous media which allows for the emission of radiative energy from the combustion chamber length through a small opening.

CHAPTER FOUR: EXPRIMENTAL SETUP

Design and refinement of experimental devices is a challenge. Whatever changes made to a device are done so in order to optimize and perfect their operation. Such processes are iterative, undergoing design, testing, analysis, and cycling in order to further improve the system. However, it is imperative that the learned knowledge during one stage reflects the next rendition of the design contributing to a better system.

4.1 Double Feedback Loop Burner

Initial investigations into porous media combustion were performed on a combustor designed to operate over a wide range of equivalence ratios, and volumetric flow rates. Considerations were also undertook in order to investigate the differences between simple hydrocarbon fuels such as gaseous methane, compared to longer hydrocarbons, n- dodecane or n-heptane, which would exist in standard conditions in their liquid form. While complications of liquid fuel use resulted in failure of the device, much was learned about the nature of the design of the porous combustor and its operating characteristics; demonstrating such technology offered the stable operation at equivalences of 0.5 with combustion temperatures exceeding 1383 K as the K-Type thermocouple recording temperature melted.

4.1.1 Flow Loop Design

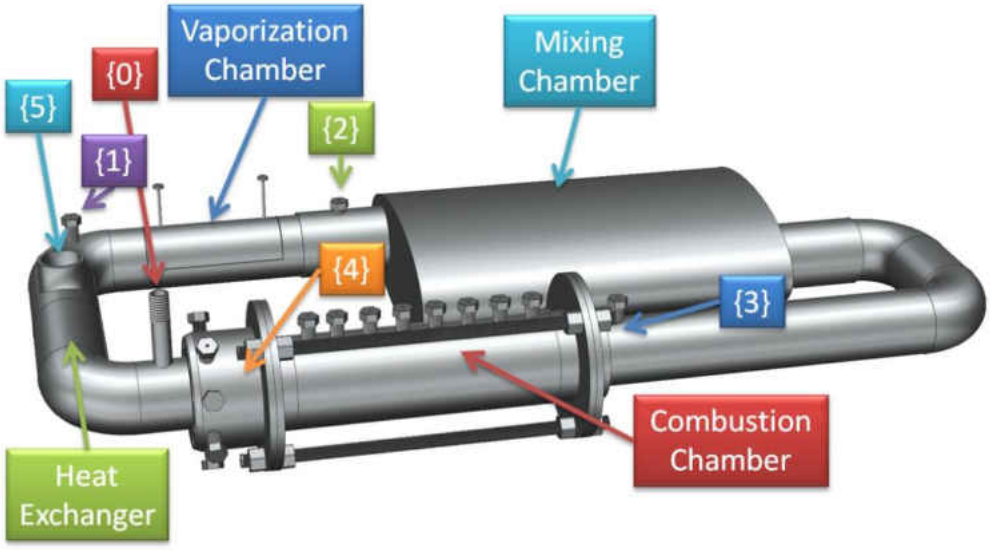

Figure 31) Flow loop of the double feedback burner with each component outlined and the location of the 6 steady states as they correspond to the location of the burner.

The double feedback loop burner, Figure 31, was designed with a flow loop consisting of four interlinked devices, with six thermodynamic states, supplementary reactant delivery, and sensory systems. Design of the burner focused on steady state analysis and operation. At state *0*, dried-pressure regulated air, and gaseous fuels, are introduced to the concentric heat exchanger, Figure 32. Upon entering the heat exchanger, thermal energy would be extracted from the post combustion exhaust gasses. In order to allow the burner the ability to utilize multiple fuels with various boiling points, user controllable bypass valves were also incorporated to the design allowing some of the hot exhaust gasses to be extracted from the system prior to entering the heat exchanger.

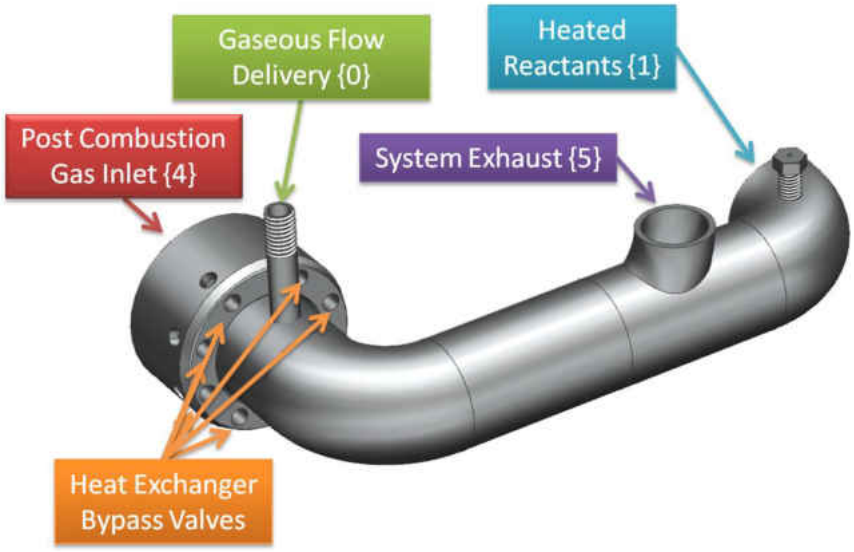

Figure 32) CAD Depiction of concentric heat exchanger.

State *1* identifies the preheated fluid at the vaporization chamber inlet. Within the vaporization chamber, Figure 33, liquid fuel can be injected into metallic foam, Figure 34, driven by an external fuel pump. Gases which exit the heat exchanger are used to maintain the temperature of the steel foam at the boiling point of the liquid fuel. Upon the liquid fuel's contact with the metallic foam, the high surface area offered by the foam allows complete vaporization of the liquid fuel. Fuel vapors and the gaseous reacting flow are then assumed to be unevenly distributed and at State *2*; the vaporized fuel mixture enters the Mixing Chamber. Within the Mixing Chamber, baffles disrupt the flow of the incoming fluid forcing the transition to a homogeneous reactant mixture upon the fluids exit of the mixing chamber.

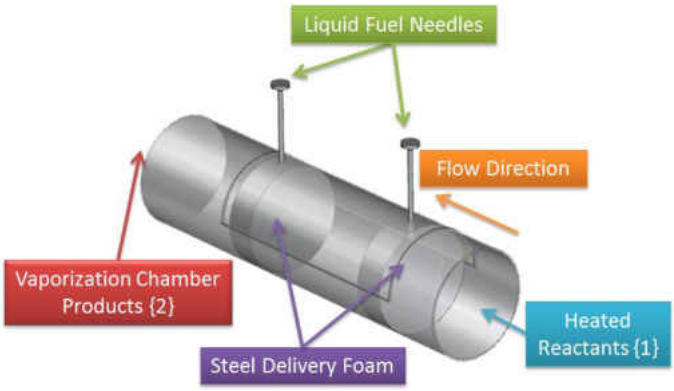

Figure 33) Vaporization Chamber showing liquid fuel needles and method of reactant delivery.

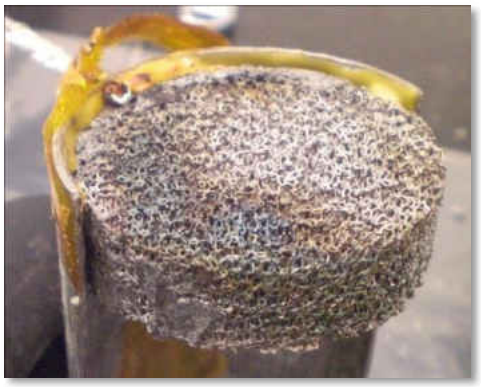

Figure 34) Steel foam as attached to the access hatch of the vaporization chamber.

At State *3* the homogeneous mixture enters the Combustion Chamber depicted. Within the Combustion Chamber, a sustained heterogeneous combustion reaction occurs within ceramic porous media; the ceramic porous media acts to re-circulate heat upstream to the incoming reactants, promoting efficient combustion and marking the first feedback mechanism. Post combustion gasses exiting the Combustion Chamber at *4* then enter the hot side of the Heat Exchanger where heat is transferred into the incoming reactants at State *0*, marking the second feedback mechanism. An idealized thermodynamic cycle of the burner is presented in Figure 35 with each of the six states identified.

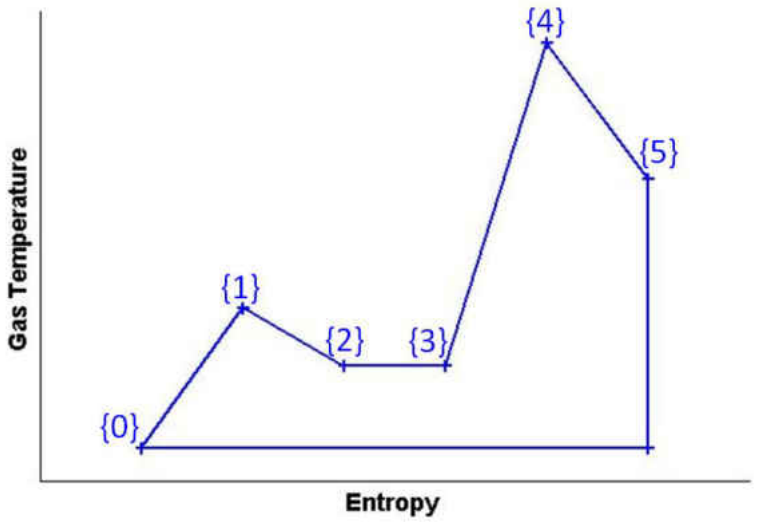

Figure 35) Outlined thermodynamic Cycle outlining the relative locations of the thermodynamic states between the sections within the combustor.

By design, the maximum working total pressure is experienced at the inlet *0*, and is limited to 4.0 atm. Quantitatively, analysis of the system is then characterized by the deviation from the specific entropy and temperature from *0*; net extractable heat from the system is a result of the enthalpy difference between the inlet temperature at state *0* with the experimentally specific exit pressure and the conditions of the fluids exit from the burner at state *5*.

4.1.2 Combustion Chamber Design

A combustion chamber must be able to contain and sustain a combustion reaction, though it is also important to allow for examination of the reaction. Instrumentation ports along the "top" of the combustion chamber allow for a thermal mapping of the reaction. From literature, the range of equivalence ratios which a stable flame could be sustained within is directly dictated by the length of the porous solid [67] therefore a "long" combustion media was implemented. A cutaway diagram of the combustion chamber can be seen in Figure 36.

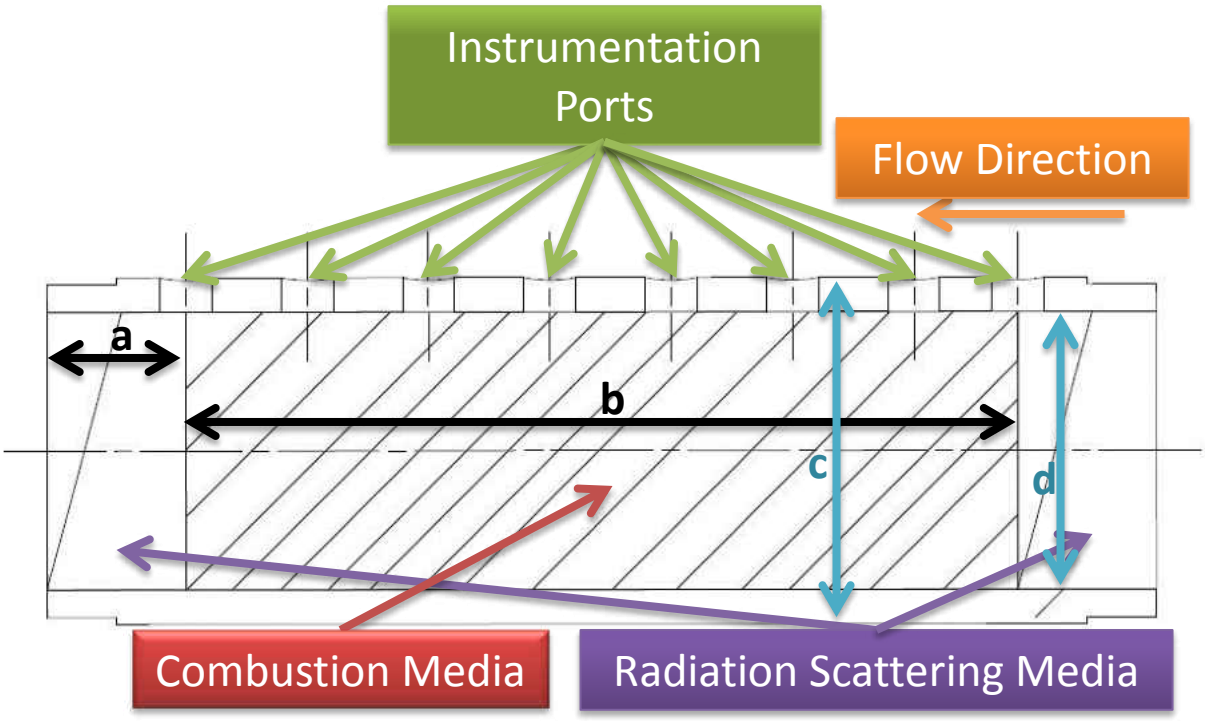

Figure 36) 2D representation of the combustion chamber showing dimensions, green alumina inserts, red silicon carbide porous media, thermocouple ports, as well as the silicon carbide structure. From right to left, each of the instrumentation ports are referred to as *0~7*. Dimension a) 25.4mm, b) 152.4, c) 63.5mm, d)50.8mm.

A cross sectional representation of the combustion chamber is displayed in Figure 36. Containing the combustion reaction is the combustion chamber housing, machined from SAE 316 stainless steel. 316 steel was selected as it is commonly used in the manufacturing of boilers [101] and nuclear reactors [102], with continuous ratings for structural loading at temperatures of 1198K with a maximum temperature limit of 1650K [103].

Figure 37, Depicts the packing arrangement of the combustion chamber internals. A large combustion media was selected made of silicon carbide and lies between two alumina oxide medias which were used to scatter radiation emitted from the silicon carbide media. SiC and Al_2O_3 were selected as these materials exhibit a high melting point, favorable radiative properties and a high thermal resistance, these values are presented in Table 4. Complementing the ceramic

structures, a fine steel mesh was employed to prevent flashback into the mixing chamber. A discardable steel mesh was also employed around the boundary of the combustion media to facilitate the disassembly process.

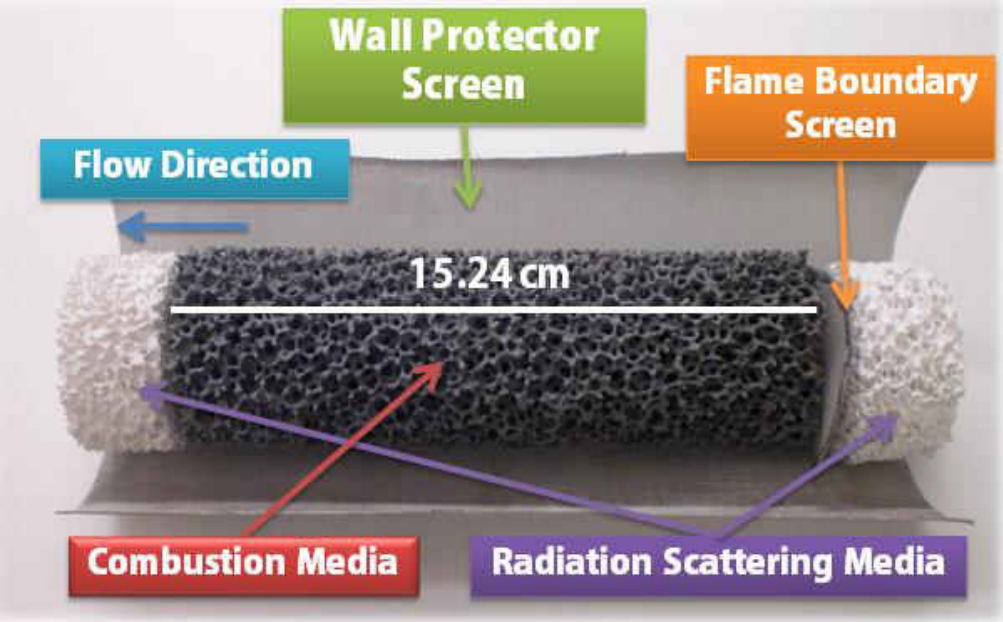

Figure 37) Arrangement and packing of the combustion media, radiation scattering media and wall screen protectors.

Table 4) Selected materials properties of SiC and Al_2O_3.

[104-106]	SiC	Al_2O_3
Melting Point	3100 K	2323 K
ε (1000~1500 K)	0.87~0.85	0.55~0.41
***k* (1200~1500 K)**	58~30 W/(m· K)	6.55~5.66 W/(m· K)
R_T (1273K)	2.5 kW/m	2.2 kW/m

Emplacement of a passive device which inhibited the progression of the flame in the event of flashback was crucial to the safety during operation of the combustor. However, arbitrarily assigning mesh would not ensure it would serve the purpose intended. As the Peclet Number quantity exhibited a high comparative uncertainty, verifications to ensure the flame was unable to travel through the screen were conducted. By subjecting a free flame emitted from a

blow torch up against the screen, examinations were considered across various flame speeds to ensure the flame would be unable to progress through the steel screen. The uninsulated assembled burner flow loop can be seen in Figure 38.

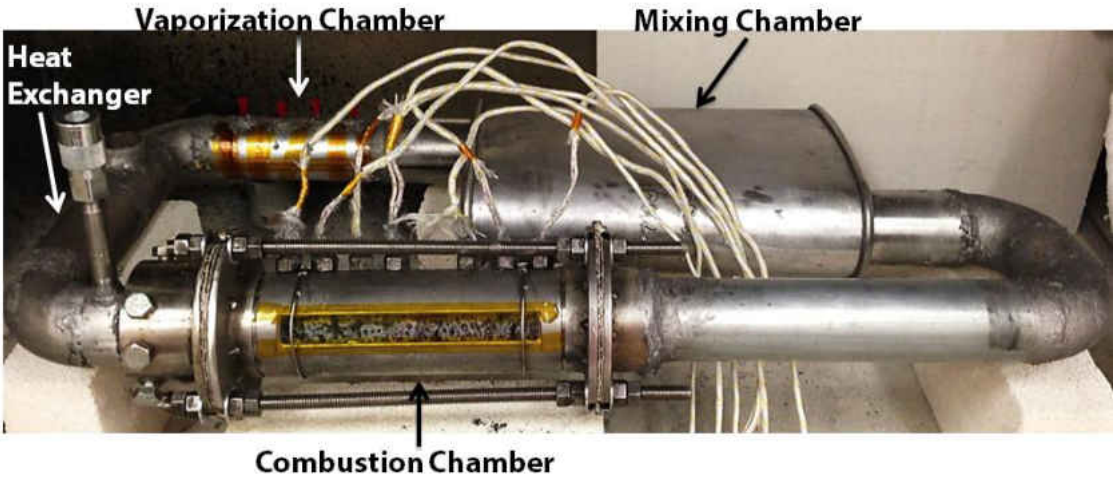

Figure 38) Assembled porous combustor with instrumentation hookups shown on the combustion chamber.

4.2 Combustion Event Modeling

To supplement the examination of phenomena observed within the combustor's experimental operation, shortly following the completion of the first design iteration combustion was investigated utilizing CHEMKIN-PRO. CHEMKIN-PRO allowed for the manipulation of various design characteristics quickly without necessitating further time and costs associated with fabrication. Following preliminary operations of the double feedback loop combustor, construction of a model which accurately reflected the experimental observations was constructed using methane fuel and the GRI 3.0 Chemistry package. Secondly, the construction of a reduced chemical mechanism was incorporated to better focus on the geometric considerations of the porous reactor.

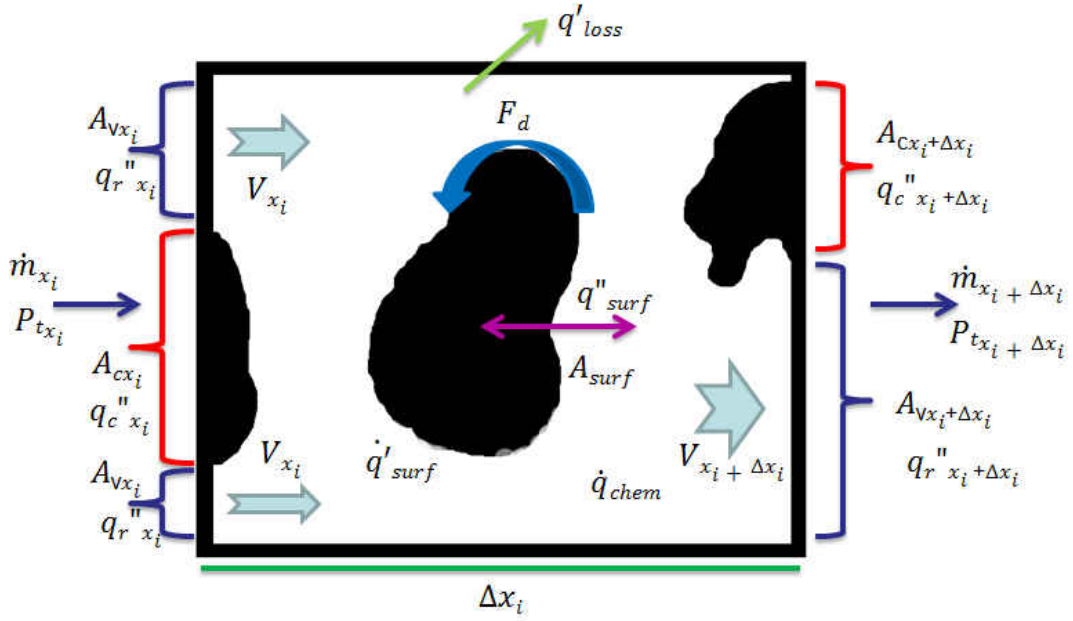

Figure 39) Control volume analysis of porous media.

From the presented terms in Figure 39 all of the necessary conservation equations can be constructed for the control volume of the porous combustion element. A full steady state analysis would mandate the use of the following equations: continuity of mass and atomic species flux, momentum conservation, and a thermochemical energy balance. An energy balance must be considered individually for both the solid and gas phases within the element; the solid phase balance consists of radiative flux from other elements, as well as conductive flux into the porous structure external heat loss, any heat generated from surface chemical reactions, and lastly the interlinking term merging the gas and solid phase. Energy conservation for the gas phase would also contain the interlinking term, heat generation as a result of gas phase chemical reactions, and advection associated with the mass flux in and out of the control element. Under lean conditions, diffusion characteristics of the gasses is able to be neglected [55].

Examination of the solid phase within the combustion chamber is highly scale dependent as exhibited in Figure 9 and Figure 10. Therefore, vapor deposition or other similar methods will

reveal the active surface area of the structure, but not the effective convection boundary. Figure 40 exemplifies this, examining the red outline several cavities can be seen; within these cavities or pores, the effective mode of atomic transport is diffusion related. Using the real surface area which takes into account the diffusion exposed area will not truly represent the surface area of the structure as would be convection dominant; the convective boundary is conveyed by the blue line on the right.

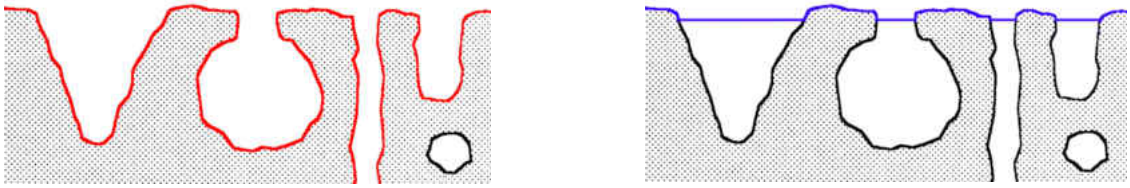

Figure 40) Comparison between real surface area (red) of micro and mesio pores as compared to effective convective surface area (blue) [107].

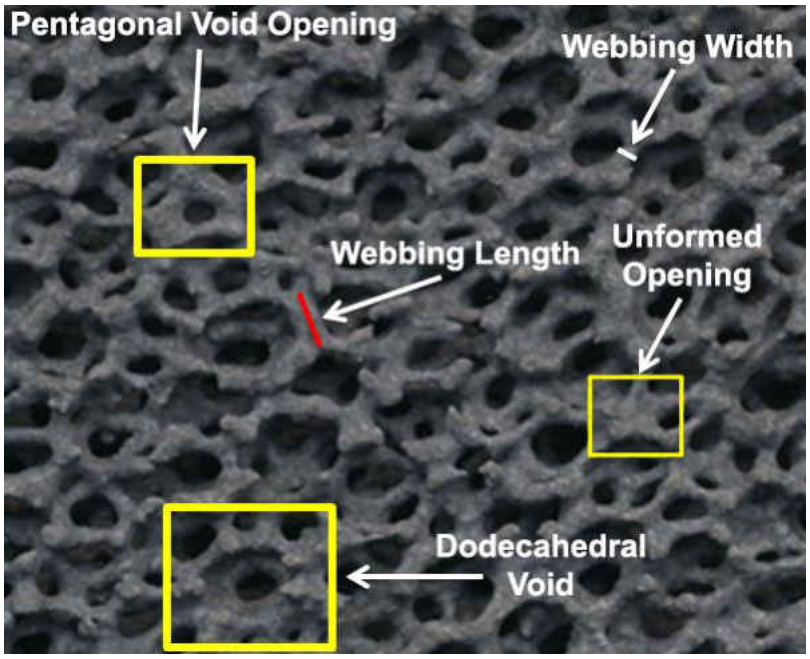

Figure 41) In depth geometric analysis of porous media showing void openings, voids, and unformed openings. These are shown in conjunction with characteristic webbing lengths and widths used in calculations.

Examining Figure 41, openings of the porous media are roughly pentagonal, examples of which are boxed within the figure. The vertices of the opening are termed “webbing” and have their own characteristic length and width; these measurements are shown in red and white, respectively. The porous media regularly encloses to form voids in the shape of a dodecahedron, arranged in a close configuration. Defects such as unformed openings act to increase the effective surface area of such geometry.

From observation, the utilized porous media is best characterized as a lattice of irregular dodecahedrons. For the sake of convince equations pertaining to the characterization of a single void are considered to be that of a regular dodecahedron, Figure 42. In such an analysis, the length of each vertex, *a*, represents the webbing length and it is assumed the porous media exists in the shape of a cylinder around each of the vertices with the diameter of the webbing width; With the given webbing length, the radius of a sphere which is the mid-radii between the circumscribed and inscribed spheres about the polyhedron is expressed as equation (30). Considerations are also taken bounding the volume of each of the cylinders within the circumscribed sphere.

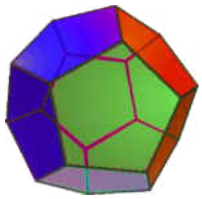

Figure 42) Regular dodecahedron. Used to illustrate idealized structure of the porous media.

$$r_u = a \cdot \frac{\mathbf{1}}{\mathbf{4}} \cdot (\mathbf{3} + \sqrt{\mathbf{5}}) \tag{30}$$

As a dodecahedron is unable to form a lattice, it is assumed the randomness of the porous solid allows for the geometric predictability of the dodecahedron. Using the dodecahedron as a model for a single pore, it was then assumed the series of pores were arranged in a face centered

cubic structure where the radius of each sphere within the arrangement exhibits the mid-radi of the polyhedron's inscribed and circumscribed spheres.

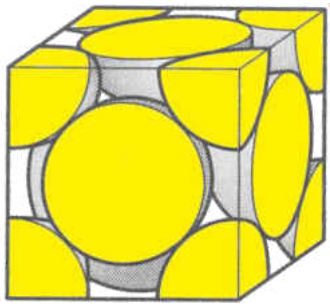

Figure 43) FCC Crystal Structure. Used to orchestrate the arrangement of voids within a porous structure.

Using the FCC crystal structure, the packing factor is used to determine the number of pores arranged in a plane N_p and the number arranged along the solids length N_L. The net surface area is then calculated from these parameters and the term which describes the net surface area per dodecahedron per void in accordance with the webbing length a and width D_w. The equivalent effective radius of the combustion chamber r_e is then calculated according to the atomic packing factor.

$$\frac{APF^{2/3} \cdot A_c}{\pi \cdot {r_u}^2} = N_P \tag{31}$$

$$\frac{APF^{1/3} \cdot L_c}{2 \cdot r_u} = N_L \tag{32}$$

$$S_A = \pi \cdot D_c \cdot L_c + N_L \cdot N_P \cdot \left(a \cdot 20 \cdot \pi \cdot D_w \cdot \frac{1}{3}\right) \tag{33}$$

$$APF^{1/3} \cdot r_c = r_e \tag{34}$$

Using the above method, comparisons were drawn between the measured value of volume of the solid structure through water immersion and the calculated volume of the irregular dodecahedron. Measurements of the water immersion testing were limited due to the resolution

of the instrument, and have an uncertainty of 2.5 cm^3. Through immersion the average volume of the porous media was found to be 55 cm^3 with a standard deviation of 5.463 cm^3 of the twenty recorded samples. For the porous media whose average recorded webbing length was found to be .305 cm and webbing width of 0.025 cm a porous solid volume of 55.8 cm^3 was found. Based on the above method of solid volume approximation, the bulk surface area can then be derived for interfacial heat transfer and the fractions of cross sectional planar area corresponding to both void and solid surface area.

As to the knowledge of the author at the writing of this manuscript, there are no closed form expressions which express the Nusselt Number or convection coefficient for porous media. An approximation was constructed utilizing an assumed similarity of entrance length pipe flow with correction parameters for the corresponding drop in pipe diameter associated with the volume occupied by the solid structure represented in (35) [108] corresponding to the length of an open pore.

$$Nu_D = \frac{h \cdot D_e}{k_f} = 3.66 + \frac{0.668 \cdot \frac{D_e}{2 \cdot r_u}}{\left[1 + .04 \cdot \frac{D_e}{2 \cdot r_u} \cdot Re_D \cdot Pr\right]^{2/3}} \tag{35}$$

With rigidly defined conditions for the characteristics of the solid structure, it was then possible to construct a physical model to represent the combustion system. Within CHEMKIN-PRO, networks of zero dimensional reactor points were arranged. Heat transfer was allowed to occur within the reactors as would be presented in three space flow. At each point, the incoming gasses are assumed perfectly mixed with no partiality of the properties of the porous media corresponding to arrangement. Each of the nodes were affixed thermal losses in the form of a heat flux which would correspond to the behavior of the system, however the end nodes were

also offered additional heat loss which reflected radiative emissions from the combustion media on the planes normal to the direction of flow.

In order to validate the model, prior to drawing any conclusions between model outputs and experimental data, comparisons regarding fixed inlet conditions were implemented with the number of nodes as a variable to demonstrate convergence. From the eight thermocouples which are on the physical combustion chamber, the number of discrete sections which comprised the combustion chamber was increased until asymptotic convergence of the system results was observed using the GRI 3.0 Mechanism [38]. . Kerosene fuel was not utilized as burn data to validate such models was limited.

The domain over which combustion is allowed to occur was constructed from a linear arrangement of reactor points, matching Figure 44. Which yield a lump sum of the properties over the discrete span the point encompasses. At each point, the incoming gasses are assumed perfectly mixed, and the rate limiting step of the reaction is assumed to be the Arrhenius behavior. At each discretization, the assumed random geometry of the porous media was assumed constant, and as a result no bias according to any section within the reaction model is implemented within the combustion section. However, an extension of the reactor model was considered to reflect the change in flow between the combustion chamber and the thermocouple sensor at *4* reflected in the experiment; this node is boxed within the figure comparing the combustion chamber to the cross section.

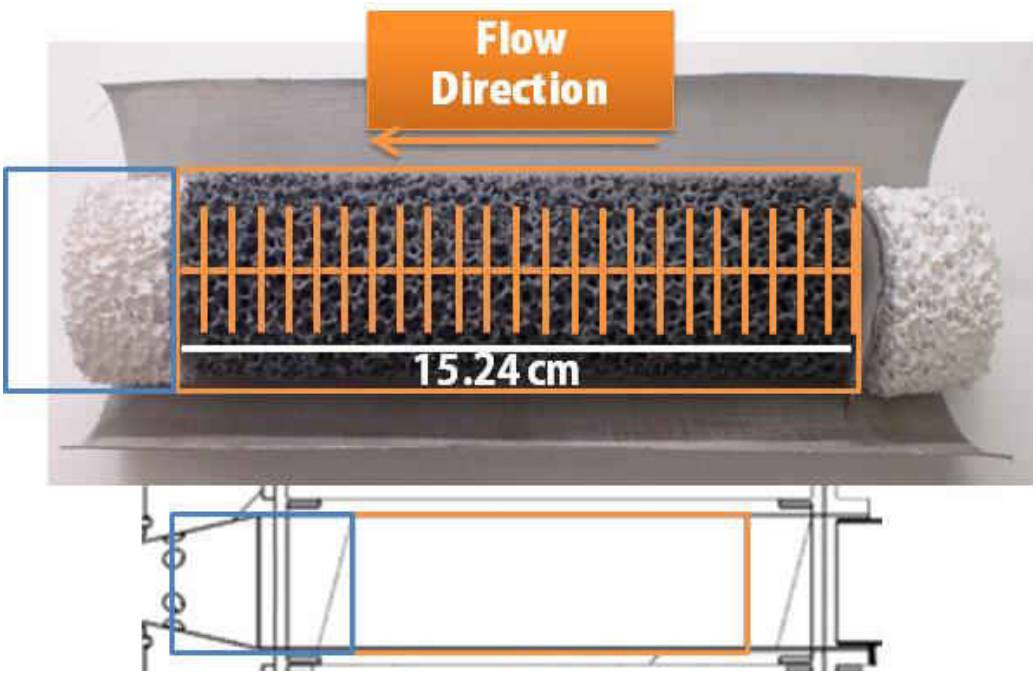

Figure 44) Discretization of porous section overlaid on the combustion media for comparison purposes.

To prevent failure of the exterior housing, heat losses are necessary from the combustion event. As the enclosure of the fume hood is reflective, it is assumed the only present losses are derived from natural convection (37) [108]. A plot for the convection coefficient for an air temperature of 296K of an isothermal horizontal cylinder, of diameter 5.08 cm, is presented in Figure 45 as a function dependent only on the temperature of a hot surface.

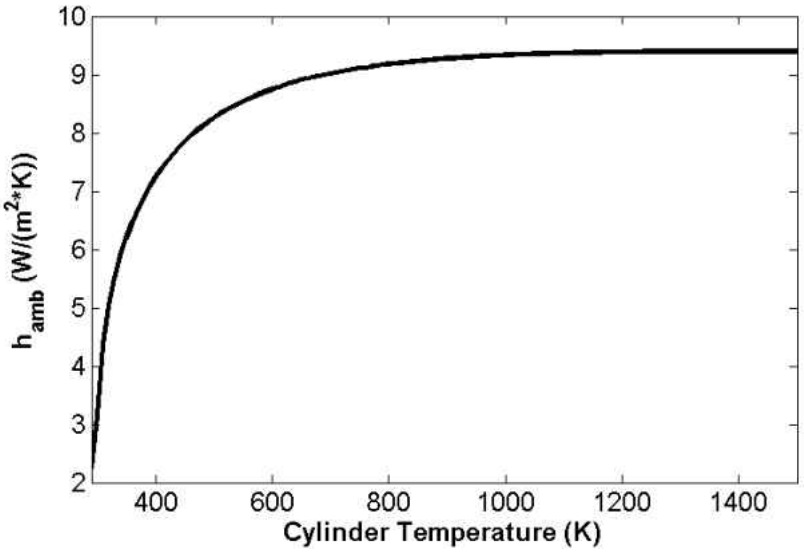

Figure 45) Convection coefficient for an isothermal horizontal cylinder as a function of exterior surface temperature.

$$Ra_D = \frac{g \cdot \beta}{\alpha \cdot \nu} \cdot D^3 \cdot (T_s - T_{inf}) \tag{36}$$

$$Nu_D = \frac{h \cdot D}{k_f} = \left\{ 0.6 + \frac{0.387 \cdot {Ra_D}^{1/6}}{\left[1 + \left(0.599/Pr\right)^{9/16}\right]^{8/27}} \right\}^2 \tag{37}$$

In order to validate the model, prior to drawing any conclusions between model outputs and experimental data, comparisons regarding fixed inlet conditions were implemented with the number of nodes as a variable to demonstrate convergence of the numerical system. As the combustion chamber is further discretized, effects of increased sensitivity of heat transfer within the reactor as well as the likely hood of examining intermediate reaction compounds were observed. However, due to computational limitations the model was never able to reveal superadiabatic combustion conditions which are present within the peak intensity of the flame.

CHAPTER FIVE: RESULTS AND DISCUSSION

5.1 Double Feedback Burner

5.1.1 Double Feedback Burner Experimental Results

Experimental results from the double feedback burner can be analyzed through the time history. From Figure 46 three regions can be observed from the vertical bars emplaced over the time history data. Between the green bars, is an associated warm-up period with the burner. Operation of the burner between the green and red bars, correspond to various flow rates with a fixed equivalence ratio as an examination of the ability to throttle the burner while operating on gaseous methane fuel. Verification of the burner's ability to run liquid fuel is proudly presented between the red bars.

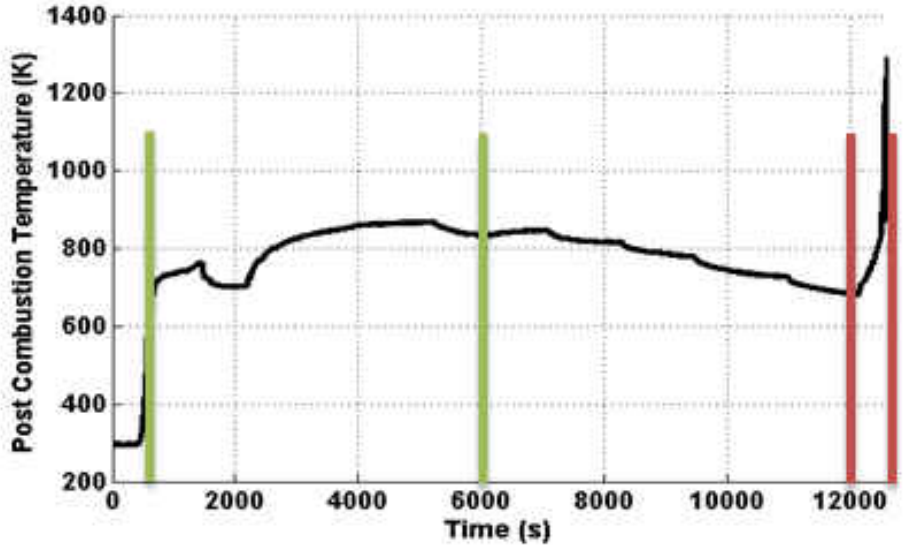

Figure 46) Temporal dependency of an experimental run of the double feedback burner, temperature profile is taken from *4*.

From operation of the experimental burner, the thermal operation of the heat exchanger was spot on with calculations used in the development of the model. A Joule Thompsons effect was observed with the steel delivery foam as a non ideal temperature drop was incurred with the

addition of each piece of porous foam, indicating the higher pore density foam induced a significant pressure drop [109]. It was also observed at the inlet to the combustion chamber, a significant drop in temperature was incurred regardless of insulation on the surface; it is assumed the long residence time allowed constant enthalpy changes in chemical potential of the flow. Due to the placement and design of the thermocouples the data extracted from them produces a qualitative examination of the combustion event and the most reliable temperature profile data for post reaction quantification can be taken from the thermocouple at *4*.

5.1.1.1 Results of Utilizing Liquid Fuel

Liquid fuel was successfully utilized as a combustion fuel within the burner. Maintaining a base flow rate at 36.5 SLPM and equivalence of 0.5 using methane fuel, an additional fuel source of 10 ml/min of K-2 grade kerosene was utilized.

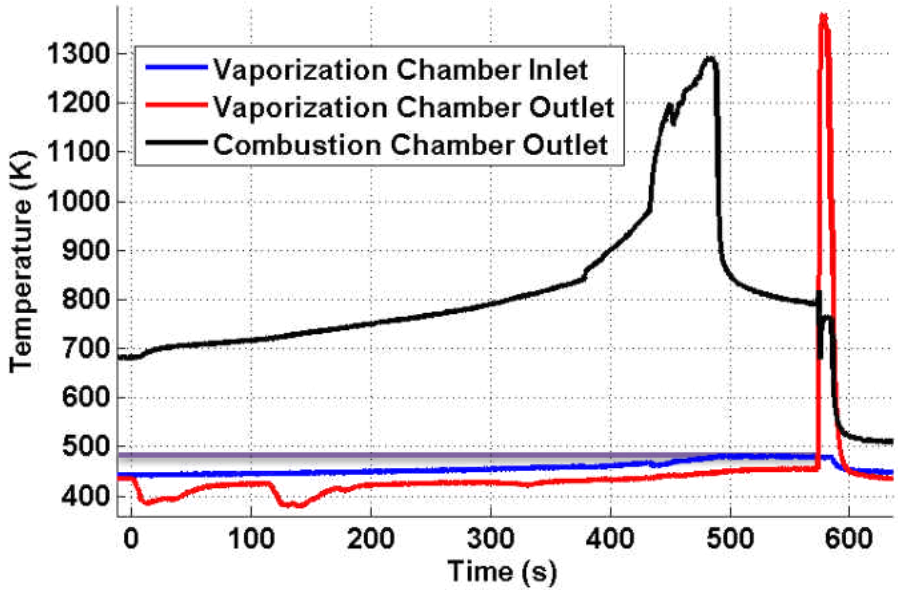

Figure 47) Temperature plot of the vaporization chamber for the double feedback burner.

Figure 46 displays the temperature profiles of the combustion chamber outlet at *4* and the vaporization chamber temperatures at *1* and 2. Immediately a temperature increase can be

observed in the thermal output, the inclusion of kerosene flow assuming it is approximately $C_{12}H_{26}$ [110] greatly increases the equivalence ratio of the reacting flow.

During this time period, the availability of enthalpy to be passed through the hot side of the heat exchanger increases, resulting in a steadily increasing vaporization chamber inlet temperature. Analyzing the steady rise in temperature over the period of approximately 15 seconds to 380 seconds following liquid fuel introduction the combustion chamber temperature profile reveals the flame progressing downstream. Examining Figure 48, the downstream thermocouples record an increasing temperature corresponding to the increase in post combustion chamber temperature observed in Figure 46.

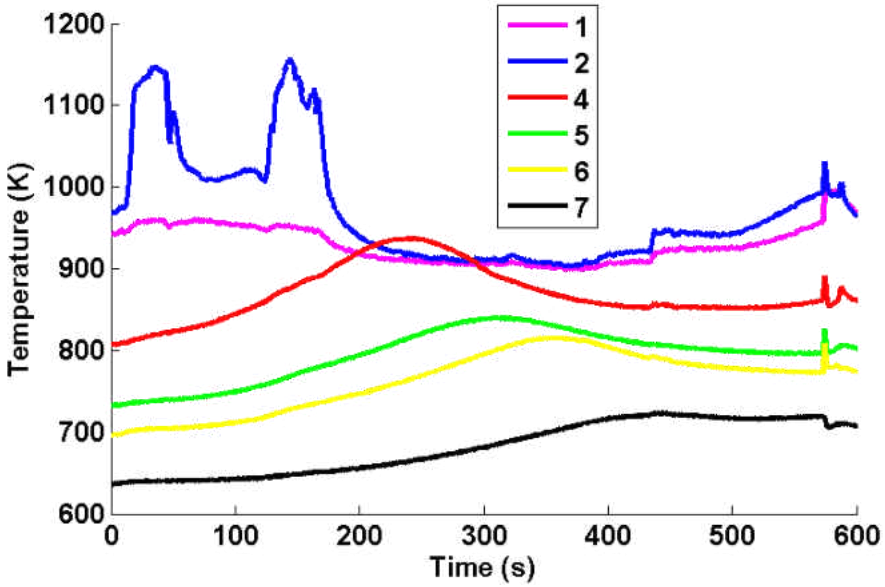

Figure 48) Partial combustion chamber thermocouple plot missing thermocouples 0 and 3 as these were damaged at an earlier point in the experiment.

At roughly 450 seconds following the flow of kerosene into the system, the flame had propagated outside of the combustion media and had entered the converging section where the post combustion chamber thermocouple was located. To prevent damage to the system, allowing

the flame to be swallowed back into the combustion media the flow of liquid fuel was terminated.

While this immediately sought to reduce the danger to the system, a sizeable amount of enthalpy was still being transferred to the unreacted stream. Upon reaching the vaporization chamber, residual buildup on the steel delivery foam of the liquid fuel along with the increased tendency to ignite a reactive mixture occurred and ignition happened within the vaporization chamber. Unfortunately this resulted in failure of the experimental device.

5.1.1.2 Results of Using Gaseous Fuels

Operating the burner on strictly methane provided more fruitful data which demonstrated the applicability of the system to throttling and allowed for the construction of data for model validation. Maintaining constant equivalence ratio, the mass flux was varied discreetly from 49.3 to 26.3 SLPM. Referencing Figure 49 a correlation between the thermal output of the system directly coincides with the reactant flux through the system. Segmenting the data from Figure 49, between 6000 and 12000s, to coincide with each step change in the flow rate of the reactants through the system, a plot of augmented times is displayed in Figure 50.

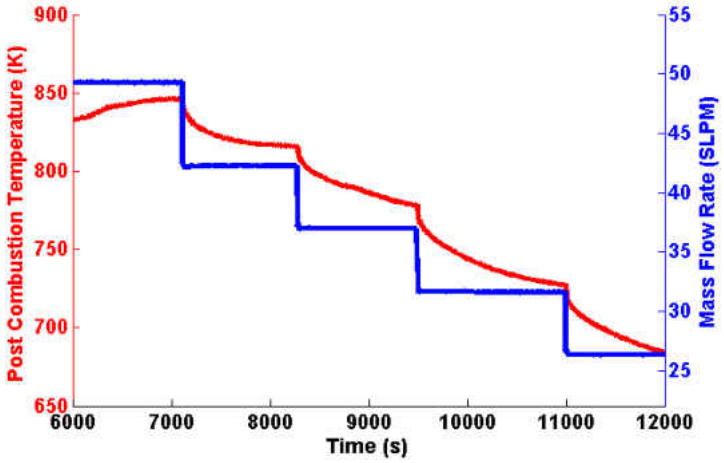

Figure 49) Step wise flow rate drops maintaining constant equivalence of 0.50, plotted along with the output temperature at *4*.

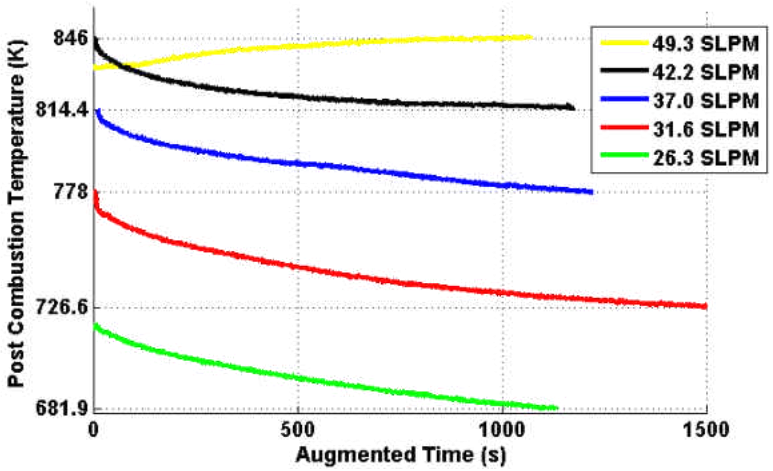

Figure 50) Combustion chamber outlet temperature *4* time evolution starting from initial point at which mass flux was changed.

5.1.2 Double Feedback Burner Modeling Considerations

Having gathered sufficient data from the experimental device, a similar throttling examination was considered of the modeled system. The results of which were used to validate the model.

Figure 51 presents this comparison. It is important to note, any output derived from the experimental model is going to be "ideal." Also, as the quantification of the internal surface area is vague, an uncertainty of 20% is considered, as well as an uncertainty of 20% for the internal and external convection coefficients. Examinations of the sensitivity of the chemical model were also considered, though the maximum temperature difference of the most pertinent reactions was on the order of 1K. Experimental thermocouple data was treated with a prescribed error of 1.5% on the limitations of the thermocouple, with cold junction errors on the order of 13K. As a 24-bit DAQ was used over a small full scale range, numerical errors associated with data binning are assumed negligible.

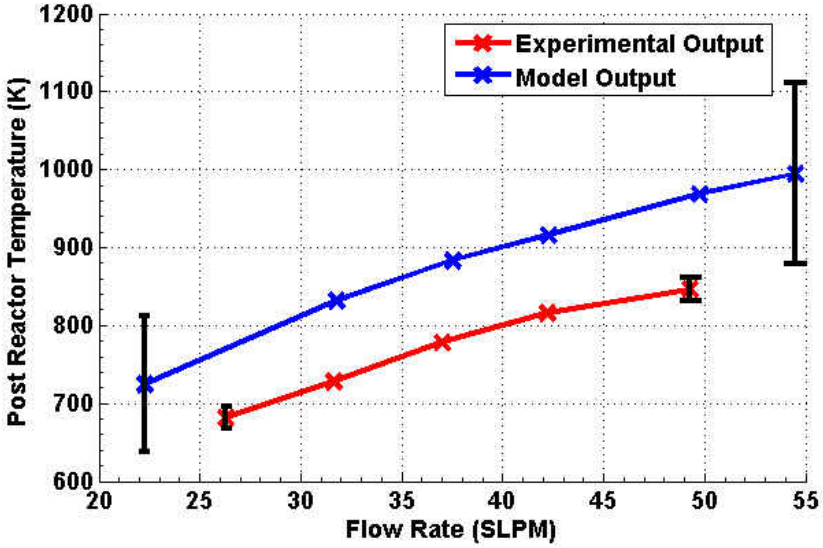

Figure 51) Comparative data between the model, and experimental system using gaseous fuel at an equivalence of 0.50 over a range of flow rates.

Analyzing the data presented within Figure 51, it can be seen both the model and experimental apparatus show an increased output at higher flow rates, indicating the work potential of a porous combustor responds favorable to higher fluxes as the increased mass flux and exergy content of the gasses are favorable at these regions. It is also interesting to note there is a decay in the thermal potential with reactant flux increases that is exhibited in both the model and experiment.

5.2 Exploratory Modeling Work

5.2.1 Determination of Solid Length

An excessively long porous structure within the combustion chamber is detrimental to the performance of a heterogeneous combustor. The solid structure exerts a drag force on the reactants as they pass over the solid [45]. In addition there are substantial losses in the exergy of the reaction byproducts with an excessively long combustion chamber as the chamber body

allows a substantial release of thermal energy to the environment. An examination was considered for the calculation of internal parameters to length parameters to appropriately size the combustion chamber's length for a fixed diameter and pore size.

From the analytical model [67], it has been established that at a higher equivalence ratio the flame will lengthen this will also happen at higher mass fluxes. As a means of determining the appropriate distance of length for the combustion chamber, a temperature profile was constructed from a simulation conducted at an equivalence of 0.60 and a flux of 55 SLPM. This profile is presented in Figure 52

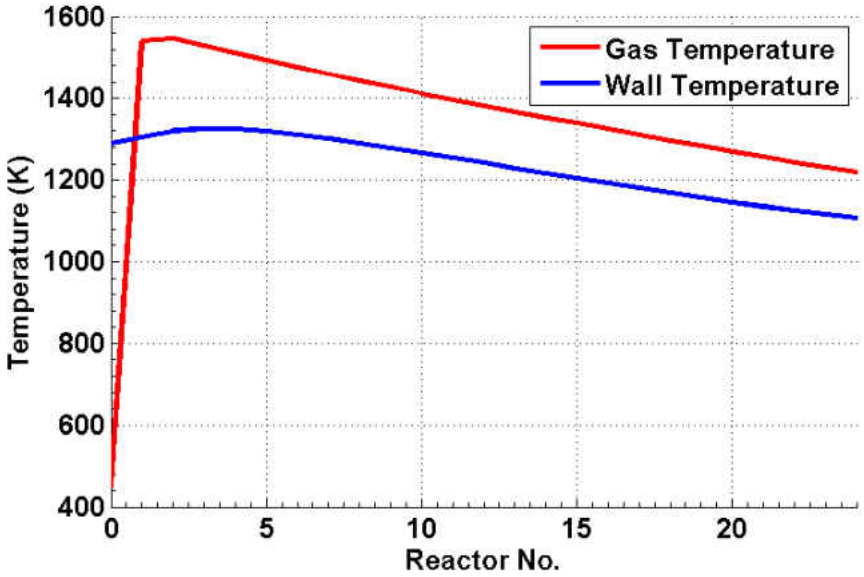

Figure 52) CHEMKIN-PRO temperature profiles of Double-Feedback Burner at 49.75 SLPM.

A further comparison between the solid and gas temperatures is abstracted using a augmented temperature profile difference between the solid and gas phase, Figure 53 described in (38). Examining the temperature profile, the early length has initially a large negative value, crosses zero, then peaks. The observed peak corresponds to the location of the highest temperature of the gas. Beyond this peak a nonlinear drop in temperature is then observed, with a

linear drop off in temperature until the end of the combustion chamber. Based from the model an appropriate length is on the size of 4.45 cm, compared to the experimental systems length of 15.24 cm.

$$\theta(x) = \frac{T_g(x) - T_s(x)}{T_{g_{max}}} \tag{38}$$

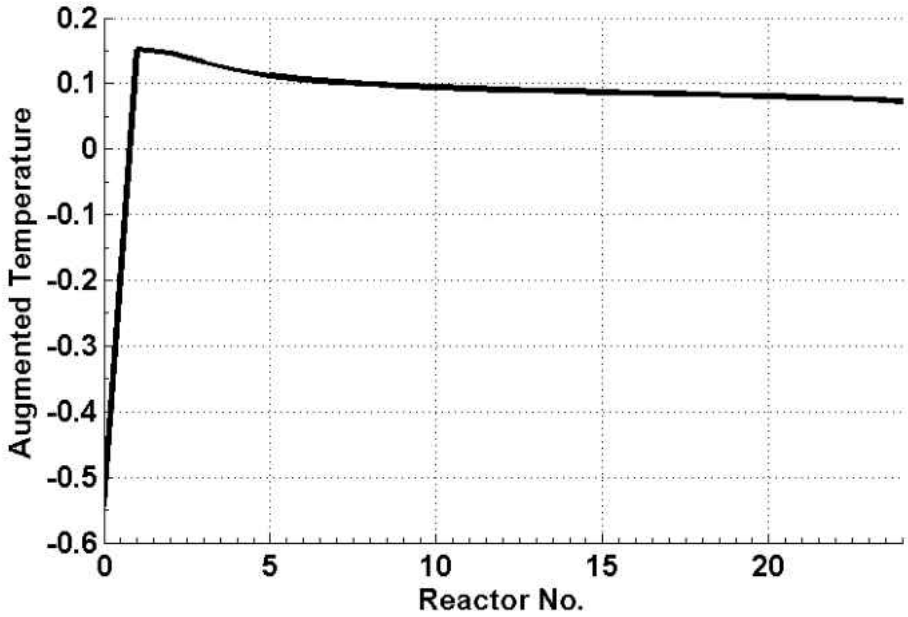

Figure 53) Augmented temperature profile corresponding to the Double-Feedback burner at 55.00 SLPM and equivalence ratio of 0.60.

A comparison between the experimental system and model was conducted to examine the validity of this analysis. Referencing Figure 54, black carbon deposition can be seen along the wall, spanning between the first and third thermocouples. Knowing the distances between the thermocouples is 2.166 cm and the threaded holes for the thermocouples are 3/8-16 UNC threads, the active length of the combustion chamber experimentally produced revels a length of 4.62 cm.

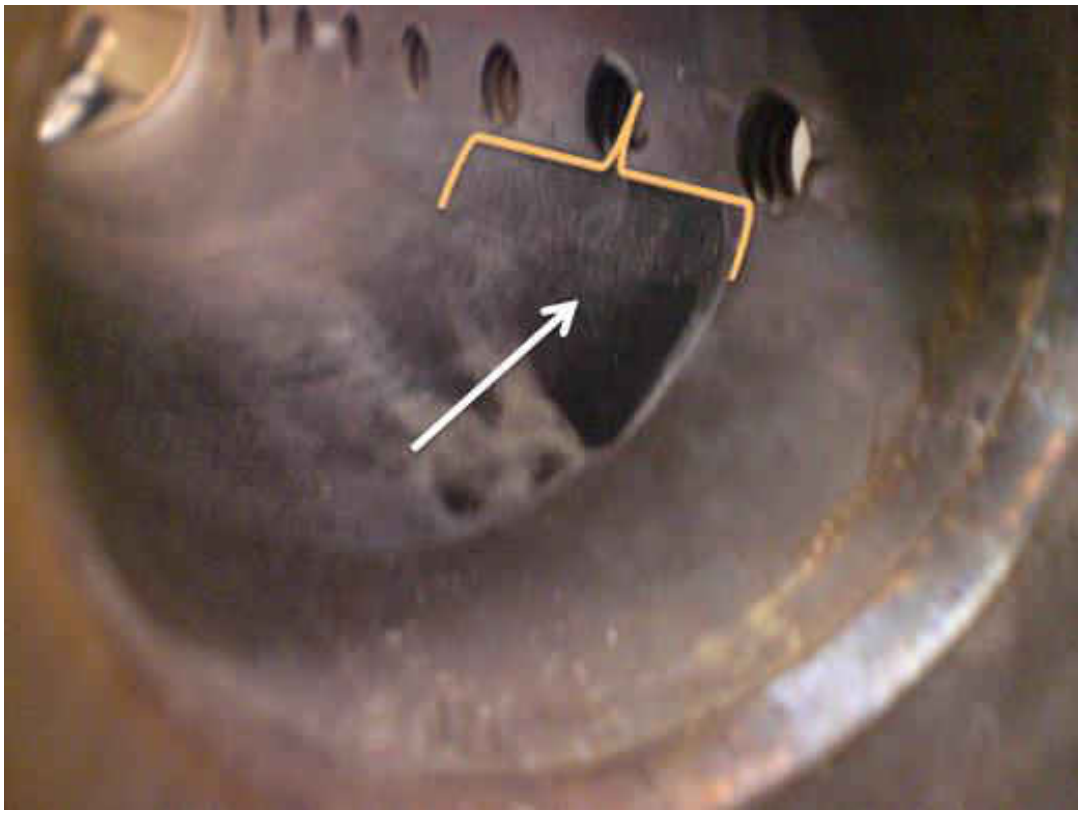

Figure 54) Carbon deposition along the combustion chamber inlet, white arrow pointing to carbon deposition along the wall, with the apparent reaction zone outlined in orange. Spacing between each thermocouple tap center is 2.166 cm.

5.2.2 Exhaust Gas Recirculation Analysis

Exhaust gas recirculation or EGR introduces a small fraction of the combustion byproducts to the combustion event, and aids in the reduction of pollutant formation [111]. Using the experimental model, optimized for length from the existing combustion reactor, a combustion chamber design featuring an EGR, Figure 55, is used to numerically investigate the effects of EGR on heterogeneous combustors. In this example a pressure driven flow reroutes exhaust gasses back to the inlet with a fixed recirculation flux of 2.5% of the mass flux of the inlet.

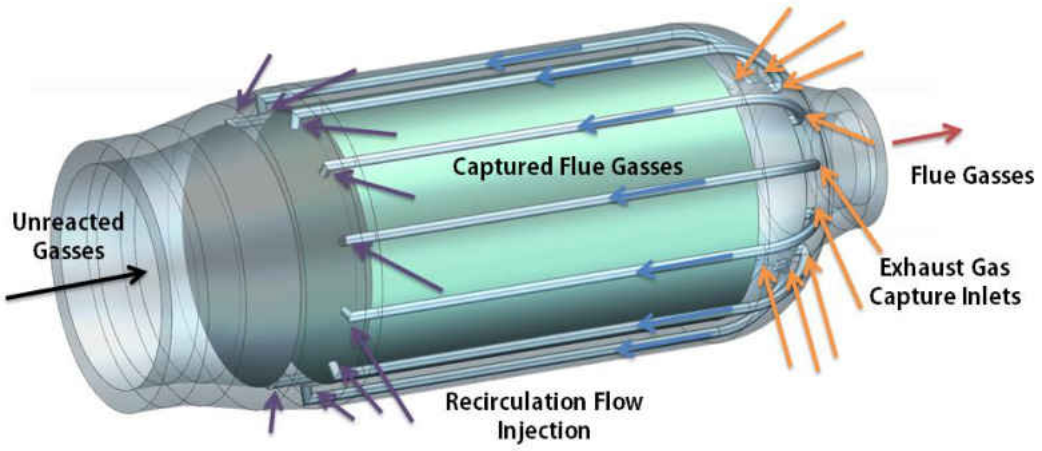

Figure 55) Representation of an EGR system which features pathways for the exhaust to reroute.

Comparing the exhaust gas temperature profiles between the non-recirculating and EGR burners, Figure 56, it can be observed there is a negligible difference in the thermal output of the combustor with the nominal change in exhaust temperature being less than 0.05 K over a range of lean equivalence ratios. However, over the equivalence ratio between 0.80 and 0.94, there is a localized region where there is an increase in the thermal output of the combustion gasses.

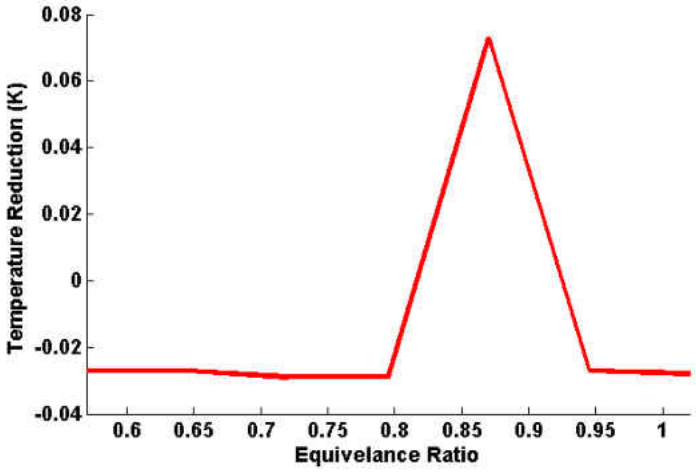

Figure 56) Temperature reduction as a result of EGR implementation at a recirculation flux of 2.5%.

Examining the reduction in NO_x it can be seen there is a significant improvement, which increases as the equivalence ratio gets richer, until it peaks at an equivalence of 0.87.

Dissimilarly, there is a negligible change in CO output, however over the range of equivalence ratios under the same band which there is an increase in exergy of the exhaust gasses, there is a correlation of CO reduction. Conveniently, this band also features peak reductions in NO_x.

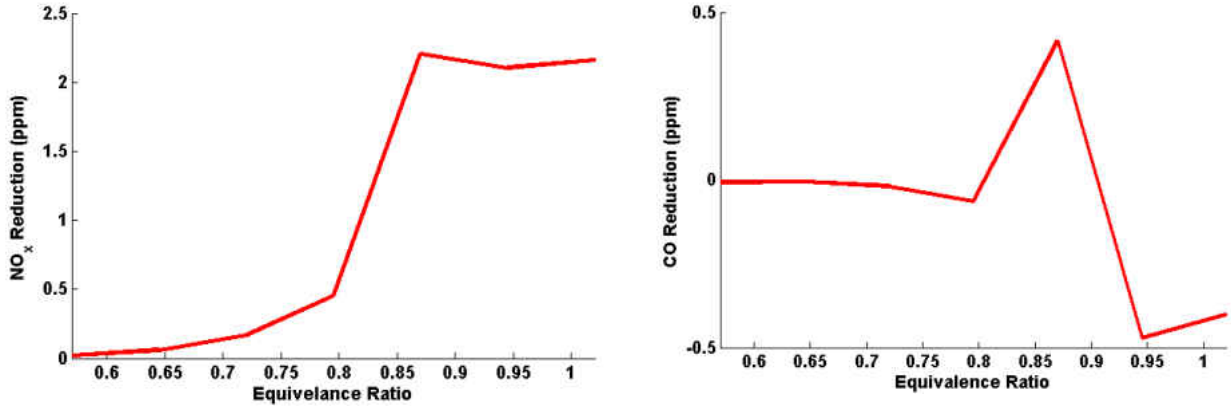

Figure 57) Reductions in the NO_x and CO concentrations, respectively, for a heterogeneous combustor featuring EGR with a recirculation flux of 2.5%.

5.2.3 Staged Injection

Building from series combustor [92], which featured two discrete porous structures with a separate injection, for each stage, a modification of this design which employs a single porous structure with a secondary inlet, Figure 58. Two Series of tests were carried out to examine the scope of applicability for staged reactant injection. As similar to the exhaust gas recirculation tests, the same model features for the experimental reactor were implemented; however, considerations of a length reduction to that of the appropriately sized porous combustor were also employed.

Featured in Figure 58, is the conceptual burner used. A primary inlet with the larger corresponding mass flux lies upstream of a flashback inhibiting screen. Between the primary and secondary inlets, a span of porous media which gives sufficient length to have the primary phase

of the reaction at near completion before the secondary inlet, marks the upstream third of the reactor. At the entrance to the secondary inlet, the reaction temperatures are already going to be at appreciable levels, to prevent pre-ignition of the secondary inlet, separate oxidizer and fuel streams are employed.

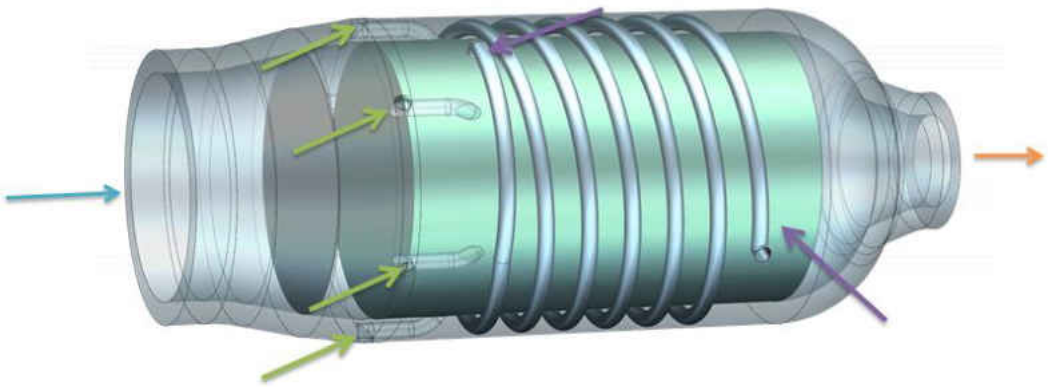

Figure 58) Porous combustor with staged inlet.

To reduce the likelihood of failure, the secondary inlets are used to cool off the reaction. The shorter pathways which travel from the upstream section to the inlet plane would ideally be used for fuel or water injection. Downstream, a helical coil is employed within the walls of the combustion chamber which is to be used for the oxidizer. As this device features multiple inlets, in order to keep a common base measure, an "overall equivalence ratio" $\bar{\varphi}$, was employed to give a mass flux based average for a reactor with multiple inlet planes.

$$\bar{\varphi} = \frac{\sum \dot{m}_i \cdot \varphi_i}{\sum \dot{m}_i} \tag{39}$$

5.2.3.1 Spanned Reactant Flux Examinations

The first of two investigations considered for a split plane system dealt with the investigation of a fixed mass flux spread over multiple inlets. A net mass flux of 80 SLPM and fixed equivalence ratio of 0.55 SLPM is employed for both cases; case one features a single inlet carrying 100% of the mass flux through the system, whereas the second case employs a split

mass flux of 60 SLPM at the primary inlet with an additional 20 SLPM at the secondary inlet both of which are at a fixed equivalence ratio of 0.55.

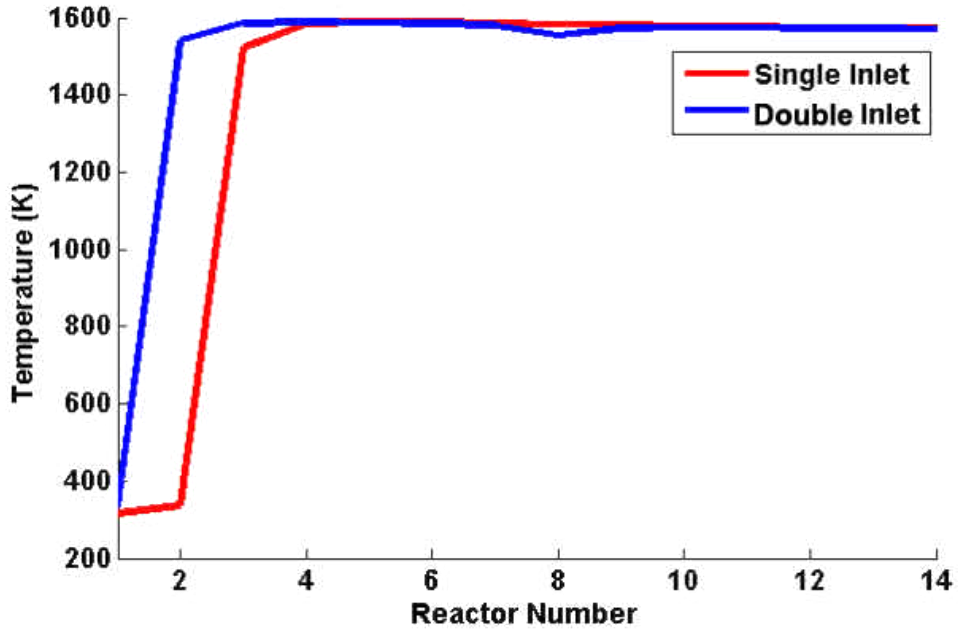

Figure 59) Temperature profile of the gas phase for 80 SLPM at an equivleance ratio of 0.55 through a heterogenous reactor.

Examining the thermal output Figure 59, it can be seen the single inlet configuration increases the preheating length as the gasses need an increased length to obtain the sufficient energy to ignite. Whereas the double inlet design gas phase temperature profile reveals ignition occurs much earlier; there is also a corresponding temperature drop where the second stage gasses are injected. At the exit plane, the difference in thermal potential of the two reactors is negligible, however the split design features a 7.65 ppm CO increase and a 274 ppb NO_x increase indicating there is a correlation with the pollutant formation and flame speed.

5.2.3.2 Varied Equivalence Multiple Inlet Examinations

As it is known there is a correlation between reactant flux and emissions, an examination was undertaken to measure the effectiveness of a varied equivalence ratio multiple inlet design, where the reactant flux is directly increased with the secondary inlet. In this test case, the primary inlet with a mass flux of 80 SLPM and a secondary inlet of 20 SLPM in series; for each inlet the equivalence ratio was varied from 0.54 to 1.02 and differences were marked between the two. In the case of the double inlet design, the upstream equivalence ratio was maintained at 0.84.

Using the staged inlet design, the exergy content of the reaction byproducts is of negligible difference over the range of presented overall equivalence ratios, however the multiple inlet design features a higher reactant flux. While the decreased exergy may be less beneficial in terms of Carnot Efficiency[4], it is more favorable as at these heightened temperatures the reaction byproducts will need to be cooled prior to their introduction to nozzles used for turbine cooling and there is a higher mass flux associated.

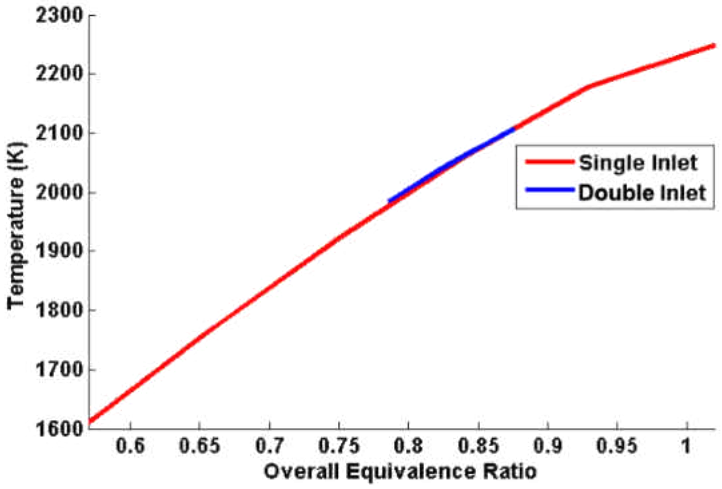

Figure 60) Comparison of a single inelt and double inlet reactor by examination of the thermal output.

While the thermodynamic potential of the two designs may not mandate their further interest, the associated environmental benefits of the staged inlet design are highly preferable. In both cases, the ability of the combustor to respond to changes at the secondary inlet convey a reduction in CO, examining the magnitude of its formation, whereas a significant reduction in NOx is observed comparatively speaking with a tendency to have increased benefit at equivalence ratios tending to 1.0.

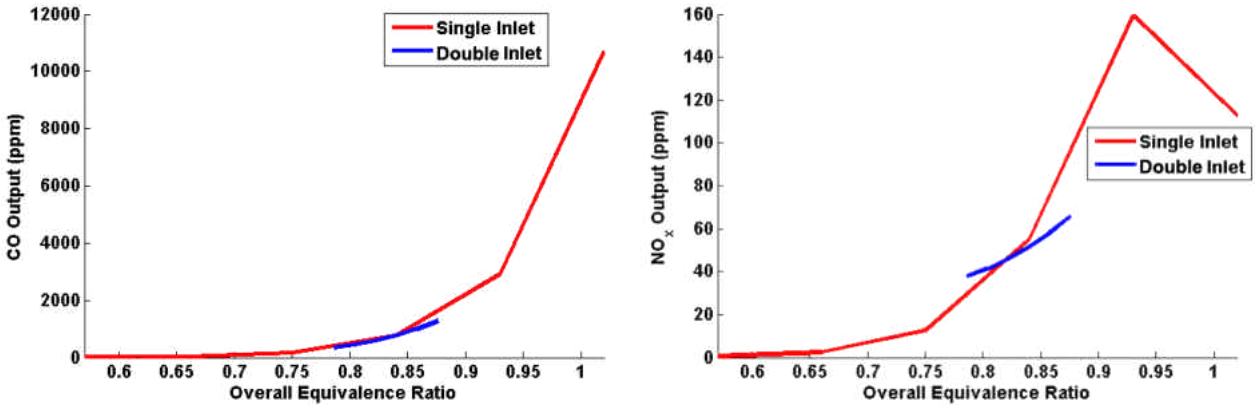

Figure 61) Comparison of CO and NOx output for single inlet and double inlet deisgn over varying overall equivleance ratios.

CHAPTER SIX: CONCLUSIONS

Based on the literature review and the work presented within this text, heterogeneous combustion is an interesting means of combustion with several applications in the advancement of emissions reduction and applications to reclaimed fuel sources. Combustion with a high surface area continuous solid immersed within the flame, as the solid within the flame acts as an internal regenerator distributing heat from the combustion byproducts to the upstream reactants. By including the solid structure, radiative energy extraction becomes viable, while the solid enables a vast extension of flammability limits compared to conventional flames, while offering dramatically reduced emissions of NO_x and CO, and dramatically increased burning velocities.

For the scope of study a combustor was built to operate on liquid fuel and demonstrated the ability to throttle output at constant equivalence by varying the reactant flux through the system. Furthermore a reactor network model was constructed within CHEMKIN-PRO and verified using experimentally gathered data.

From the development of the experimental model, a series of investigations were made to study the effectiveness of optimizing a porous combustor in the form of: solid length profiling, exhaust gas recirculation and staged reactant injection. Reducing the length of the solid phase enabled a higher fraction of energy to be available in the form of sensible enthalpy of the reaction byproducts. While the impact of exhaust gas recirculation is minimal, it is still a valid control technique when properly configured to target NO_x reduction, and should be employed as a final step in the combustor design process. Furthermore, the benefits of multiple reactant inlets offer a dramatic reduction in CO and NO_x emissions while maintaining exergy content of the combustor's exhaust stream.

APPENDIX A: REDUCED CHEMICAL MECHANISM RATES

```
!
! ************************************************************************
!    Extension of Hindiyarti, Glarborg and Marshall, JPCA 2007          *
! ************************************************************************
!
! ************************************************************************
!    GRI 3.0 Merged in allowing for N2/CH4/C2H6/C3H8 Oxidation           *
!                    H/O & Some CO chemistry was reserved from Glarborg  *
! ************************************************************************
!
! ************************************************************************
!   Units of Cal Mol K Atm                                               *
!   GRI reactions denoted by <=> if no hyperlink is given                *
!   Glarborg Reactions Denoted by =                                      *
!   Externally Sourced Reactions have Hyperlink Included                 *
! ************************************************************************
ELEMENTS
   O  H  C  N   AR
END
!
SPECIES
!
 AR                ! Argon
!
! H/O SPECIES
!
H                 ! Hydrogen radical
H2                ! Hydrogen
O                 ! Oxygen radical
O2                ! Oxygen
OH                ! Hydroxide
H2O               ! Water
HO2               ! Hydrogen peroxyl
H2O2              ! Hydrogen peroxide
!
! C1 SPECIES
!
HCO                                   !
CO                ! Carbon monoxide
CO2               ! Carbon dioxide
HOCO              ! Hydroxyoxomethyl radical
CH2                                   ! Metyhlene Radical
CH2(S)                            !
CH2O                                  !
CH2OH                                 ! Methelenohol
CH3                           ! Methyl Radical
CH3O                              !
CH3OH                                 ! Methanol
CH4                                   ! Methane
!
! C2 Species
!
C2H3                                  !
C2H4                          ! Ethylene
```

```
C2H5                                    !
C2H6                                    ! Ethane
HCCO                                    !
CH2CO                                   !
!
! C3 Species
!
C3H7                                    !
C3H8                                    ! Propane
!
! N SPECIES
!
N                                               ! Nitrogen Radical
N2              ! Nitrogen
NNH                                             !
NH                                      !
NH2                                             ! Amidogen
NH3                                     ! Ammonina
NO                              ! N=O
NO2                             ! O-N=O
N2O                             !
HNO                             ! H-N=O
!
! S SPECIES
!
S               ! Sulfur
SH              ! Mercapto radical (H-S*)
H2S             ! Hydrogen sulfide (H-S-H)
SO              ! Sulfur monoxide (triplet) (S=O) ground state
SO(S)           ! Sulfur monoxide (singlet) (S=O) excited state
SO2             ! Sulfur dioxide (O=S=O)
SO3             ! Sulfur trioxide (O=S(=O)=O)
HSO             ! H-S*=O
HOSO            ! HO-S*=O
!
! Mixed Base Species
HCN                                             !
NCO                                             !
HNCO                                    !
!
END
```

```
REACTIONS

!
! ************************************************************************
!   H2/O2 subset                                                       *
! ************************************************************************
!
H+O2=O+OH                       3.550E+15   -0.410   16600.00 ! RAS/GLA07_CO HES98
H+O2(+M)=HO2(+M)                1.480E+12    0.600       0.00 ! RAS/GLA07_CO MUE/DRY98
  LOW  / 3.5E+16 -0.41 -1116 /                              !
  TROE / 0.5 1.0E-30 1.0E+30 /                              !
  N2/0/ AR/0/ H2O/11/ H2/2/ O2/0.78/                        !
H+O2(+AR)=HO2(+AR)              1.480E+12    0.600       0.00 ! RAS/GLA07_CO MUE/DRY99
  LOW  / 9.04E+19 -1.500 490 /                              !
  TROE / 0.5 1.0E-30 1.0E+30 /                              !
H+O2(+N2)=HO2(+N2)              1.480E+12    0.600       0.00 ! RAS/GLA07_CO LI/DRY04
  LOW  / 6.37E+20 -1.720 520 /                              !
  TROE / 0.8 1.0E-30 1.0E+30 /                              !
O+H2=OH+H                       3.818E+12    0.000    7948.00 ! RAS/GLA07_CO CEC05
  DUP                                                       !
O+H2=OH+H                       8.792E+14    0.000   19175.00 ! RAS/GLA07_CO CEC05
  DUP                                                       !
OH+H+M=H2O+M                    4.500E+22   -2.000       0.00 !          CON/WES04
  AR/0.38/ H2/0.73/ H2O/12/ !HE/0.38/                       !
OH+H2=H+H2O                     2.140E+08    1.520    3449.00 ! RAS/GLA07_CO MIC92
O+H2O=OH+OH                     4.500E+04    2.700   14550.00 ! RAS/GLA07_CO MIC92
HO2+H=OH+OH                     8.400E+13    0.000     400.00 ! RAS/GLA07_CO
HO2+O=OH+O2                     1.630E+13    0.000    -445.00 ! RAS/GLA07_CO CEC05
HO2+OH=H2O+O2                   3.600E+21   -2.100    9000.00 ! RAS/GLA07_CO
  DUP                                                       !
HO2+OH=H2O+O2                   2.000E+15   -0.600       0.00 !
  DUP                                                       !
HO2+OH=H2O+O2                  -2.200E+96  -24.000   49000.00 !
  DUP                                                       !
H2O2(+M)=OH+OH(+M)              4.000E+11    0.000   37137.00 ! RAS/GLA07_CO KAP/TRO02
  LOW  /2.291E+16 0.0 43638/                                !
  TROE /0.5 1E-30 1E+30 1E+30/                              !         (Fc=0.5)
  H2O/12/ H2/2.5/ AR/0.64/                                  !
H2O2+O=HO2+OH                   9.550E+06    2.000    3970.00 ! RAS/GLA07_CO NBS86
H2O2+OH=H2O+HO2                 1.000E+12    0.000       0.00 ! RAS/GLA07_CO HEL/DRY98
  DUP                                                       !
H2O2+OH=H2O+HO2                 5.800E+14    0.000    9560.00 !
  DUP                                                       !
H+2O2<=>HO2+O2                  2.080E+19   -1.240        .00 ! GRI 3.0
H+O2+H2O<=>HO2+H2O               11.26E+18    -.760        .00 ! GRI 3.0
H+O2+N2<=>HO2+N2                2.600E+19   -1.240        .00 ! GRI 3.0
H+O2+AR<=>HO2+AR                 7.000E+17    -.800        .00 ! GRI 3.0
OH+HO2<=>O2+H2O                 1.450E+13     .000    -500.00 ! GRI 3.0
 DUP
OH+H2O2<=>HO2+H2O                2.000E+12     .000     427.00 ! GRI 3.0
 DUP
OH+H2O2<=>HO2+H2O                1.700E+18     .000   29410.00 ! GRI 3.0
 DUP
```

```
OH+HO2<=>O2+H2O                  0.500E+16     .000   17330.00 ! GRI 3.0
 DUP
!
! ************************************************************************
!   C1 subset                                          *
! ************************************************************************
!
CO+O(+M)=CO2(+M)                1.800E+10   0.0      2384 ! RAS/GLA07_CO ALL/DRY97
  LOW  /1.35E+24 -2.79 4191/                          !
  TROE /1.0 1E-30 1E+30 1E+30/                        !         Fc=1
  H2/2.5/ H2O/12/ CO/1.9/ CO2/3.8/                    !
CO+OH=CO2+H                     8.000E+10   0.000       0 ! RAS/GLA07_CO (1 bar, 300<T<2000K)
  DUP                                                 !
CO+OH=CO2+H                     8.800E+05   1.770     954 ! RAS/GLA07_CO (1 bar, 300<T<2000K)
  DUP                                                 !
CO+OH=HOCO                      6.000E+26  -5.600    2881 ! RAS/GLA07_CO (1 bar, 300<T<2000K)
CO+HO2=CO2+OH                    6.919E+06   1.609   17496 ! Klippenstein ab initio
HOCO+OH=CO2+H2O                   4.558E+12   0.0       -89 !          YU/FRA05
  DUP                                                 !
HOCO+OH=CO2+H2O                   9.544E+06   2.000     -89 !          YU/FRA05
  DUP                                                 !
HOCO+O2=CO2+HO2                  9.910E+11   0.0         0 !          NOL/WAG93
O+CH3<=>H+CH2O                    5.060E+13     .000       .00 ! GRI 3.0
O+CH4<=>OH+CH3                    1.020E+09    1.500    8600.00 ! GRI 3.0
O2+CO<=>O+CO2                    2.500E+12     .000   47800.00 ! GRI 3.0
H+CH4<=>CH3+H2                    6.600E+08    1.620   10840.00 ! GRI 3.0
H+CH2O(+M)<=>CH2OH(+M)                5.400E+11     .454    3600.00 ! GRI 3.0
    LOW  /  1.270E+32   -4.820   6530.00/
    TROE/   .7187  103.00  1291.00  4160.00 /
H2/2.00/ H2O/6.00/ CH4/2.00/ CO/1.50/ CO2/2.00/ C2H6/3.00/
H+CH2O(+M)<=>CH3O(+M)                 5.400E+11     .454    2600.00 ! GRI 3.0
    LOW  /  2.200E+30   -4.800   5560.00/
    TROE/   .7580   94.00  1555.00  4200.00 /
H2/2.00/ H2O/6.00/ CH4/2.00/ CO/1.50/ CO2/2.00/ C2H6/3.00/
H+CH2OH<=>OH+CH3                    1.650E+11     .650    -284.00 ! GRI 3.0
H+CH2OH<=>CH2(S)+H2O                  3.280E+13    -.090     610.00 ! GRI 3.0
OH+CH3(+M)<=>CH3OH(+M)                2.790E+18   -1.430    1330.00 ! GRI 3.0
    LOW  /  4.000E+36   -5.920   3140.00/
    TROE/   .4120  195.0  5900.00  6394.00/
H2/2.00/ H2O/6.00/ CH4/2.00/ CO/1.50/ CO2/2.00/ C2H6/3.00/
OH+CH3<=>CH2+H2O                   5.600E+07    1.600    5420.00 ! GRI 3.0
OH+CH3<=>CH2(S)+H2O                  6.440E+17   -1.340    1417.00 ! GRI 3.0
OH+CH4<=>CH3+H2O                   1.000E+08    1.600    3120.00 ! GRI 3.0
OH+CH2O<=>HCO+H2O                    3.430E+09    1.180    -447.00 ! GRI 3.0
OH+CH3OH<=>CH2OH+H2O                  1.440E+06    2.000    -840.00 ! GRI 3.0
OH+CH3OH<=>CH3O+H2O                   6.300E+06    2.000    1500.00 ! GRI 3.0
CH2+O2=>OH+H+CO                    5.000E+12     .000    1500.00 ! GRI 3.0
CH2(S)+N2<=>CH2+N2                   1.500E+13     .000     600.00 ! GRI 3.0
CH2(S)+AR<=>CH2+AR                    9.000E+12     .000     600.00 ! GRI 3.0
CH2(S)+O2<=>H+OH+CO                   2.800E+13     .000       .00 ! GRI 3.0
CH2(S)+O2<=>CO+H2O                   1.200E+13     .000       .00 ! GRI 3.0
CH2(S)+H2O(+M)<=>CH3OH(+M)            4.820E+17   -1.160    1145.00 ! GRI 3.0
    LOW  /  1.880E+38   -6.360   5040.00/
    TROE/   .6027  208.00  3922.00  10180.0 /
```

```
H2/2.00/ H2O/6.00/ CH4/2.00/ CO/1.50/ CO2/2.00/ C2H6/3.00/
CH2(S)+H2O<=>CH2+H2O                 3.000E+13     .000        .00 ! GRI 3.0
CH2(S)+CO2<=>CH2+CO2                 7.000E+12     .000        .00 ! GRI 3.0
CH2(S)+CO2<=>CO+CH2O                 1.400E+13     .000        .00 ! GRI 3.0
CH3+O2<=>O+CH3O                    3.560E+13     .000   30480.00 ! GRI 3.0
HO2+CH3<=>OH+CH3O                    3.780E+13     .000        .00 ! GRI 3.0! Near Stoich Ignition Specific
CH3+O2<=>OH+CH2O                   2.310E+12     .000   20315.00 ! GRI 3.0
HCO+H2O<=>H+CO+H2O                   1.500E+18   -1.000   17000.00 ! GRI 3.0
HCO+M<=>H+CO+M                                                    5.150E+14         -1.200         17734.00
!http://kinetics.nist.gov/kinetics/Detail?id=2002FRI/HER5778-5788:4
H2/2.00/ H2O/ .00/ CH4/2.00/ CO/1.50/ CO2/2.00/ C2H6/3.00/
HCO+O2<=>HO2+CO                    13.45E+12     .000     400.00 ! GRI 3.0
CH2OH+O2<=>HO2+CH2O                  1.800E+13     .000     900.00 ! GRI 3.0
O+CH3=>H+H2+CO                     3.370E+13     .000        .00 ! GRI 3.0
H+CH3(+M)<=>CH4(+M)                  13.90E+15    -.534     536.00 ! GRI 3.0
    LOW  /  2.620E+33   -4.760   2440.00/
    TROE/   .7830   74.00  2941.00  6964.00 /
H2/2.00/ H2O/6.00/ CH4/3.00/ CO/1.50/ CO2/2.00/ C2H6/3.00/ AR/ .70/
!
! ************************************************************************
!   C2 subset                                          *
! ************************************************************************
!
O+C2H6<=>OH+C2H5                   8.980E+07    1.920    5690.00 ! GRI 3.0
H+C2H4(+M)<=>C2H5(+M)                0.540E+12     .454    1820.00 ! GRI 3.0
    LOW  /  0.600E+42   -7.620   6970.00/
    TROE/   .9753  210.00   984.00  4374.00 /
H2/2.00/ H2O/6.00/ CH4/2.00/ CO/1.50/ CO2/2.00/ C2H6/3.00/ AR/ .70/
OH+C2H4<=>C2H3+H2O                 3.600E+06    2.000    2500.00 ! GRI 3.0
C2H3+O2<=>CH3+CO2                                                 4.167E+12         -0.100              -60.43   !
http://www.sciencedirect.com/science/article/pii/S0009261402004025
OH+C2H6<=>C2H5+H2O                 3.540E+06    2.120     870.00 ! GRI 3.0
OH+CH2CO<=>HCCO+H2O                  7.500E+12     .000    2000.00 ! GRI 3.0
CH2+CO(+M)<=>CH2CO(+M)               8.100E+11     .500    4510.00 ! GRI 3.0
    LOW  /  2.690E+33   -5.110   7095.00/
    TROE/   .5907  275.00  1226.00  5185.00 /
H2/2.00/ H2O/6.00/ CH4/2.00/ CO/1.50/ CO2/2.00/ C2H6/3.00/ AR/ .70/
2CH3(+M)<=>C2H6(+M)                  6.770E+16   -1.180     654.00 ! GRI 3.0
    LOW  /  3.400E+41   -7.030   2762.00/
    TROE/   .6190  73.20  1180.00  9999.00 /
H2/2.00/ H2O/6.00/ CH4/2.00/ CO/1.50/ CO2/2.00/ C2H6/3.00/ AR/ .70/
C2H5+O2<=>HO2+C2H4                   8.400E+11     .000    3875.00 ! GRI 3.0
HCCO+O2<=>OH+2CO                   3.200E+12     .000     854.00 ! GRI 3.0
OH+CH3=>H2+CH2O                    8.000E+09     .500   -1755.00 ! GRI 3.0
CH2+O2=>2H+CO2                     5.800E+12     .000    1500.00 ! GRI 3.0
CH2+O2<=>O+CH2O                    2.400E+12     .000    1500.00 ! GRI 3.0
```

```
!
! ************************************************************************
!   C3 subset                                                  *
! ************************************************************************
!
CH3+C2H5(+M)<=>C3H8(+M)                .9430E+13     .000       .00 ! GRI 3.0
    LOW/ 2.710E+74  -16.82  13065.0 /
    TROE/ .1527  291.0  2742.0  7748.0 /
H2/2.00/ H2O/6.00/ CH4/2.00/ CO/1.50/ CO2/2.00/ C2H6/3.00/ AR/ .70/
O+C3H8<=>OH+C3H7                     1.930E+05    2.680   3716.00 ! GRI 3.0
OH+C3H8<=>C3H7+H2O                     3.160E+07    1.800    934.00 ! GRI 3.0
CH3+C2H4(+M)<=>C3H7(+M)                2.550E+06    1.600   5700.00 ! GRI 3.0
     LOW/ 3.00E+63  -14.6  18170./
     TROE/ .1894  277.0  8748.0  7891.0 /
H2/2.00/ H2O/6.00/ CH4/2.00/ CO/1.50/ CO2/2.00/ C2H6/3.00/ AR/ .70/
!
! ************************************************************************
!   N subset                                                   *
! ************************************************************************
!
N+NO<=>N2+O                          2.700E+13     .000     355.00 ! GRI 3.0
N+O2<=>NO+O                          9.000E+09    1.000    6500.00 ! GRI 3.0
N2O+O<=>N2+O2                         1.400E+12     .000   10810.00 ! GRI 3.0
N2O+H<=>N2+OH                         3.870E+14     .000   18880.00 ! GRI 3.0
N2O+OH<=>N2+HO2                       2.000E+12     .000   21060.00 ! GRI 3.0
N2O(+M)<=>N2+O(+M)                    7.910E+10     .000   56020.00 ! GRI 3.0
    LOW  /  6.370E+14     .000  56640.00/
H2/2.00/ H2O/6.00/ CH4/2.00/ CO/1.50/ CO2/2.00/ C2H6/3.00/ AR/ .625/
HO2+NO<=>NO2+OH                       2.110E+12     .000    -480.00 ! GRI 3.0
NO+O+M<=>NO2+M                        1.060E+20   -1.410       .00 ! GRI 3.0
H2/2.00/ H2O/6.00/ CH4/2.00/ CO/1.50/ CO2/2.00/ C2H6/3.00/ AR/ .70/
NO2+O<=>NO+O2                        3.900E+12     .000    -240.00 ! GRI 3.0
NO2+H<=>NO+OH                         1.320E+14     .000     360.00 ! GRI 3.0
NH+OH<=>HNO+H                         2.000E+13     .000       .00 ! GRI 3.0
NH+OH<=>N+H2O                         2.000E+09    1.200       .00 ! GRI 3.0
NH+O2<=>HNO+O                         4.610E+05    2.000    6500.00 ! GRI 3.0
NH+O2<=>NO+OH                         1.280E+06    1.500     100.00 ! GRI 3.0
NH+H2O<=>HNO+H2                       2.000E+13     .000   13850.00 ! GRI 3.0
NH+NO<=>N2+OH                         2.160E+13    -.230       .00 ! GRI 3.0
NH+NO<=>N2O+H                         3.650E+14    -.450       .00 ! GRI 3.0
NH2+O<=>H+HNO                         3.900E+13     .000       .00 ! GRI 3.0
NH2+OH<=>NH+H2O                       9.000E+07    1.500    -460.00 ! GRI 3.0
H+NO+M<=>HNO+M                        4.480E+19   -1.320     740.00 ! GRI 3.0
H2/2.00/ H2O/6.00/ CH4/2.00/ CO/1.50/ CO2/2.00/ C2H6/3.00/ AR/ .70/
HNO+OH<=>NO+H2O                       1.300E+07    1.900    -950.00 ! GRI 3.0
HNO+O2<=>HO2+NO                       1.000E+13     .000   13000.00 ! GRI 3.0
NH3+OH<=>NH2+H2O                      5.000E+07    1.600     955.00 ! GRI 3.0
NH3+O<=>NH2+OH                        9.400E+06    1.940    6460.00 ! GRI 3.0
NH+CO2<=>HNO+CO                       1.000E+13     .000   14350.00 ! GRI 3.0
```

```
!
! ************************************************************************
!    Multi Base subset                                 *
! ************************************************************************
!
NCO+OH<=>NO+H+CO                    0.250E+13     .000       .00 ! GRI 3.0
NCO+NO<=>N2O+CO                     1.900E+17   -1.520     740.00 ! GRI 3.0
NCO+NO<=>N2+CO2                     3.800E+18   -2.000     800.00 ! GRI 3.0
HCN+OH<=>HNCO+H                                                    2.520E+06          4.710      493.00
! http://kinetics.nist.gov/kinetics/Detail?id=1991TSA/HER609-663:8
CH2+NO<=>H+HNCO                                                    2.510E+12       0.000       5981.00 !
http://kinetics.nist.gov/kinetics/Detail?id=1995BAU/KLA97-104:2
CH2+NO<=>OH+HCN                     2.900E+14    -.690     760.00 ! GRI 3.0
HNCO+O<=>NCO+OH                      2.200E+06    2.110   11400.00 ! GRI 3.0
HNCO+OH<=>NCO+H2O                    3.300E+07    1.500    3600.00 ! GRI 3.0
HNCO+OH<=>NH2+CO2                    3.300E+06    1.500    3600.00 ! GRI 3.0
HNCO+H<=>NH2+CO                     2.250E+07    1.700    3800.00 ! GRI 3.0 ! .5 Eq ignition Specific
NCO+NO2<=>N2O+CO2                    3.250E+12     .000    -705.00 ! GRI 3.0
END
```

APPENDIX B: THERMODYNAMICS DATA

```
THERMO
   300.000  1000.000  5000.000
! GRI-Mech Version 3.0 Thermodynamics released 7/30/99
! NASA Polynomial format for CHEMKIN-II
! see README file for disclaimer

AR        BUR0302 L 6/88AR  1    0    0    0G   200.000  6000.000 1000.        1
 0.25000000E+01 0.00000000E+00 0.00000000E+00 0.00000000E+00 0.00000000E+00    2
-0.74537500E+03 0.43796749E+01 0.25000000E+01 0.00000000E+00 0.00000000E+00    3
 0.00000000E+00 0.00000000E+00-0.74537500E+03 0.43796749E+01 0.00000000E+00    4
! H2/O2
H         BUR0302 L 6/94H   1    0    0    0G   200.000  6000.000 1000.        1
 0.25000000E+01 0.00000000E+00 0.00000000E+00 0.00000000E+00 0.00000000E+00    2
 0.25473660E+05-0.44668285E+00 0.25000000E+01 0.00000000E+00 0.00000000E+00    3
 0.00000000E+00 0.00000000E+00 0.25473660E+05-0.44668285E+00 0.26219035E+05    4
H2                121286H   2               G  0300.00   5000.00  1000.00      1 !LI/DRY04 (v6.1)
 2.99142337E+00 7.00064411E-04-5.63382869E-08-9.23157818E-12 1.58275179E-15    2
-8.35033997E+02-1.35511017E+00 3.29812431E+00 8.24944174E-04-8.14301529E-07    3
-9.47543433E-11 4.13487224E-13-1.01252087E+03-3.29409409E+00                   4
O                 120186O   1               G  0300.00   5000.000  1000.00     1 !LI/DRY04 (v6.1)
 2.54205966E+00-2.75506191E-05-3.10280335E-09 4.55106742E-12-4.36805150E-16    2
 2.92308027E+04 4.92030811E+00 2.94642878E+00-1.63816649E-03 2.42103170E-06    3
-1.60284319E-09 3.89069636E-13 2.91476445E+04 2.96399498E+00                   4
O2        BUR0302 RUS 89O   2    0    0    0G   200.000  6000.000 1000.        1
 3.66096083E+00 6.56365523E-04-1.41149485E-07 2.05797658E-11-1.29913248E-15    2
-1.21597725E+03 3.41536184E+00 3.78245636E+00-2.99673415E-03 9.84730200E-06    3
-9.68129508E-09 3.24372836E-12-1.06394356E+03 3.65767573E+00 0.00000000E+00    4
OH                S 9/01O   1H   1    0    0G   200.000  6000.000 1000.        1 !LI/DRY04 (v6.1)
 2.86472886E+00 1.05650448E-03-2.59082758E-07 3.05218674E-11-1.33195876E-15    2
 3.68362875E+03 5.70164073E+00 4.12530561E+00-3.22544939E-03 6.52764691E-06    3
-5.79853643E-09 2.06237379E-12 3.34630913E+03-6.90432960E-01 4.51532273E+03    4
H2O               20387H   2O   1          G  0300.00   5000.00  1000.00      1 !LI/DRY04 (v6.1)
 2.67214561E+00 3.05629289E-03-8.73026011E-07 1.20099639E-10-6.39161787E-15    2
-2.98992090E+04 6.86281681E+00 3.38684249E+00 3.47498246E-03-6.35469633E-06    3
 6.96858127E-09-2.50658847E-12-3.02081133E+04 2.59023285E+00                   4
HO2               L 5/89H   1O   2   00   00G   200.000  3500.000  1000.000    1 !LI/DRY04 (v6.1)
 4.01721090E+00 2.23982013E-03-6.33658150E-07 1.14246370E-10-1.07908535E-14    2
 1.11856713E+02 3.78510215E+00 4.30179801E+00-4.74912051E-03 2.11582891E-05    3
-2.42763894E-08 9.29225124E-12 2.94808040E+02 3.71666245E+00 1.00021620E+04    4
H2O2              120186H   2O   2          G  0300.00   5000.00  1000.00      1 !LI/DRY04 (v6.1)
 4.57316685E+00 4.33613639E-03-1.47468882E-06 2.34890357E-10-1.43165356E-14    2
-1.80069609E+04 5.01136959E-01 3.38875365E+00 6.56922581E-03-1.48501258E-07    3
-4.62580552E-09 2.47151475E-12-1.76631465E+04 6.78536320E+00                   4
!C1
HCO               L12/89H   1C   1O   1     G   200.000  3500.000  1000.000    1
 2.77217438E+00 4.95695526E-03-2.48445613E-06 5.89161778E-10-5.33508711E-14    2
 4.01191815E+03 9.79834492E+00 4.22118584E+00-3.24392532E-03 1.37799446E-05    3
-1.33144093E-08 4.33768865E-12 3.83956496E+03 3.39437243E+00                   4
```

```
CO        BUR0302 RUS 79C   1O   1    0    0G   200.000  6000.000 1000.       1
 0.30484859E+01 0.13517281E-02-0.48579405E-06 0.78853644E-10-0.46980746E-14    2
-0.14266117E+05 0.60170977E+01 0.35795335E+01-0.61035369E-03 0.10168143E-05    3
 0.90700586E-09-0.90442449E-12-0.14344086E+05 0.35084093E+01-0.13293628E+05    4
CO2       BUR0302 L 7/88C   1O   2    0    0G   200.000  6000.000 1000.       1
 0.46365111E+01 0.27414569E-02-0.99589759E-06 0.16038666E-09-0.91619857E-14    2
-0.49024904E+05-0.19348955E+01 0.23568130E+01 0.89841299E-02-0.71220632E-05    3
 0.24573008E-08-0.14288548E-12-0.48371971E+05 0.99009035E+01-0.47328105E+05    4
HOCO      CLR est L 7/88C   1O   2H   1    0G   200.000  6000.000 1000.       1  !CLR est based on CO2 data and
SANDIA
 0.46365111E+01 0.27414569E-02-0.99589759E-06 0.16038666E-09-0.91619857E-14    2  !H298=-45.19 kcal/mol
-2.44401027E+04  2.54925146E+00  0.23568130E+01  0.89841299E-02-0.71220632E-05         3    !S298=  60.00
cal/mol/K
 0.24573008E-08-0.14288548E-12-2.37871697E+04 1.43850505E+01-0.47328105E+05    4
CH2               L S/93C   1H   2         G   200.000  3500.000  1000.000    1
 2.87410113E+00 3.65639292E-03-1.40894597E-06 2.60179549E-10-1.87727567E-14    2
 4.62636040E+04 6.17119324E+00 3.76267867E+00 9.68872143E-04 2.79489841E-06    3
-3.85091153E-09 1.68741719E-12 4.60040401E+04 1.56253185E+00                  4
CH2(S)            L S/93C   1H   2         G   200.000  3500.000  1000.000    1
 2.29203842E+00 4.65588637E-03-2.01191947E-06 4.17906000E-10-3.39716365E-14    2
 5.09259997E+04 8.62650169E+00 4.19860411E+00-2.36661419E-03 8.23296220E-06    3
-6.68815981E-09 1.94314737E-12 5.04968163E+04-7.69118967E-01                  4
CH2O              L 8/88H   2C   1O   1     G   200.000  3500.000  1000.000    1
 1.76069008E+00 9.20000082E-03-4.42258813E-06 1.00641212E-09-8.83855640E-14    2
-1.39958323E+04 1.36563230E+01 4.79372315E+00-9.90833369E-03 3.73220008E-05    3
-3.79285261E-08 1.31772652E-11-1.43089567E+04 6.02812900E-01                  4
CH2OH             GUNL93C   1H   3O   1     G   200.000  3500.000  1000.000    1
 3.69266569E+00 8.64576797E-03-3.75101120E-06 7.87234636E-10-6.48554201E-14    2
-3.24250627E+03 5.81043215E+00 3.86388918E+00 5.59672304E-03 5.93271791E-06    3
-1.04532012E-08 4.36967278E-12-3.19391367E+03 5.47302243E+00                  4
CH3               L11/89C   1H   3         G   200.000  3500.000  1000.000    1
 2.28571772E+00 7.23990037E-03-2.98714348E-06 5.95684644E-10-4.67154394E-14    2
 1.67755843E+04 8.48007179E+00 3.67359040E+00 2.01095175E-03 5.73021856E-06    3
-6.87117425E-09 2.54385734E-12 1.64449988E+04 1.60456433E+00                  4
CH3O              121686C   1H   3O   1     G   300.00   3000.00   1000.000    1
 0.03770799E+02 0.07871497E-01-0.02656384E-04 0.03944431E-08-0.02112616E-12    2
 0.12783252E+03 0.02929575E+02 0.02106204E+02 0.07216595E-01 0.05338472E-04    3
-0.07377636E-07 0.02075610E-10 0.09786011E+04 0.13152177E+02                  4
CH3OH             L 8/88C   1H   4O   1     G   200.000  3500.000  1000.000    1
 1.78970791E+00 1.40938292E-02-6.36500835E-06 1.38171085E-09-1.17060220E-13    2
-2.53748747E+04 1.45023623E+01 5.71539582E+00-1.52309129E-02 6.52441155E-05    3
-7.10806889E-08 2.61352698E-11-2.56427656E+04-1.50409823E+00                  4
CH4               L 8/88C   1H   4         G   200.000  3500.000  1000.000    1
 7.48514950E-02 1.33909467E-02-5.73285809E-06 1.22292535E-09-1.01815230E-13    2
-9.46834459E+03 1.84373180E+01 5.14987613E+00-1.36709788E-02 4.91800599E-05    3
-4.84743026E-08 1.66693956E-11-1.02466476E+04-4.64130376E+00                  4
!C2
C2H3              L 2/92C   2H   3         G   200.000  3500.000  1000.000    1
 3.01672400E+00 1.03302292E-02-4.68082349E-06 1.01763288E-09-8.62607041E-14    2
 3.46128739E+04 7.78732378E+00 3.21246645E+00 1.51479162E-03 2.59209412E-05    3
-3.57657847E-08 1.47150873E-11 3.48598468E+04 8.51054025E+00                  4
```

```
C2H4            L 1/91C   2H   4         G   200.000  3500.000  1000.000    1
 2.03611116E+00 1.46454151E-02-6.71077915E-06 1.47222923E-09-1.25706061E-13    2
 4.93988614E+03 1.03053693E+01 3.95920148E+00-7.57052247E-03 5.70990292E-05    3
-6.91588753E-08 2.69884373E-11 5.08977593E+03 4.09733096E+00                   4
C2H5            L12/92C   2H   5         G   200.000  3500.000  1000.000    1
 1.95465642E+00 1.73972722E-02-7.98206668E-06 1.75217689E-09-1.49641576E-13    2
 1.28575200E+04 1.34624343E+01 4.30646568E+00-4.18658892E-03 4.97142807E-05    3
-5.99126606E-08 2.30509004E-11 1.28416265E+04 4.70720924E+00                   4
C2H6            L 8/88C   2H   6         G   200.000  3500.000  1000.000    1
 1.07188150E+00 2.16852677E-02-1.00256067E-05 2.21412001E-09-1.90002890E-13    2
-1.14263932E+04 1.51156107E+01 4.29142492E+00-5.50154270E-03 5.99438288E-05    3
-7.08466285E-08 2.68685771E-11-1.15222055E+04 2.66682316E+00                   4
HCCO            SRIC91H   1C   2O   1     G   300.00   4000.00   1000.000    1
 0.56282058E+01 0.40853401E-02-0.15934547E-05 0.28626052E-09-0.19407832E-13    2
 0.19327215E+05-0.39302595E+01 0.22517214E+01 0.17655021E-01-0.23729101E-04    3
 0.17275759E-07-0.50664811E-11 0.20059449E+05 0.12490417E+02                   4
CH2CO           L 5/90C   2H   2O   1     G   200.000  3500.000  1000.000    1
 4.51129732E+00 9.00359745E-03-4.16939635E-06 9.23345882E-10-7.94838201E-14    2
-7.55105311E+03 6.32247205E-01 2.13583630E+00 1.81188721E-02-1.73947474E-05    3
 9.34397568E-09-2.01457615E-12-7.04291804E+03 1.22156480E+01                   4
!C3
C3H7            L 9/84C   3H   7         G   300.000  5000.000  1000.000    1
 0.77026987E+01 0.16044203E-01-0.52833220E-05 0.76298590E-09-0.39392284E-13    2
 0.82984336E+04-0.15480180E+02 0.10515518E+01 0.25991980E-01 0.23800540E-05    3
-0.19609569E-07 0.93732470E-11 0.10631863E+05 0.21122559E+02                   4
C3H8            L 4/85C   3H   8         G   300.000  5000.000  1000.000    1
 0.75341368E+01 0.18872239E-01-0.62718491E-05 0.91475649E-09-0.47838069E-13    2
-0.16467516E+05-0.17892349E+02 0.93355381E+00 0.26424579E-01 0.61059727E-05    3
-0.21977499E-07 0.95149253E-11-0.13958520E+05 0.19201691E+02                   4
! N
N               L 6/88N   1             G   200.000  6000.000  1000.000    1
 0.24159429E+01 0.17489065E-03-0.11902369E-06 0.30226245E-10-0.20360982E-14    2
 0.56133773E+05 0.46496096E+01 0.25000000E+01 0.00000000E+00 0.00000000E+00    3
 0.00000000E+00 0.00000000E+00 0.56104637E+05 0.41939087E+01                   4
N2        BUR0302 G 8/02N  2.   0.   0.   0.G   200.000  6000.000 1000.       1
 2.95257637E+00 1.39690040E-03-4.92631603E-07 7.86010195E-11-4.60755204E-15    2
-9.23948688E+02 5.87188762E+00 3.53100528E+00-1.23660988E-04-5.02999433E-07    3
 2.43530612E-09-1.40881235E-12-1.04697628E+03 2.96747038E+00 0.00000000E+00    4
NNH             T07/93N   2H   1         G   200.000  6000.000  1000.000    1
 0.37667544E+01 0.28915082E-02-0.10416620E-05 0.16842594E-09-0.10091896E-13    2
 0.28650697E+05 0.44705067E+01 0.43446927E+01-0.48497072E-02 0.20059459E-04    3
-0.21726464E-07 0.79469539E-11 0.28791973E+05 0.29779410E+01                   4
NH              And94 N   1H   1         G   200.000  6000.000  1000.000    1
 0.27836928E+01 0.13298430E-02-0.42478047E-06 0.78348501E-10-0.55044470E-14    2
 0.42120848E+05 0.57407799E+01 0.34929085E+01 0.31179198E-03-0.14890484E-05    3
 0.24816442E-08-0.10356967E-11 0.41880629E+05 0.18483278E+01                   4
NH2             And89 N   1H   2         G   200.000  6000.000  1000.000    1
 0.28347421E+01 0.32073082E-02-0.93390804E-06 0.13702953E-09-0.79206144E-14    2
 0.22171957E+05 0.65204163E+01 0.42040029E+01-0.21061385E-02 0.71068348E-05    3
-0.56115197E-08 0.16440717E-11 0.21885910E+05-0.14184248E+00                   4
NH3             J 6/77N   1H   3         G   200.000  6000.000  1000.000    1
 0.26344521E+01 0.56662560E-02-0.17278676E-05 0.23867161E-09-0.12578786E-13    2
-0.65446958E+04 0.65662928E+01 0.42860274E+01-0.46605230E-02 0.21718513E-04    3
-0.22808887E-07 0.82638046E-11-0.67417285E+04-0.62537277E+00                   4
```

```
NO              RUS 78N   1O   1         G   200.000  6000.000  1000.000    1
 0.32606056E+01 0.11911043E-02-0.42917048E-06 0.69457669E-10-0.40336099E-14    2
 0.99209746E+04 0.63693027E+01 0.42184763E+01-0.46389760E-02 0.11041022E-04    3
-0.93361354E-08 0.28035770E-11 0.98446230E+04 0.22808464E+01                   4
NO2             L 7/88N   1O   2         G   200.000  6000.000  1000.000    1
 0.48847542E+01 0.21723956E-02-0.82806906E-06 0.15747510E-09-0.10510895E-13    2
 0.23164983E+04-0.11741695E+00 0.39440312E+01-0.15854290E-02 0.16657812E-04    3
-0.20475426E-07 0.78350564E-11 0.28966179E+04 0.63119917E+01                   4
N2O             L 7/88N   2O   1         G   200.000  6000.000  1000.000    1
 0.48230729E+01 0.26270251E-02-0.95850874E-06 0.16000712E-09-0.97752303E-14    2
 0.80734048E+04-0.22017207E+01 0.22571502E+01 0.11304728E-01-0.13671319E-04    3
 0.96819806E-08-0.29307182E-11 0.87417744E+04 0.10757992E+02                   4
HNO             And93 H   1N   1O   1    G   200.000  6000.000  1000.000    1
 0.29792509E+01 0.34944059E-02-0.78549778E-06 0.57479594E-10-0.19335916E-15    2
 0.11750582E+05 0.86063728E+01 0.45334916E+01-0.56696171E-02 0.18473207E-04    3
-0.17137094E-07 0.55454573E-11 0.11548297E+05 0.17498417E+01                   4
! S
S    BUR0302    J 9/82S   1    0    0    0G   200.000  6000.000 1000.       1
 2.87936498E+00-5.11050388E-04 2.53806719E-07-4.45455458E-11 2.66717362E-15    2
 3.25013791E+04 3.98140647E+00 2.31725616E+00 4.78018342E-03-1.42082674E-05    3
 1.56569538E-08-5.96588299E-12 3.25068976E+04 6.06242434E+00 3.33128471E+04    4
SH   BUR0302    s06/01S  1.H  1.   0.   0.G   200.000  6000.000 1000.       1
 3.03153188E+00 1.25805478E-03-4.05525688E-07 6.19651478E-11-3.50864386E-15    2
 1.63428914E+04 6.15027214E+00 3.68468234E+00 3.24598115E-03-1.28632474E-05    3
 1.69509712E-08-7.07586975E-12 1.60405724E+04 2.01782467E+00 1.71999456E+04    4
H2S  BUR0302    RUS 89H   2S   1    0    0G   200.000  6000.000 1000.       1
 0.29770813E+01 0.36005325E-02-0.12328487E-05 0.19692654E-09-0.11677327E-13    2
-0.35155970E+04 0.67868340E+01 0.41194112E+01-0.18771599E-02 0.82066045E-05    3
-0.70594243E-08 0.21405829E-11-0.36819294E+04 0.15345832E+01-0.24775964E+04    4
SO   BUR0302    J 6/77S   1O   1    0    0G   300.000  5000.000 1000.       1
 4.01428730E+00 2.70228170E-04 8.28966670E-08-3.43237410E-11 3.11214440E-15    2
-7.10519560E+02 3.49973505E+00 3.14902330E+00 1.18393470E-03 2.57406860E-06    3
-4.44434190E-09 1.87351590E-12-4.04075710E+02 8.31987915E+00 6.02271219E+02    4
SO(S)       SO+deltaH  H   0O   1S   1    0G   300.000  5000.000 1000.00     1
 4.01428730E+00 2.70228170E-04 8.28966670E-08-3.43237410E-11 3.11214440E-15    2 !S298 = 50.89 cal/mol/K
 1.07137380E+04 2.41770183E+00 3.14902330E+00 1.18393470E-03 2.57406860E-06    3
-4.44434190E-09 1.87351590E-12 1.10201820E+04 7.23784593E+00 6.02271219E+02    4
SO2  BUR0302    J 6/61S   1O   2    0    0G   300.000  5000.000 1000.       1
 5.24513640E+00 1.97042040E-03-8.03757690E-07 1.51499690E-10-1.05580040E-14    2
-3.75582270E+04-1.07404892E+00 3.26653380E+00 5.32379020E-03 6.84375520E-07    3
-5.28100470E-09 2.55904540E-12-3.69081480E+04 9.66465108E+00-3.57007867E+04    4
SO3  BUR0302    J 9/65S   1O   3    0    0G   300.000  5000.000 1000.       1
 7.07573760E+00 3.17633870E-03-1.35357600E-06 2.56309120E-10-1.79360440E-14    2
-5.02113760E+04-1.11875176E+01 2.57803850E+00 1.45563350E-02-9.17641730E-06    3
-7.92030220E-10 1.97094730E-12-4.89317530E+04 1.22651384E+01-4.75978348E+04    4
HSO  BUR0302    T 4/93H   1S   1O   1    0G   200.000  6000.000 1000.       1 !BURCAT
 0.45416010E+01 0.22648458E-02-0.83152058E-06 0.13614796E-09-0.82290966E-14    2
-0.21608556E+04 0.23357633E+01 0.34130925E+01 0.32105128E-02 0.38960721E-05    3
-0.81958128E-08 0.37789804E-11-0.17554966E+04 0.86522782E+01-0.57517665E+03    4
HOSO DAG/GLA03 GOU/MAR99H   1O   2S   1    0G   300.000  1500.000 1500.00    0 1
 0.16184697E+01 0.21164061E-01-0.26690482E-04 0.16272216E-07-0.37779005E-11    2
-0.30255641E+05 0.19477260E+02 0.16184697E+01 0.21164061E-01-0.26690482E-04    3
 0.16272216E-07-0.37779005E-11-0.30255641E+05 0.19477260E+02                   4
```

```
! Mixed Base
HCN             GRI/98H   1C   1N   1     G   200.000  6000.000  1000.000    1
 0.38022392E+01 0.31464228E-02-0.10632185E-05 0.16619757E-09-0.97997570E-14    2
 0.14407292E+05 0.15754601E+01 0.22589886E+01 0.10051170E-01-0.13351763E-04    3
 0.10092349E-07-0.30089028E-11 0.14712633E+05 0.89164419E+01                   4
NCO             EA 93 N   1C   1O   1     G   200.000  6000.000  1000.000    1
 0.51521845E+01 0.23051761E-02-0.88033153E-06 0.14789098E-09-0.90977996E-14    2
 0.14004123E+05-0.25442660E+01 0.28269308E+01 0.88051688E-02-0.83866134E-05    3
 0.48016964E-08-0.13313595E-11 0.14682477E+05 0.95504646E+01                   4
HNCO            BDEA94H   1N   1C   1O   1G   300.000  5000.000  1478.000    1
 6.22395134E+00 3.17864004E-03-1.09378755E-06 1.70735163E-10-9.95021955E-15    2
-1.66599344E+04-8.38224741E+00 3.63096317E+00 7.30282357E-03-2.28050003E-06    3
-6.61271298E-10 3.62235752E-13-1.55873636E+04 6.19457727E+00                   4


END
```

REFRENCES

1. Zeng, X., et al., *Pilot verification of a low-tar two-stage coal gasification process with a fluidized bed pyrolyzer and fixed bed gasifier.* Applied Energy, 2014. 115: p. 9-16.

2. Higman, C. and S. Tam, *Advances in Coal Gasification, Hydrogenation, and Gas Treating for the Production of Chemicals and Fuels.* Chemical reviews, 2014.

3. Murphy, D.J., *The implications of the declining energy return on investment of oil production.* Philosophical Transactions of the Royal Society A: Mathematical, Physical and Engineering Sciences, 2014. 372(2006): p. 20130126.

4. Cengel, Y.A., M.A. Boles, and M. Kanoğlu, *Thermodynamics: an engineering approach*. Vol. 5. 2011: McGraw-Hill New York.

5. Weinberg, F., *Combustion temperatures: the future?* Nature, 1971. 233: p. 239-241.

6. Howell, J., M. Hall, and J. Ellzey, *Combustion of hydrocarbon fuels within porous inert media.* Progress in Energy and Combustion Science, 1996. 22(2): p. 121-145.

7. Trimis, D., et al., *Porous medium combustor versus combustion systems with free flames.* Advances in Heat Transfer Enhancement and Energy Conservation, 1997: p. 339-345.

8. Hayes, R.E. and S.T. Kolaczkowski, *Introduction to catalytic combustion*. 1997: CRC Press.

9. Wood, S. and A.T. Harris, *Porous burners for lean-burn applications.* Progress in energy and combustion science, 2008. 34(5): p. 667-684.

10. Hoffmann, J., et al., *Experimental study on combustion in porous media with a reciprocating flow system.* Combustion and Flame, 1997. 111(1): p. 32-46.

11. Marbach, T.L., V. Sadasivuni, and A.K. Agrawal, *Investigation of a miniature combustor using porous media surface stabilized flame.* Combustion science and technology, 2007. 179(9): p. 1901-1922.

12. Williams, A., R. Woolley, and M. Lawes, *The formation of NO< sub> x</sub> in surface burners.* Combustion and Flame, 1992. 89(2): p. 157-166.

13. Tong, T. and S. Sathe, *Heat transfer characteristics of porous radiant burners.* Journal of Heat Transfer (Transactions of the ASME (American Society of Mechanical Engineers), Series C);(United States), 1991. 113(2).

14. Hanamura, K., R. Echigo, and S.A. Zhdanok, *Superadiabatic combustion in a porous medium.* International Journal of Heat and Mass Transfer, 1993. 36(13): p. 3201-3209.

15. Brenner, G., et al., *Numerical and experimental investigation of matrix-stabilized methane/air combustion in porous inert media.* Combustion and Flame, 2000. 123(1): p. 201-213.

16. Beer, J., *Combustion Aerodynumics.* Combustion Technology: Some Modern Developments, 1974: p. 61.

17. Steinberg, A.M., et al., *Effects of Flow Structure Dynamics on Thermoacoustic Instabilities in Swirl-Stabilized Combustion.* AIAA journal, 2012. 50(4): p. 952-967.

18. Candel, S.M. *Combustion instabilities coupled by pressure waves and their active control*. in *Symposium (International) on Combustion*. 1992. Elsevier.

19. McNaught, A.D. and A. Wilkinson, *Compendium of chemical terminology*. Vol. 1669. 1997: Blackwell Science Oxford.

20. Normann, F., et al., *High-temperature reduction of nitrogen oxides in oxy-fuel combustion.* Fuel, 2008. 87(17): p. 3579-3585.

21. Chase, M.W. and J.A.N.A. Force, *NIST-JANAF thermochemical tables.* 1998.

22. Pechukas, P., *Transition state theory.* Annual Review of Physical Chemistry, 1981. 32(1): p. 159-177.

23. Upadhyay, S.K., *Chemical kinetics and reaction dynamics*. 2006: Springer.

24. Huang, H., et al., *Structure of a covalently trapped catalytic complex of HIV-1 reverse transcriptase: implications for drug resistance.* Science, 1998. 282(5394): p. 1669-1675.

25. Zhou, Q., et al., *Flue gas NOx reduction using ammonia radical injection.* Journal of the Air & Waste Management Association, 1992. 42(9): p. 1193-1197.

26. Vatcha, S.R., *Low-emission gas turbines using catalytic combustion.* Energy conversion and Management, 1997. 38(10): p. 1327-1334.

27. Delimaris, D. and T. Ioannides, *VOC oxidation over MnO< sub> x</sub>–CeO< sub> 2</sub> catalysts prepared by a combustion method.* Applied Catalysis B: Environmental, 2008. 84(1): p. 303-312.

28. Paik, S.C. and J.S. Chung, *Selective catalytic reduction of sulfur dioxide with hydrogen to elemental sulfur over Co-Mo/Al< sub> 2</sub> O< sub> 3</sub>*. Applied Catalysis B: Environmental, 1995. 5(3): p. 233-243.

29. Hayes, R. and S. Kolaczkowski, *Mass and heat transfer effects in catalytic monolith reactors.* Chemical Engineering Science, 1994. 49(21): p. 3587-3599.

30. Rosten, R., et al. *Characterization of (La0. 9Sr0.) 0.95Cr0. 85Mg0. 1Ni0. 05O3 Perovskite Ceramics for a Perovskite Related Membrane Reactor*. in *MRS Proceedings*. 2006. Cambridge Univ Press.

31. Weinrotter, M., et al., *Laser ignition of ultra-lean methane/hydrogen/air mixtures at high temperature and pressure.* Experimental thermal and fluid science, 2005. 29(5): p. 569-577.

32. Glassman, I. and R. Yetter, *Combustion*. 2008: Academic press.

33. Zhou, X. and J. Pereira, *Comparison of four combustion models for simulating the premixed combustion in inert porous media.* Fire and Materials, 1998. 22(5): p. 187-197.

34. William H. Green, J.W.A., Beat A. Buesser, Robert W. Ashcraft, Gregory J. Beran, Caleb A. Class, Connie Gao, C. Franklin Goldsmith, Michael R. Harper, Amrit Jalan, Murat Keceli, Gregory R. Magoon, David M. Matheu, Shamel S. Merchant, Jeffrey D. Mo, Sarah Petway, Sumathy Raman, Sandeep Sharma, Jing Song, Yury Suleymanov, Kevin M. Van Geem, John Wen, Richard H. West, Andrew Wong, Hsi-Wu Wong, Paul E. Yelvington, Nathan Yee, Joanna Yu. *RMG - Reaction Mechanism Generator v 4.0.1*. 2013; Available from: http://rmg.sourceforge.net/.

35. Petersen, E.L., et al. *High-pressure methane oxidation behind reflected shock waves*. in *Symposium (International) on Combustion*. 1996. Elsevier.

36. Li, J., et al., *A comprehensive kinetic mechanism for CO, CH2O, and CH3OH combustion.* International Journal of Chemical Kinetics, 2007. 39(3): p. 109-136.

37. Ranzi, E., et al., *Wide-range kinetic modeling study of the pyrolysis, partial oxidation, and combustion of heavy n-alkanes.* Industrial & engineering chemistry research, 2005. 44(14): p. 5170-5183.

38. Smith, G., et al., *GRI 3.0.* Gas Research Institute, Chicago, IL, http://www. me. berkeley. edu/gri_mech, 2000.

39. Glarborg, P. and P. Marshall, *Oxidation of Reduced Sulfur Species: Carbonyl Sulfide.* International Journal of Chemical Kinetics, 2013. 45(7): p. 429-439.

40. Bowman, C., et al., *The GRI 3.0 chemical kinetic mechanism.* University of California: Berkeley, CA, 1999.

41. Friedrichs, G., et al., *Quantitative detection of HCO behind shock waves: The thermal decomposition of HCO.* Physical Chemistry Chemical Physics, 2002. 4(23): p. 5778-5788.

42. Feng, W. and B. Wang, *Reaction of vinyl radical with O< sub> 2</sub> studied by time-resolved infrared emission spectroscopy.* Chemical physics letters, 2002. 356(5): p. 505-510.

43. Tsang, W. and J.T. Herron, *Chemical kinetic data base for propellant combustion I. Reactions involving NO, NO2, HNO, HNO2, HCN and N2O.* Journal of physical and chemical reference data, 1991. 20(4): p. 609-663.

44. Bauerle, S. and M. Klatt, *Investigation of the Reaction of 3CH2 with NO at high Temperatures.* Berichte der Bunsengesellschaft für physikalische Chemie, 1995. 99(2): p. 97-104.

45. Mishra, S., et al., *Heat transfer analysis of a two-dimensional rectangular porous radiant burner.* International communications in heat and mass transfer, 2006. 33(4): p. 467-474.

46. Ingham, D.B. and I. Pop, *Transport phenomena in porous media III*. Vol. 3. 2005: Access Online via Elsevier.

47. Mujeebu, M.A., et al., *Combustion in porous media and its applications–A comprehensive survey.* Journal of environmental management, 2009. 90(8): p. 2287-2312.

48. TAKENO, T. and K. SATO, *An excess enthalpy flame theory.* Combustion Science and Technology, 1979. 20(1-2): p. 73-84.

49. WAWRZINEK, I.K. and D. TRIMIS, *Flame Stabilization of Highly Diffusive Gas Mixtures in Porous Inert Media.* Modelling Fluid Flow: The State of the Art, 2004: p. 107.

50. Eckert, E. and R. Drake, *Analysis of heat and mass transfer, 1972.* McGraw− Hil1 など.

51. Ding, Y., et al., *High sensitivity cw-cavity ringdown and Fourier transform absorption spectroscopies of< sup> 13</sup> CO< sub> 2</sub>*. Journal of molecular spectroscopy, 2004. 226(2): p. 146-160.

52. Tashkun, S.A., et al., *CDSD-1000, the high-temperature carbon dioxide spectroscopic databank.* Journal of Quantitative Spectroscopy and Radiative Transfer, 2003. 82(1): p. 165-196.

53. Edwards, D., *Absorption by infrared bands of carbon dioxide gas at elevated pressures and temperatures.* JOSA, 1960. 50(6): p. 617.

54. Leonardi, S., J. Gore, and R. Viskanta. *Experimental investigation of partially-premixed combustion in a novel porous radiant burners*. in *Proceedings of the thirty-fifth national heat transfer conference (NHTC2001), Anaheim*. 2001.

55. Zhdanok, S., L.A. Kennedy, and G. Koester, *Superadiabatic combustion of methane air mixtures under filtration in a packed bed.* Combustion and Flame, 1995. 100(1): p. 221-231.

56. Kaplan, M. and M.J. Hall, *The combustion of liquid fuels within a porous media radiant burner.* Experimental thermal and fluid science, 1995. 11(1): p. 13-20.

57. Barra, A.J. and J.L. Ellzey, *Heat recirculation and heat transfer in porous burners.* Combustion and Flame, 2004. 137(1): p. 230-241.

58. Fuse, T., N. Kobayashi, and M. Hasatani, *Combustion characteristics of ethanol in a porous ceramic burner and ignition improved by enhancement of liquid-fuel intrusion in the pore with ultrasonic irradiation.* Experimental thermal and fluid science, 2005. 29(4): p. 467-476.

59. Robinson, R.C. and J.L. Smialek, *SiC recession caused by SiO2 scale volatility under combustion conditions: I, experimental results and empirical model.* Journal of The American Ceramic Society, 1999. 82(7): p. 1817-1825.

60. Hornetz, B., H. Michel, and J. Halbritter, *ARXPS studies of SiO2-SiC interfaces and oxidation of 6H SiC single crystal Si-(001) and C-(001) surfaces.* Journal of materials research, 1994. 9(12): p. 3088-3094.

61. Fahrenholtz, W.G., *Thermodynamic Analysis of ZrB2–SiC Oxidation: Formation of a SiC-Depleted Region.* Journal of the American Ceramic Society, 2007. 90(1): p. 143-148.

62. Raj, R., *Chemical Potential-Based Analysis for the Oxidation Kinetics of Si and SiC Single Crystals.* Journal of the American Ceramic Society, 2013. 96(9): p. 2926-2934.

63. Kärcher, B. and D. Fahey, *The role of sulfur emission in volatile particle formation in jet aircraft exhaust plumes.* Geophysical research letters, 1997. 24(4): p. 389-392.

64. Stanger, R. and T. Wall, *Sulphur impacts during pulverised coal combustion in oxy-fuel technology for carbon capture and storage.* Progress in Energy and Combustion Science, 2011. 37(1): p. 69-88.

65. Norton, D.G. and D.G. Vlachos, *Combustion characteristics and flame stability at the microscale: a CFD study of premixed methane/air mixtures.* Chemical Engineering Science, 2003. 58(21): p. 4871-4882.

66. Hackert, C., J. Ellzey, and O. Ezekoye, *Combustion and heat transfer in model two-dimensional porous burners.* Combustion and flame, 1999. 116(1): p. 177-191.

67. Takeno, T., K. Sato, and K. Hase. *A theoretical study on an excess enthalpy flame*. in *Symposium (International) on Combustion*. 1981. Elsevier.

68. Foutko, S.I., S.I. Shabunya, and L.A. Kennedy. *Superadiabatic combustion wave in a diluted methane-air mixture under filtration in a packed bed*. in *Symposium (International) on Combustion*. 1996. Elsevier.

69. Henneke, M.R. and J.L. Ellzey, *Modeling of filtration combustion in a packed bed.* Combustion and flame, 1999. 117(4): p. 832-840.

70. Andersen, F.M., *Marshak boundary condition recurrence formulae.* Zeitschrift für angewandte Mathematik und Physik ZAMP, 1997. 48(1): p. 165-170.

71. Khanna, V., R. Goel, and J. Ellzey, *Measurements of emissions and radiation for methane combustion within a porous medium burner.* Combustion science and technology, 1994. 99(1-3): p. 133-142.

72. Twarowski, A., *The temperature dependence of H+ OH recombination in phosphorus oxide containing post-combustion gases.* Combustion and flame, 1996. 105(3): p. 407-413.

73. Larson, C., P. Stewart, and D. Golden, *Pressure and temperature dependence of reactions proceeding via a bound complex. An approach for combustion and atmospheric chemistry modelers. Application to HO+ CO→[HOCO]→ H+ CO2.* International journal of chemical kinetics, 1988. 20(1): p. 27-40.

74. Akihama, K., et al., *Mechanism of the smokeless rich diesel combustion by reducing temperature.* Training, 2001. 2011: p. 03-15.

75. Glarborg, P., et al. *A reduced mechanism for nitrogen chemistry in methane combustion*. in *Symposium (International) on Combustion*. 1992. Elsevier.

76. Hori, M., et al. *An experimental and kinetic calculation of the promotion effect of hydrocarbons on the NO-NO< sub> 2</sub> conversion in a flow reactor*. in *Symposium (International) on Combustion*. 1998. Elsevier.

77. Lu, T. and C.K. Law, *A directed relation graph method for mechanism reduction.* Proceedings of the Combustion Institute, 2005. 30(1): p. 1333-1341.

78. Keck, J.C. and D. Gillespie, *Rate-controlled partial-equilibrium method for treating reacting gas mixtures.* Combustion and Flame, 1971. 17(2): p. 237-241.

79. Løvs, T., D. Nilsson, and F. Mauss, *Automatic reduction procedure for chemical mechanisms applied to premixed methane/air flames.* Proceedings of the Combustion Institute, 2000. 28(2): p. 1809-1815.

80. Maas, U. and S.B. Pope, *Simplifying chemical kinetics: intrinsic low-dimensional manifolds in composition space.* Combustion and Flame, 1992. 88(3): p. 239-264.

81. Frouzakis, C.E. and K. Boulouchos, *Analysis and reduction of the CH4-air mechanism at lean conditions.* Combustion science and technology, 2000. 159(1): p. 281-303.

82. Sung, C., C. Law, and J.-Y. Chen. *An augmented reduced mechanism for methane oxidation with comprehensive global parametric validation*. in *Symposium (International) on Combustion*. 1998. Elsevier.

83. Voss, S., et al., *Investigation on the thermal flame thickness for lean premixed combustion of low calorific H< sub> 2</sub>/CO mixtures within porous inert media.* Proceedings of the Combustion Institute, 2012.

84. Zheng, C., et al., *Partial Oxidation of Methane in Porous Reactor: Part I. Unidirectional Flow.* Energy & Fuels, 2012. 26(8): p. 4849-4856.

85. Lown, A.L., et al., *Cold flow properties for blends of biofuels with diesel and jet fuels.* Fuel, 2014. 117: p. 544-551.

86. Judson, D.G., *Diesel fuel heater*. 1985, Google Patents.

87. Mujeebu, M.A., et al., *A review of investigations on liquid fuel combustion in porous inert media.* Progress in Energy and Combustion Science, 2009. 35(2): p. 216-230.

88. Zhao, Z. and M. Xie, *Numerical simulation about interaction between pressure swirl spray and hot porous medium.* Energy Conversion and Management, 2008. 49(5): p. 1047-1055.

89. Vijaykant, S. and A.K. Agrawal, *Liquid fuel combustion within silicon-carbide coated carbon foam.* Experimental Thermal and Fluid Science, 2007. 32(1): p. 117-125.

90. Hayashi, S. and S. Kumagai. *Flame propagation in fuel droplet-vapor-air mixtures*. in *Symposium (International) on Combustion*. 1975. Elsevier.

91. Kamal, M. and A. Mohamad, *Enhanced radiation output from foam burners operating with a nonpremixed flame.* Combustion and flame, 2005. 140(3): p. 233-248.

92. Abbasi, H.A., T.D. Briselden, and M.J. Khinkis, *Staged combustion in a porous-matrix surface combustor to promote ultra-low NO. sub. x Emissions*. 1995, Google Patents.

93. ELLZEY, J.L. and R. Goel, *Emissions of CO and NO from a two stage porous media burner.* Combustion science and technology, 1995. 107(1-3): p. 81-91.

94. Hanamura, K., K. Bohda, and Y. Miyairi, *A study of super-adiabatic combustion engine.* Energy conversion and management, 1997. 38(10): p. 1259-1266.

95. Xie, M.-Z., et al., *Experimental and numerical investigation on performance of a porous medium burner with reciprocating flow*. Fuel, 2009. 88(1): p. 206-213.

96. Weinberg, F.J., *Advanced combustion methods*. 1986, Imperial College of Science and Technology, London.

97. Durst, F. and M. Weclas, *A new type of internal combustion engine based on the porous-medium combustion technique*. Proceedings of the Institution of Mechanical Engineers, Part D: Journal of Automobile Engineering, 2001. 215(1): p. 63-81.

98. Gnesdilov, N., K. Dobrego, and I. Kozlov, *Parametric study of recuperative VOC oxidation reactor with porous media.* International journal of heat and mass transfer, 2007. 50(13): p. 2787-2794.

99. Teodorita Al Seadi, D.R., Heinz Prassl, Michael Köttner, Tobias Finsterwalder, and R.J. Silke Volk, *Biogas*. University of Southern Denmark Esbjerg, Niels Bohrs Vej 9-10,. 126.

100. *Landfill Gas*. [cited 2014; Available from: http://www.epa.gov/lmop/faq/landfill-gas.html.

101. Lai, J., *A study of precipitation in AISI type 316 stainless steel.* Materials Science and Engineering, 1983. 58(2): p. 195-209.

102. Weiss, B. and R. Stickler, *Phase instabilities during high temperature exposure of 316 austenitic stainless steel.* Metallurgical transactions, 1972. 3(4): p. 851-866.

103. *The Atlas Steels Technical Handbook of Stainless Steels*. 2013 ed. 2013: Atlas Steels Technical Department. 49.

104. Incropera, F.P., *Introduction to heat transfer*. 2011: John Wiley & Sons.

105. MUNRO, M., *Evaluated Material Properties for a Sintered alpha-Alumina.* Journal of the American Ceramic Society, 1997. 80(8): p. 1919-1928.

106. Munro, R., *Material properties of a sintered α-SiC*. Journal of Physical and Chemical Reference Data, 1997. 26(5): p. 1195-1203.

107. Leofanti, G., et al., *Surface area and pore texture of catalysts.* Catalysis Today, 1998. 41(1): p. 207-219.

108. Bejan, A., *Heat Transfer*. 1st ed. 1993, New York: John Wiley & Sons, Inc. 675.

109. Callen, H., *Thermodynamics and Thermostatistics*. 1985, Wiley, New York.

110. Honnet, S., et al., *A surrogate fuel for kerosene.* Proceedings of the Combustion Institute, 2009. 32(1): p. 485-492.

111. Turns, S.R., *An Introduction to Combustion: Concepts and Applications*. Third ed, ed. B. Steinquist. 2012: McGraw Hill.